Doctoral Dissertation
Doctoral Program in Materials Science and Technology (35^{h} Cycle)

Investigation of Different Types of Biochar on the Thermal Stability and Fire Retardancy of Polymer Composites

By

Samuele Matta

******

Supervisors:
Prof. Giulio Malucelli, Supervisor
Prof. Alberto Frache, Co-Supervisor

Doctoral Examination Committee:
Prof. Claudia Marano, Politecnico di Milano
Prof. Martino Colonna, Università di Bologna
Prof. Silvia Spriano, Politecnico di Torino
Prof. Sabrina Grassini, Politecnico di Torino
Prof. Marco Zanetti, Università di Torino

Politecnico di Torino
01/06/2023

Declaration

I hereby declare that, the contents and organization of this dissertation constitute my own original work and does not compromise in any way the rights of third parties, including those relating to the security of personal data.

Samuele Matta

Turin, 2023

* This dissertation is presented in partial fulfillment of the requirements for **Ph.D. degree** in the Graduate School of Politecnico di Torino (ScuDo).

I would like to dedicate this thesis to my Family

Abstract

Fire is a very important and severe hazard that involves all flammable materials, in particular polymers. In this context, it becomes very important to provide flammable materials with flame retardant features, so that the former can withstand the application of a flame or of an irradiative heat flux, hence becoming suitable for specific applications (civil construction engineering, transportation, furniture, among a few to mention). Besides, the way employed for imparting flame retardant properties is a key issue: in fact, it is possible to incorporate the flame retardant in the bulk material, or to selectively locate it on the material surface. It is worthy to note that, being equal the content, usually the application of the flame retardants (FRs) onto the material surface has some advantages, namely: the overall mechanical behavior of the flame retarded material is not affected and it is possible to lower the FR loading required for an acceptable fire performance. The aim of this Ph.D. dissertation is to explore various flame retardant systems using bio-sourced FRs. In this way it is possible to combine the 'green' character of these materials with the current need to provide wastes and by-products with further added value In view of sustainability, the use of biochar (BC), a solid product obtained from the thermo-chemical conversion of wastes/biomasses in an oxygen-limited environment, represents a renewable/bio-sourced material that has been widely utilized in environmental management and agriculture. In addition, it has been exploited as a low-cost carbon sequester and a natural adsorbent, as well as in soil remediation and amendment, thanks to its remarkably stable honeycomb-like carbonaceous structure. All these peculiarities suggest the possibility of using biochar either as a filler in polymer composites with enhanced thermal and flame retardant properties, or as a component of flame retardant coatings, hence further widening its potential uses. In this Ph.D, dissertation, thermoplastic polymers have been chosen (i.e. ethylene vinyl acetate

and polyethylene), and with compound technique the biochar was incorporated into the polymers as flame retardants. Using the thermo-compression and injection molding processes, the specimens were molded and used for forced combustion and flammability tests (i.e., cone calorimeter and UL-94). Furthermore, various masterbatch of biochar and polymer were prepared and then applied to the surface of unfilled matrix by thermocompression. Both the systems turned out to significantly improve the overall flame retardant features of the polymer. In this thesis, different types of BC were used from various feedstock and the properties of their respective compounds were thoroughly investigated.

PhD framework and objectives

The objective of this dissertation is to investigate the effect of biochar as a filler for flame retardant systems. In this regard, two different polymers were chosen as the matrix for the study of biochar used as an alternative flame retardant to conventional ones. The first one is the ethylene vinyl acetate (EVA), a copolymer widely studied in the scientific literature because of its poor performance against fire and which typically requires a very high amount of flame retardants, even above 60 wt.%. The second one is the high-density polyethylene (HDPE), a commercially common polymer which, however, requires a flame retardant treatment in almost all applications in which it is used. The thesis project explores different strategies to impart a flame retardancy to the above matrices. For this purpose, biochars were produced starting from various biomasses or waste. All the new materials obtained were then thoroughly characterized.

Thesis structure

The thesis is structured in the following chapters:

- Chapter 1 introduces the topic of the flame retardancy of polymers by describing polymer combustion and the various types of flame retardants used in polymer matrices. The state of the art of these has been discussed and examples from the literature has been reported.
- Chapter 2 describes the synthesis methods to produce biochar and lists its main properties. In addition, the state of the art regarding composite polymers containing biochar (BC) are reported from the literature focusing on polymer-biochar flame retardant systems.
- From Chapter 3 to Chapter 7 the results of the experimental trials of the thesis are reported. In particular, Chapter 3 describes the pyrolysis of kraft lignin: both the biomass and products were investigated thoroughly, reporting the results obtained. Various BCs were produced and incorporated by compounding into ethylene vinyl acetate (EVA) to obtain flame retardant system that have been studied.
- In Chapter 4 different biomasses are treated using a pyrolysis process designed for obtaining BC. The various BCs have been studied and used as filler for EVA copolymer to create innovative fire retardant systems, which have been characterized.
- Chapter 5 reports experiments conducted on systems containing both BC and humic acid to improve the fire resistance of EVA composites.
- In Chapter 6, experiments on Tetra Pak materials that are pyrolyzed to obtain char are reported. Fire retardant systems are prepared and characterized, and the results are presented.
- Finally, in Chapter 7 the effect of char from Tetra Pak as flame retardant in high density polyethylene matrices is investigated.

The materials, experimental tests, and the characterization methods used to discuss the results are reported in the Appendix.

Contents

List of Figures

List of Tables

List of the abbreviations

BC: biochar

CC: cellulose

DSC: differential scanning calorimetry

DTG: derivative thermogravimetry

EDX: energy dispersive X-ray

FC: fixed carbon

FESEM: Field Emission Scanning Electron Microscopy

FIGRA: Fire Growth Rate Index

FPI: fire performance index

FR: flame retardant

FRI: flame retardancy index

HA: humic acid

HC: hemicellulose

HHV: higher heating value

HPLC: High Performance Liquid Chromatography

HRR: heat rate release

HV: high viscosity

L/D: length/diameter

LC: lignin

LD: low viscosity

LOI: limiting oxygen index

MFI: melt flow index

MFR: melt flow rate

NP: nano particles

pkHRR: peak of heat rate release

SEA: specific extinction area

SEM: scanning electron microscopy

SPR: smoke production rate

TGA: thermogravimetric analyses

THR: total heat release

TSR: total smoke release

TTI: time to ignition

XPS: X-ray photoelectron spectroscopy

Chapter 1

Flame retardancy of polymers

1.1 Introduction

Polymer materials are widely used in daily life due to their extraordinary combination of characteristics, low weight, and ease of production. In addition to the many benefits that polymers offer, there is one clear drawback connected to the high flammability of many synthetic polymers. Furthermore, polymers are also utilized to create thin things like films, fibers, coatings, and foams, which are even more flammable than molded parts. Flammability, ease of extinguishment, flammability of the volatile products formed, amount of heat released during burning, rate of heat release, flame propagation, smoke obscuration, smoke toxicity, and the fire scenario are all elements that affect the risk of fire [1] [2] [3].

Safety requirements are becoming increasingly stringent in terms of polymer response to fire and fire resistance performance, while several flame retardant additives, such as halogenated compounds, are being phased out because of their proven or suspected negative effects on the environment. The development of efficient and environmentally friendly flame retardant systems for polymeric materials is therefore a significant challenge. The nature and chemical structure of the polymer in question, its mode of decomposition, the required level of fire safety, as well as the overall performances of the resulting materials, play a key role in the assessment of effective strategies for improving polymer fire resistance. The design of flame retardant materials and the understanding of the

phenomena that occur during combustion often involve different scientific fields (such as macromolecular chemistry and physics, mass and heat transfer physics, rheology, etc.) [4].

It is evident that flame retardants are crucial components of polymer formulations for applications where polymers have a high possibility of being exposed to an ignition source (electrical and electronic goods), where polymers are easily ignited, or where the rapid spread of a fire could result in serious issues (related to building materials and transportation) when evacuating people [5].

1.2 Polymer combustion

Polymers are highly combustible due to their mostly carbon and hydrogen chemical composition. One or more combustible species (reducing agents) and an oxidizing agent (usually the oxygen in the air) are required for a combustion reaction to occur. Typically, the procedure begins with a heat source raising the temperature of the polymeric material to a point where it causes polymer bond scissions. The volatile component of the resulting polymer fragments diffuses into the atmosphere and produces a flammable gaseous mixture (the fuel). When the self-ignition temperature is reached, which is the temperature at which the activation energy of the combustion reaction is achieved, this gaseous mixture ignites. As an alternative, the ignition occurs at a lower temperature if the fuel comes in contact with an intense external energy, such as a spark or a flame. During combustion, the fuel releases a certain amount of heat that can promote new decomposition reactions in the solid phase, which, in turn, generate other fuels [4].

Figure 1 is used to illustrate the combustion of polymers. A loop shows the cyclic relationship between the two successive reactions of pyrolysis (R1) and oxidation (R2), which supports the overall combustion and results in a specific kinetic interdependence of the two reactions. Indeed, the two responses influence each another. Through the formation of volatiles, the rate of polymer pyrolysis influences the oxidation-combustion rate, which in turn affects the pyrolysis through the combustion heat response [6].

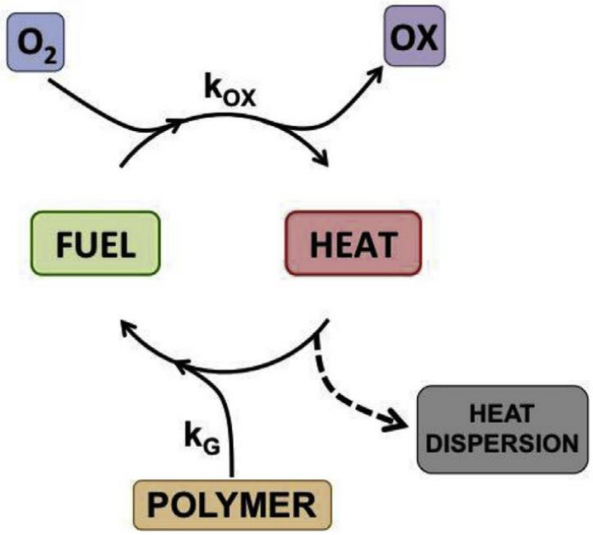

Figure 1. The Fire Loop: FUEL = volatile pyrolysis products (G), OX = combustion products, k_G and k_{OX} are the overall specific rates of volatiles G products formation by polymer pyrolysis and of their oxidation, respectively. Reprinted with the permission from [6].

This process occurs in the solid, gaseous, and interfacial phases and includes several complex reactions and transport phenomena. In general, polymer combustion involves four main steps: ignition, pyrolysis, combustion, and feedback [7]. The energy required for the thermal decomposition of a polymer must be greater than the binding energy between the carbon atoms that are covalently connected. The presence or absence of oxygen in the solid and gas phases, have a significant impact on the decomposition mechanisms. Indeed, the thermal decomposition is the result of the effects of heat and oxygen. It is then possible to distinguish between oxidizing and non-oxidizing thermal degradation. The first mechanism is commonly started by chain scissions under the influence of temperature only, and it is called pyrolysis. Chemical defects in polymer chains, the presence of weak bonds, the oxygen atoms in the chain, catalyst residues, and previous oxidation residues, are some of the factors that affect the initial scission. Chain scission can take place as free radicals are produced (Equation (1)); in this situation, the reaction doesn't cease because these radicals set off a chain reaction that may happen in both oxidative and non-oxidizing conditions. Alternatively, the chain scission can start by migration of hydrogen atoms which causes the formation of a molecule with a reactive double bond (Equation (2)).

$$R_1 - CH_2 - CH_2 - R_2 \rightarrow R_1 - CH_2 \cdot + \cdot CH_2 - R_2 \quad (1)$$

$$R_1 - CH_2 - CH_2 - CH_2 - R_2 \rightarrow R_1 - CH = CH_2 + CH_3 - R_2 \quad (2)$$

In oxidizing thermal conditions, a wide range of low molecular weight compounds (carboxylic acids, alcohols, ketones, aldehydes, etc.) is produced when the polymer combines with oxygen in the air. This breakdown also releases H· and OH·, an extremely reactive species. By means of the macromolecular radical recombination processes, oxidation can result in crosslinking, but bond scission is still the main reaction. The release of hydrogen atoms from the polymer chains causes a reaction that regulates the rate at which the degradation process spreads. Thus, the C-H bond energy determines the polymer stability toward oxidation. By both convection and diffusion into the layer near the surface, the decomposition gases produced by pyrolysis first combine with oxygen, produce free radicals, and then, when the critical point is reached, ignite. This ignition can be started by an external source (flash-ignition) or self-induced (self-ignition). The gas combustion raises the temperature of the polymer, promoting pyrolysis and the creation of new combustible gases. If the polymer receives enough heat from the flame to keep its rate of degradation above the minimum value, the combustion process will continue, and the polymer will be completely consumed [8]. The combustion process is schematized in Figure 2.

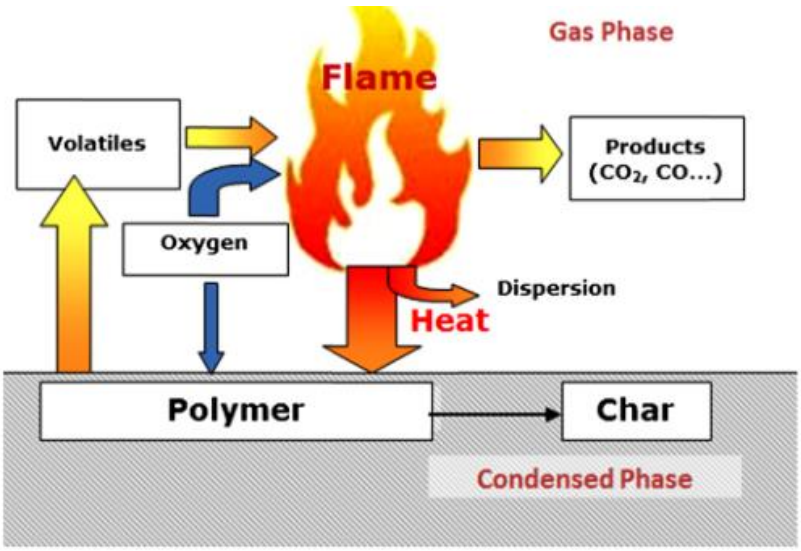

Figure 2. Schematic representation of the polymer combustion cycle. Reprinted with the permission from [9].

The reaction of polymers to flame or heat can be defined by their flammability, speed of flame spread and heat release. One or more of these parameters must be measured by specific tests depending on the desired application of the polymeric material. Several small-, intermediate-, or full-scale flammability tests are employed in academic or industrial laboratories to screen materials when exposed to flame or heat. As many polymers melt and are prone to produce flammable drops or flow, the ability of polymers to disperse flames away from a fire source is critical. Therefore, it is essential to test the flammability of polymeric materials in environments like those in which they are usually employed. The heat and mass transfer properties of fires vary significantly, depending on factors including applied heat flux, temperature, length scales, and ventilation. Figure 3 shows a typical example of a fire scenario, in which three stages can be identified.

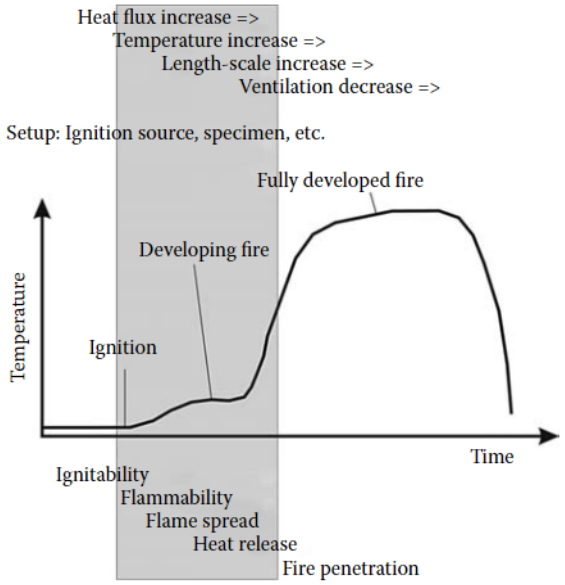

Figure 3. The stages of a fire, fire properties, and the range of fire scenarios. Reprinted with the permission from [10]**.**

- Ignition. The beginning of flame is known as piloted ignition, which is defined by an ignition source (flame, cigarette, glow wire, etc.), ignition temperatures (ranging from 325 to 425 °C), and high ventilation. For some time, the fire only involves a small region, and its growth is confined.

- Developing fire. This stage of the fire's development is marked by an external heat flux about 20 - 60 kW m^{-2}, larger size, ambient temperatures above the ignition temperature (425 - 625 °C), and persistently high ventilation. The transition from ignition to fully developed fire is called *flashover*, and at this point all exposed combustible materials are included in the fire.

- Fully developed fire. This stage presents a high external flux > 50 kW m^{-2}, great length scales, ambient temperature above 625 °C and a low ventilation. This is the most critical stage of fire when the peak in the fire growth occurs.

- Decay. Following a sustained period of combustion, fire experiences a dramatic drop in burning rate when combustibles are exhausted, entering the decay phase before the flame is finally extinguished.

The various characteristics of fire and materials are highlighted by these fire stages and can be identified as in Table 1.

Table 1. Parameters identified at each stage of the fire.

Stage	Parameters
Ignition	Ignitability: time to ignition (TTI), heat flux for ignition, temperature at ignition, etc. Flammability: behavior under ambient conditions after the removal of a flame (extinguishing of flame).
Developing fire	Flame spreading. Heat rate release (HRR). Total heat release (THR).
Fully developed fire	Heat penetration. Fire resistance. Heat release.

Most fire testing and fire science focus on specific protection objectives such as preventing sustained ignition, minimizing the contribution to fire spread, or acting as a fire barrier. Most well-established fire tests seek to recreate a specific realistic fire scenario and monitor a specific fire hazard or risk from a specific material inside that scenario [10]. The most significant tests for studying the flame

retardancy and thermal stability in polymeric materials are discussed in details in the Appendix.

1.3 Flame retardants

Flame retardant systems are designed to prevent polymers from burning or to slow down the combustion process. Various physical and chemical solutions have been developed to comply with fire safety requirements and reduce fire hazards. The importance of flame retardants (FRs) is highlighted in situations where polymers are likely to come into contact with an ignition source (such as in electrical and electronic applications) and where they can easily spread fire (like in residential and industrial buildings and transportation) [9]. Flame retardants affect the polymer combustion during a specific stage of this process: heating, decomposition, ignition, or flame spread. They are not singular events, but rather complicated processes, in which several distinct stages occur concurrently, with one stage dominating. There are different ways that physical action can slow down the polymer combustion [11]:

a. through the formation of a protective layer. The additives can provide under an external heat flux, a shield with a low thermal conductivity, which can decrease the amount of heat that is transferred from the heat source to the material. The polymer degradation rate is therefore slowed down, and the "fuel flow" (pyrolysis gases produced as a result of the material's degradation) decreases, making it harder for flammable molecules to fuel the flame.
b. By cooling. The energy balance of combustion can be influenced by the degradation reactions of the additives. The substrate can cool down as the additive degrades endothermally, which lowers the temperature needed to support combustion process.
c. By dilution. The fuel is diluted in the solid and gaseous phases by the addition of substances and additives that produce inert gases during decomposition, preventing the gas mixture from exceeding its lower ignition limit.

The majority of the chemical processes that interfere with combustion occur in the condensed and gas phases.

a. Condensed phase reaction. In this phase, two types of reactions are possible. The flame retardant can accelerate the breaking of the polymer by increasing the polymer flow, which leads to a separation from the flame that falls off. Second, the flame retardant can develop a coating of carbon on the polymer surface. This process, named “charring”, is the most common condensed-phase type of action [12]. It provides a barrier to heat and mass flow which prevents its transformation into flammable gases [13].
b. Gas phase reaction. The flame retardant or its degradation products interfere with the radical mechanism of the combustion process, which occurs in the gas phase. Thus, the exothermic flame processes are interrupted, the system cools down, and the supply of flammable gases is decreased until it is eventually totally suppressed.

Additive flame retardants are typically mineral fillers, hybrids, or organic compounds, which are incorporated into a polymer matrix during the transformation process. They do not react with the polymer at this point but only at higher temperatures, during the degradation of the polymers or at the beginning of a fire.

1.3.1 Halogenated flame retardants

Halogenated flame retardants are molecules that contain the elements from group VII of the periodic table (i.e., F, Cl, Br, and I), as suggested by their name. They can have a wide range of chemical structures, from aliphatic to aromatic carbon substrates that have been per-halogenated (all hydrogen atoms have been replaced with halogen counterparts), or they can be found in inorganic forms, however organo-halogen compounds are more efficient as flame retardant additives for polymers [14]. Due to their low cost of chemical synthesis and efficacy in a wide variety of polymers, brominated flame retardants are the most extensively used [15]. Through the continuous flow of free radicals produced, they stop polymer combustion in the gas phase. According to Equations (3) to (6) (where RX is a hydrocarbon halide), high energy OH and H radicals produced during combustion interact with free radicals released by the flame retardants.

$$RX \rightarrow R\cdot + X\cdot \quad (3)$$

$$X\cdot + R'H \rightarrow R'\cdot + HX \quad (4)$$

$$HX + H\cdot \rightarrow H_2 + X\cdot \quad (5)$$

$$HX + OH\cdot \rightarrow H_2O + X\cdot \quad (6)$$

The primary aspect affecting the effectiveness of halogenated FRs is the type of halogen involved. Halogenated bromine- and chlorine-based FRs present low bond energies of connection with carbon atoms in polymers. They can thus easily participate in the combustion process with the previously mentioned mechanism. In relation to polymer fire retardancy, more thermally stable forms like fluorine compounds are not common. Fluorine radicals are typically released at very high temperatures, far above the point at which most polymers begin to decompose. Due to their poor thermal stability, iodine-based compounds are therefore not very frequent in thermoplastic polymers. Indeed, they typically release halogen radicals in the temperature range where many polymers are processed. Due to their exceptional performance, five compounds based on brominated FRs are particularly used, namely: TBBPA (Tetrabromobisphenol A), HBCD (Hexabromocyclododecane), PBDE (Polybromodiphenylether), and TBPA (Tetrabromophthalic anhydride) [9] [16]. However, due to their intrinsic toxicity, the possibility that they could produce polybrominated dioxins and furans, and their severe effects on the environment, the use of some brominate flame retardants is limited. They also have the potential to produce large amounts of corrosive gases, which can have disastrous effects in confined spaces, as they corrode metal parts and damage sensitive electronics [7].

1.3.2 Hydroxides

By decreasing the overall amount of fuel, the rate of oxygen diffusion into the polymer bulk, and by improving the heat capacity, thermal conductivity, reflectivity, and emissivity, the incorporation of any non-combustible filler decreases the flammability of a polymer. Additionally, some inorganic materials exhibit endothermic decomposition with the production of inert gases or vapors, potentially increasing their fire-retardant properties. Their degradation must take place within a small window above the polymer processing temperature, but at or

below its decomposition temperature, in order to be successful. Group II or III carbonates or hydroxides are the most suited materials. In addition to the previously mentioned inert filler effects, they contain three additional fire-retardant properties. Indeed, they are able to thermally decompose by absorbing heat and consequently cooling the surrounding polymer. In addition, they can produce inert gases, such as water or carbon dioxide, capable of extinguishing the flame. Finally, they can lead to the accumulation of an inert layer on the degrading polymer surface. This layer acts as a shield for the incoming radiation and as a barrier to oxygen [17] [18]. Typical examples of this class of FRs include aluminum trihydrate (ATH) and magnesium hydroxide (MH). Polymer systems with adequate decomposition temperatures must be chosen based on their endothermic decomposition temperatures. When incorporated in polymers with higher processing temperatures, such as polyamides, endothermic degradation of ATH, which occurs between 180 and 220 °C, will result in a diminished flame retardant effect. The best option for these systems is MH (with an endothermic decomposition temperature > 300 °C). However, a well-known significant disadvantage of metal hydroxides is the high loading levels necessary (usually > 50 wt.%) for appropriate flame retardancy, which frequently causes processing challenges and loss in other crucial polymer properties [7].

A typical example of the use of ATH and MH refers to their incorporation in ethylene vinyl acetate (EVA) copolymer [19]. The characterization of composites filled with ATH at 50 and 60 wt.%, performed by Cross et al. [20], showed a substantial decrease in peak of heat rate release (pkHRR) from 1404 to 472 and 322 kW m^{-2}, respectively, while the same composites with MH reduced the pkHRR to 538 and 432 kW m^{-2}. The Limiting Index Oxygen (LOI) values were increased up to 32.2% with respect to 20.2% value of unfilled EVA. In this last case, the effect of ATH and MH fillers were, as expected, significantly better than the materials filled with the same amount of an “inert” filler like $CaCO_3$. In addition to their flammability, the mechanical properties of composites with inorganic filler are inevitably affected. Some mechanical properties of polymers may be negatively impacted by the large amount of filler addition, such as elongation at break and tensile strength [21]. As an example, Hobson et al. [22] demonstrated the fire retardant effect of EVA- magnesium hydroxide composites (MH loading from 50 to 55 wt.%) and studied their mechanical properties. The results show an increase in elastic modulus, from 17 to 76 MPa, accompanied by a significant decrease of elongation at break (from 722 to 167 %) and tensile strength (from 18.6 to 9.1 MPa). Furthermore, Camino et al. [23] reported the

mechanical behavior of EVA-based composites filled with 50 wt.% of MH and ATH: a substantial decrease in ultimate strength and elongation at break was reported compared to unfilled EVA. In this case, the elongation at break and tensile strength of the composites dropped by 66 and 65%, respectively, compared with unfilled EVA.

1.3.3 Phosphorous-based compounds

Phosphates, phosphonates, phosphinates, phosphine oxides, phosphates, and red phosphorus are only a few of the very numerous phosphorus-based flame retardant composites available. These phosphorated flame retardant substances are known to be active in the condensed and/or vapor phases and can be utilized as additives or introduced into the polymer chain during its production. The phosphorus-based flame retardants perform exceptionally well with oxygen-containing polymers (polyesters, polyamides, cellulose, etc.) in the condensed phase. Most of them cause thermal degradation, which produces phosphoric acid, which rapidly condenses and liberates water [24]. The oxidizing gas phase is diluted by the water emitted. Additionally, the dehydration reaction of the terminal alcohols can be catalyzed by phosphoric acid, resulting in the creation of carbocations and carbon-carbon double bonds. This may then cause the formation of crosslinked or carbonized structures at high temperatures. The char formation then occurs in combination with the carbonized residues and the phosphate anions. The polymer is thus protected from the flame by the carbonized layer (char), which also inhibits fuel volatilization and prevents the production of new free radicals, restricts oxygen diffusion (which decreases combustion) and insulates the polymer from heat. Additionally, phosphorus-based flame retardants have the ability to volatilize into the gas phase, where they can produce active radicals: $HPO_2\cdot$, $PO\cdot$, $PO_2\cdot$, and $HPO\cdot$, in decreasing order of significance. Phosphorous-based flame retardants perform remarkably better in polymers containing oxygen or nitrogen. Thus, it is important that the polymer chain contains these atoms. A strongly charring co-additive must be added in combination with the phosphorous-based flame retardant if the polymer is unable to contribute to charring due to a lack of appropriate reactive groups [4]. Among phosphorus-based flame retardants, a distinction should be noted between elemental red phosphorus, inorganic phosphates, numerous organic phosphorus products, and chlorophosphates.

Red phosphorus is the most abundant source of phosphorus for flame retardancy and it is very effective in such polymers as thermoplastic, polyesters or polyamides. One proposed mechanism of action is the reaction of red phosphorus with oxygen- or nitrogen- containing polymers that causes the char production [25] [26]. An additional mechanism involving depolymerization of red phosphorus into white phosphorus (P4) has been proposed. P4 can either diffuse from the bulk of the polymer to the burning surface, where it is oxidized to phosphoric acid derivatives that can possibly come into interaction with the flame and generate phosphoric acid, or it can volatilize at high temperatures and act in the gaseous phase. This phosphoric acid may behave as a catalyst for the formation of char, interrupting oxygen absorption and fuel volatilization [27] [28]. Red phosphorus, however, has a significant drawback. Due to its weak thermal stability, it can emit extremely toxic phosphine (PH3) during the melting process when it reacts with moisture. Interestingly, red phosphorus can be polymerically encapsulated previously to prevent phosphine formation, which can also increase its efficiency as a flame retardant [29].

Among the inorganic phosphates, the inorganic salt of polyphosphoric acid and ammonia is known as ammonium polyphosphate (APP). This polymeric molecule has a variable chain length (n), which can be higher than 1000. In comparison to longer-chain APPs, which have very low water solubility, short and linear chain APPs are more water sensitive and less thermally stable. At temperatures above 300 °C, long-chain APPs begin to break down into polyphosphoric acid and ammonia. Above 150 °C, short-chain APPs start to decompose. Therefore, it is crucial to choose a suitable APP in relation to the decomposition temperature of polymers. In general, the incorporation of APP causes char formation in such materials as polyesters [30] [31], polyamides [32] [33], and polyurethane [34] that contain oxygen and/or nitrogen. A phosphate that has been crosslinked and a polyphosphoric acid with a highly crosslinked structure are the results of the thermal decomposition of APP, which releases free acidic hydroxyl groups that condense by thermal dehydration. When incorporated into polymers containing oxygen or nitrogen, polyphosphoric acid catalyzes the dehydration process and the production of char. APP can affect the polymer degradation process in non-self-charring polymeric materials. Although many organ-phosphorus derivatives exhibit flame retardant properties, the nature of the polymer of destination and the processing temperature limit the number of commercially significant ones. Phosphate esters, phosphonates, and phosphinates are the principal categories of organophosphorus chemicals [35].

Feng et al. [36] prepared via melt blending EVA-based composites containing APP and a charring agent (CNCA-DA), finding the 3:1 ratio of APP to CNCA-DA to be optimal. Indeed, with this ratio, a LOI value greater than 27.0 % and a UL-94 V-0 classification was obtained with a charge amount starting from 20 wt.% of FR. Furthermore, the cone calorimetry results highlight a significantly overall decrease in HRR, THR and SPR parameters with addition of FR, which confirms that the FR system has an effective flame retardant and smoke suppressant effect. Specifically, the composite containing 25 wt.% of FR showed a decrease in pkHRR of up to 776 kW m^{-2} (62.6 % less than pure EVA), a THR of 131 MJ m^{-2} (163 MJ m-2 for pure EVA), and a decrease in SPR values from 0.077 of EVA to 0.043 m2 s^{-1}.

To increase the fire resistance of EVA, Bonnet et al. [37] studied a hybrid material based on EVA that contains silicon and phosphorus. The ethoxysilane groups from diethylphosphatoethoxysilane (SiP) and the acetoxy groups from EVA were exchanged to create the hybrid material. Cone calorimetry results indicated a synergistic effect between silicon and phosphorus on the thermal and fire properties. Indeed, for low amounts of filler (1.3 wt.% of silicon and 1.4 wt.% of phosphorus), a compact burned layer was developed and the pkHRR for EVA hybrid materials was found to be 35% lower than that of unfilled EVA.

1.3.4 Nitrogen-based compounds

The use of nitrogenous substances such as melamine, triazine, urea derivatives is currently growing. Among the nitrogen-containing chemicals, melamine (or its salts, such as melamine cyanurate, melamine phosphate, melamine pyrophosphate, and melamine polyphosphate) is the most widely used. Melamine can be combined with strong acids to generate thermally stable salts. Commercially available forms of melamine for various flame retardant uses include melamine itself, melamine cyanurate, melamine phosphate, melamine pyrophosphate, and melamine polyphosphate. Since there is phosphorus in the molecule, melamine phosphates also have positive features. Melamine is a thermally stable crystalline that sublimates at about 350 °C. Significant energy is absorbed during sublimation, lowering the temperature at the polymer surface. Melamine decomposes at high temperatures with the removal of ammonia,

leading to the dilution of oxygen and flammable gases and the creation of thermally stable condensates known as *melam*, *melem*, and *melon* [38]. This process prevents melamine volatilization and it is amplified if melamine volatilization is prevented, such as by trapping in the charred polymer. Melamine contributes to residue formation in the condensed phase, while ammonia dilutes the flame with incombustible gases. Melamine-based salts separate upon heating, and the newly produced melamine volatilizes similarly to pure melamine. However, compared to pure melamine, more of the melamine in melamine salts moves through progressive condensation, increasing the contribution of salts in the condensed-phase. If the anion is phosphorus-containing, the phosphoric acid that is generated will phosphorylate the polymer chains and have a similar flame-retardant effect to other common phosphorus-based additives [5].

Camino et al. [39] designed EVA systems containing a combination of melamine phosphate (MP) and phosphate-phosphonate substituted trimethylamine (I) which were able to increase the LOI values of EVA. The fire retardant effect for separate I and MP appears to stabilize (LOI = 23 %) above 13.6% for I and 22.7% for MP. Although their combination contributes additively to the growth of LOI of EVA up to LOI = 23 %, beyond this value there is evidence of synergistic action for compositions prepared with a weight ratio of I/MP in the range of 0.2 and 4.1, with a total FR loading of 20 - 30%. The maximum synergistic impact with higher loading was observed with an I/MP = 3:1 ratio.

In an interesting study, Luyt et al. [40] prepared six FR formulations mixing commercial N- and P- containing FRs and investigated their incorporation in different grades of LDPE and LLDPE, to evaluate their effects on thermal stability and fire-resistance. A FR formulation of a triazine derivative and APP (ratio of 1:3 and a total loading of 35 wt.%) was incorporated by melt blending in LDPE, reaching V-0 rating in UL-94 test and enhancing the thermal stability of the polymer (starting degradation temperature > 15 °C with respect to unfilled LDPE). Also in these cases, the mechanical properties of the polymers are subjected to significant modifications when the FRs were added. The values of tensile strength and elongation at break of LDPE decreased by 23-34%, while Young's modulus increased by 15 and 54%, depending on the FR used. In addition, the melt flow rate (MFR) values of the polymers decreased by more than 50 %, highlighting higher melt viscosity.

1.3.5 Intumescent systems

The original purpose of intumescent systems was to provide fire protection for fabrics, wood, and coatings. Intumescence is based on the development of an expanded carbonized layer on the polymer's surface when exposed to heat or fire. As an insulating barrier, this layer prevents heat transfer from the heat source to the polymer surface. Additionally, it limits the oxygen diffusion into the matrix as well as the transfer of fuel from the polymer to the flame. In general, three elements are needed to create an intumescent system:

- an acid source: an inorganic acid, acid salt, or another acid that promotes the dehydration of the carbonizing agent;
- a carbonizing agent: a carbohydrate that the acid dehydrates to form char;
- a blowing agent: a substance that decomposes and releases gas, which causes the polymer expansion and creates a swollen multicellular layer (melamine, guanidine, urea, chlorinated paraffins). To cause the growth of the carbonized layer, the gas must be released during the thermal degradation of the carbonizing agent. Table 1 lists some typical examples of the elements used in intumescent systems [41].

Table 2. List of typical elements used in intumescent systems [41]**.**

<table>
<tr><th>Acid source</th><th>Carbonization agent</th><th>Blowing agent</th></tr>
<tr><td>Acids: phosphoric, sulfuric, boric</td><td rowspan="3">Carbohydrates: starch, dextrins, sorbitol, pentaerythritol, mannitol, methylol melamine, phenol-formaldehyde resins</td><td rowspan="4">Urea, urea-formaldehyde resins, dicyandiamide, melamine</td></tr>
<tr><td>Ammonium salts: phosphates, polyphosphates, borates, polyborates, sulfates, halides</td></tr>
<tr><td>Amines-amides: urea with phosphoric acids, melamine phosphate</td><td rowspan="2">Char former polymers: PA-6, PA-6/clay nanocomposite, PU, PC, etc..</td></tr>
<tr><td>Organophosphorus</td></tr>
</table>

compounds: tricresyl phosphate, alkyl phosphates, haloalkyl phosphates	

Intumescent char production is a challenging process requiring rheology (char expansion phase and viscoelasticity), chemistry (charring), and thermo-physics (heat and mass transfer) conditions. Heat conductivity (heat transfer), viscosity (expansion), kinetic parameters (dynamic of decomposition), size and distribution of the cells (structure and morphology), and chemical composition are among the factors to be considered. The following sequences of events occur during the development of intumescence phenomena:

1. Inorganic acid is released at certain temperatures.
2. At slightly higher temperatures than that for the acid release, the acid esterifies the substances rich in carbon.
3. The mixture of substances melts either before or during esterification.
4. The ester decomposes by dehydration, leading to the formation of an inorganic carbon structure.
5. The carbonizing substance foams due to degradation products and gases generated from the aforementioned reactions.
6. As their reaction is almost over, gelation and then solidification take place, producing a multicellular foam as the final solid.

A common example is the system composed of polypropylene (PP), ammonium polyphosphate (APP), and pentaerythritol (PER) [42] [43] [44]. In the first stage (T < 280 °C), the reaction between the acidic species (APP and its decomposition products) and the char former agent (PER) results in the production of esters mixtures. The carbonization process occurs at about 280°C mostly via a free-radical process. In a subsequent step (between 280 °C and 350 °C), the blowing agent decomposes to produce gaseous products, with the subsequent char swelling. At around 430°C, the intumescent substance begins to degrade and loses its foamed characteristics. At the same time, between 280°C and 430°C the heat conductivity of char drops and the insulating capacity of the underlying material [45] [46]. In fact, the basic objective of an intumescent coating is to provide an insulating layer on the surface of the substrate to reduce heat transfer and/or diffusion. The thermal conductivity of intumescent chars is

extremely low if the char's structure is suitable, thus preventing heat transfer from the heat source to the substrate [47].

Le Bras et al. [48] investigated the combustion behavior of an EVA-based intumescent flame retardant system containing APP-PA6. The results of cone calorimetry showed a significantly different shape of the HRR curve of the composite compared with that of unfilled EVA (Figure 4). Indeed, intumescence development occurred up to 110 s with a sharp increase in HRR until a plateau was reached due to the formation of a stable intumescent protective layer. The flame retardant effect highlighted a remarkable decrease in pkHRR and an increase in TTI from 50 to 75 s.

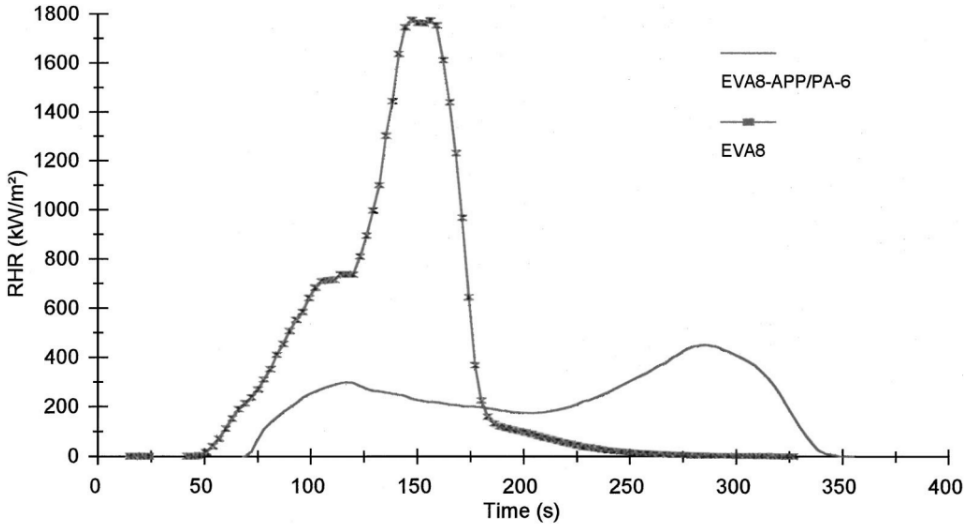

Figure 4. HRR vs time curves of EVA and its composite containing APP and PA-6. Reprinted with the permission from [48]**.**

1.3.6 Nanoparticles

Due to their exceptional behavior at the nanoscale, nanoparticles (NPs) have the potential to greatly modify a variety of properties of composites. The huge types of available NPs contribute to the significance of NP technology and applications. In comparison to micro particles, NPs have larger surface-to-volume ratios and surface energies, which promote stronger interactions with other NPs. The physical and chemical properties of composites are improved by NPs

incorporation depending on their dispersion and affinity to the matrix, as well as on the NP size [49]. When the NPs are well dispersed in polymer matrices, NPs have been shown to enhance the thermal, mechanical, and fire resistance. Additionally, they account for a significant reduction in the loading rate compared to micro-particles. More specifically, each form of NP contributes differently to flame retardancy depending on its chemical structure and geometry [50]. The geometry of NPs has, indeed, a significant impact on the flame retardant effect; NP can be classified by their geometry:

- layered particles with one nanometric dimension, such as nanoclays (i.e., montmorillonite), and referred to as 2D materials;
- fibrous particles with two nanometric dimensions (1D materials) and elongated structure, such as sepiolite and carbon nanotubes;
- particulate such as polyhedral oligosilsesquioxane (POSS) and spherical silica nanoparticles (0D materials).

The combination of polymer matrices and nano-additives plays a significant role in the effect of thermal stability and fire performance of polymer nanocomposites. For instance, in the case of clay, it is proposed a barrier mechanism [51] in the condensed phase during burning [52], schematized in Figure 5. Under pyrolysis conditions, the clay produces a char-like structure that performs as a thermal barrier, preventing further exposure of the polymer matrix to heat and oxygen; consequently, it prevents the mass transportation of the degradation products to the polymer's surface. By acting as a thermal barrier for the condensed phase, it can improve the thermal stability and fire resistance of the polymer.

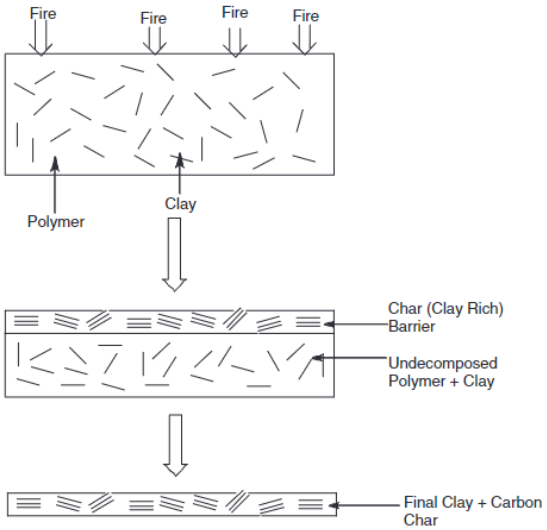

Figure 5. Mechanism of formation of the clay barrier during combustion of a polymer matrix composite. Reprinted with the permission from [53]**.**

According to research, clay can have a qualitative impact on polymer degradation [54]. The degradation process of the polymer matrix can be dramatically altered by the presence of clay, because this latter promotes the creation of oligomers rather than monomers [55]. The stability of the radicals formed during the thermal degradation of the matrix has a significant impact on how clay affects the thermal and fire resistance of polymer matrix: a stable polymer radical improves fire resistance more efficiently. The addition of clay promotes one degradation pathway rather than another when a polymer, like PS, degrades through multiple pathways. This often favors oligomers and causes the polymer matrix to degrade more slowly than the pure polymer. However, this is not the case for other polymers that degrade through only one pathway, such as PMMA; in these cases, the clay may not promote the formation of other degradation products. The way that clays improve the thermal and fire resistance of the polymer matrices can also be utilized to understand how CNTs and other nanoadditives work. The main method, through which nanoadditives improve the thermal and fire resistance of the matrix polymer is by forming a continuous carbon barrier on its surface. This barrier can significantly shield heat and oxygen from the polymer matrix, thus slowing down the burning process [56] [57].

Duquesne et al. [58] studied the fire performance of EVA-nanoclay systems at 3 to 10 wt.% filler loadings. The results showed a remarkable reduction in pkHRR

(from 28 to 47 %, depending on the loading) when clay was added to EVA due to the formation of a clay barrier on the surface of the material, which slows down the evolution of degradation products. The effect of decreasing pkHRR was most effective when the amount of clay incorporated increased, though low filler loadings were used.

1.3.7 Bio-based flame retardants

Due to their accessibility and growing awareness of the environmental challenges associated with the increased use of fossil fuels, innovative flame retardant solutions based on renewable resources are currently attracting considerable interest. In addition, the development of bio-based flame retardant systems is helpful in supporting the increasing use of bio-based polymers in various technical fields, while preserving their sustainability and positive environmental impact [59].

Biobased compounds typically refer to materials that can be obtained or derived from biomass, defined as the organic matter present on earth; it consists of microorganisms, animals, and plants. A review of the chemical composition of biomass provided the general classification of biomass into groups, subgroups, varieties, and species [60]. The following elements, listed in decreasing order of abundance, are the most prevalent: C, H, N, Ca, K, Si, Mg, Al, S, Fe, P, Cl, Na, Mn, and Ti, even though this composition greatly varies depending on the group [61].

This way, the "green" qualities of these materials can be combined with the existing requirement to provide wastes, by-products, and crops with more added value within the context of the circular economy . In the literature, there are numerous examples that demonstrate the effectiveness of using biomacromolecules or bio-sourced compounds as low environmental impact flame retardants (FRs) [62] [63] [64] [65]. These examples include tannins, phytic acid, banana pseudostem sap, lignin, to name just a few. In fact, the chemical nature of these biomacromolecules and bio-sourced products includes phosphorus, nitrogen, and/or sulfur, which are typically needed to create efficient flame retardants [66]. As example, Alongi et al [67] investigated the flame retardant effect of deoxyribonucleic acid (DNA) for EVA copolymer. For this purpose, specimens both adding the DNA in bulk by melt blending and as a surface coating

were prepared via hot compression. These systems provided a fire retardant effect to the polymer, reducing the peak of HRR (-36 and -77% for bulk and coated specimens, respectively) and increasing the TTI by 228 s (+380 %) for coated specimen, demonstrating the efficiency of DNA as a char former and thermal shield for EVA.

In terms of sustainability, biochar (BC), "the solid product obtained by the thermo-chemical conversion of wastes/biomasses in an oxygen-limited environment", is a renewable/bio-sourced material that has been extensively used in environmental management and agriculture. Due to its remarkably stable honeycomb carbonaceous structure [68] [69], it has also been used as a low-cost carbon sequester [70] [71], a natural adsorbent, soil remediation and amendment product. All these features point out the potential for employing biochar as a filler in polymer composites with improved thermal and flame retardant properties [72] or as a component of flame retardant coatings for fabrics [73], thus expanding its range of potential applications [74]. This topic will be discussed in detail in the next chapter.

Chapter 2

Biochar

2.1 Introduction

Biochar is defined as the solid product obtained from the thermochemical conversion of biomass in an oxygen-limited environment. Numerous organic wastes, including agricultural waste and municipal solid waste, can be utilized as feedstock to produce biochar. However, due to their physical, chemical and biological characteristics, biochar is an adaptable material that can be used in a wide range of applications. It is generally considered a soil modifier, which can capture carbon and improve soil health by retaining nutrients and water. In addition, its high potential exploitability in various sectors, including construction, wastewater treatment, water purification, CO_2 capture, power generation, energy storage, and soil improvement to increase soil fertility and carbon sequestration, has been explored in recent decades [75] [76] [77] [78] [79] [80]. For these reasons, biochar has gained a great attention from both industry and academia [81]. Indeed, the number of publications using the term "biochar" in the topic has been gradually increased, demonstrating a growing interest in biochar research within the scientific community (Figure 6), expanding to multidisciplinary areas for scientific research and engineering applications.

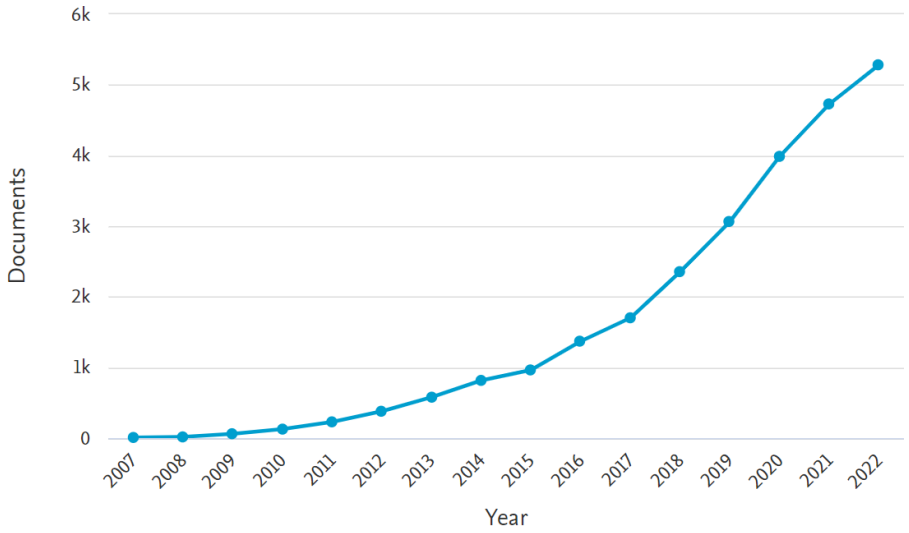

Figure 6. Documents by year containing the word "biochar" between 2007 and 2022 [data from scopus.com].

2.2 Synthesis methods

The biochar production involves a wide variety of raw materials, including woody materials, solid waste, food waste, and animal feed [82]. Several processes, including pyrolysis, gasification, torrefaction, and hydrothermal carbonization, are employed to produce BC. The main techniques mentioned are discussed in the following sections.

2.2.1 Pyrolysis

Pyrolysis is a process for thermal decomposition organic substances in an oxygen-limited atmosphere between 400 and 900 °C [83]. The purpose of pyrolysis is to maximize the production of high-value products from biomass conversion. The three components of biomass (i.e., cellulose, hemicellulose, and lignin) follow separate reaction pathways during thermal decomposition, including cross-linking, depolymerization, and fragmentation. For generic biomass, the main decomposition processes take place between 200 and 500 °C [84] [85] [86] and proceed according to four steps: partial hemicellulose decomposition, entire hemicellulose decomposition to partial cellulose decomposition, entire cellulose and partial lignin decomposition, and successive

decomposition and increasing degree of carbonization [87] [88]. This process results in a formation of different products, comprising solid, liquid, and gaseous compounds. The first two products are known as biochar and bio-oil, respectively, while the gas is a mixture that contains CO, CO_2, H_2, and C1-C2 hydrocarbons. The types of raw biomass sources and the specific pyrolysis treatments determine the yields of the pyrolysis products. The reaction temperature, heating rate, and residence time are factors that affect the end products of pyrolysis operations. Usually, when the pyrolysis temperature rises, the amount of biochar decreases and the yield of syngas increases [89] [90] [91]. Depending on the heating rate and vapour residence time, pyrolysis processes are classified as slow pyrolysis, fast pyrolysis and flash pyrolysis.

Slow pyrolysis is performed with a slow heating rate, low temperature, and extended residence time. As an example, wood will provide 30-35% biochar, 45-50% bio-oil, and 20-25% gas when subjected to slow pyrolysis with a low heating rate at temperatures between 400 and 500 °C [92]. The results of numerous research findings show that as the pyrolytic temperature rises, the carbon content also tends to increase. On the other hand, when the pyrolytic temperature increases, the concentration of nitrogen, hydrogen, and oxygen decreased [93] [94]. However, it was found that the distribution of nitrogen in biochar varied among different biomasses but was mostly unaffected by the temperature of biochar formation [95] [96].

Fast pyrolysis usually aims to yield a large amount of liquid product [97]. The vapor residence time is kept short and quick cooling is used to increase the yield of the liquid product, while the gas production caused by secondary cracking is minimized [83] occurring at a high heating rate, with quick residence time. The principal yield of fast pyrolysis is bio-oil, which ranges from 50 to 80% on a dry basis and is produced by the condensation of condensable gases [98].

Flash pyrolysis is a potential method to convert biomass into solid, liquid, and gaseous fuels obtaining a yield of bio-oil up to 75%. Specifically, depending on the feedstock employed, this method yields 15–25 wt.% of biochar, 60–75 wt.% of bio-oil, and 10–20 wt.% of non-condensable gases [99]. The specific conditions required for this process include: inert environment, rapid heating, high reaction temperatures (up to1000 °C), and a short gas residence time (less than 1 s) [100]. The main parameters that differentiate the various pyrolysis processes are listed in Table 3.

Table 3. Values of the key operating parameters for different pyrolysis processes [101]**.**

Pyrolysis technology	Solid residence time (s)	Heating rate (°C s^{-1})	Temperature (°C)
Slow	450 – 550	0.1 – 1	400 – 675
Fast	1 – 10	10 – 200	575 – 975
Flash	<1	>1000	775 – 1000

The choice of a reactor for a specific pyrolysis process is a key operation. As pyrolysis technology development continues, several reactor designs have been explored to improve pyrolysis performance and produce high-quality products. Each reactor type has unique features, yielding capacities, benefits, and drawbacks [92].

Among the various types of reactors, fluidized-bed reactors are suitable for fast pyrolysis. A pressurized fluid is flowed through solid particulate matter to create a fluid-solid mixture with fluid-like characteristics. Therefore, the system provides a fast heat transmission, controlled pyrolysis reaction and gas residence time, high surface area of contact fluid-solid, and good heat/mass transfer, which causes the feedstock particles to heat up quickly [102]. An example of this system is presented in Figure 7.

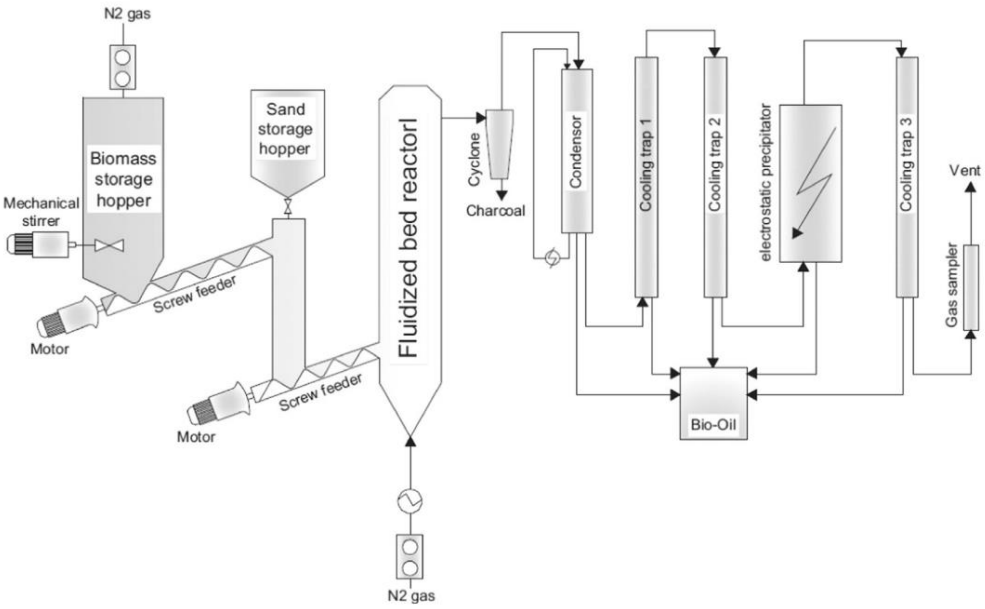

Figure 7. Schematization of a fluidized-bed reactor system. Reprinted with the permission from [103]**.**

If biochar generation is the goal, fixed-bed reactors are typically used for slow pyrolysis. A carrier gas enters the reactor and passes through the bed to flow out the condensable and non-condensable gases to the condensers. Due to its simple design, the fixed bed reactor is typically employed at the laboratory or bench size [104], as shown in Figure 8.

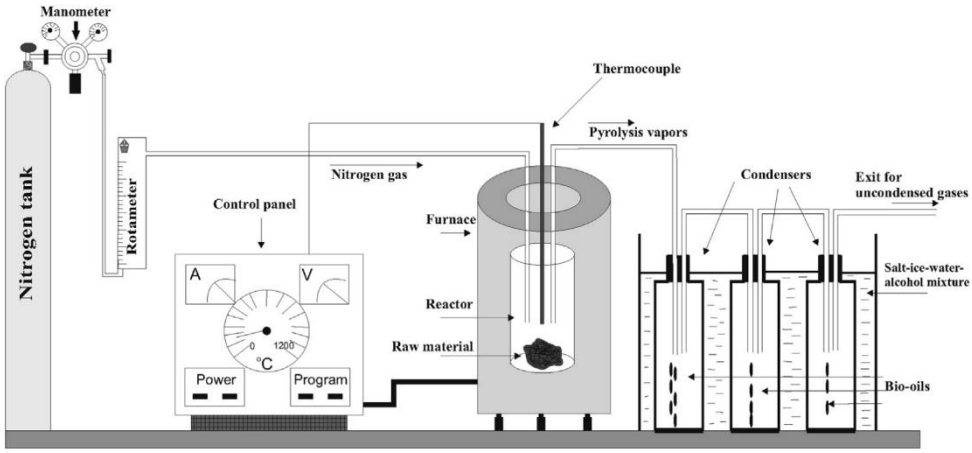

Figure 8. Scheme of a fixed-bed reactor system. Reprinted with the permission from [105]**.**

Finally, a wide variety of reactors are used in the pyrolysis process, the most common include plasma pyrolysis reactors, ablative reactors, vacuum pyrolysis reactors, rotating cone reactors [92] [104].

2.2.2 Gasification

Gasification is a thermochemical partial oxidation process that produces gaseous products from carbonaceous sources including biomass, coal, and polymers. Gasification agents such as air, steam, oxygen, CO_2 or gas mixture) are used for this process. Gaseous products (H_2, CO, CO_2, N_2, etc.), liquid products (tar and oil), and solid products (char and ash) are all produced during the gasification process. The production of biochar is only about 5-10% of the amount of the initial biomass because gasification is intended to produce gaseous products [106] [107]. The mechanism of gasification can be divided into four stages, although the differences in temperature and pressure between one phase and another make it difficult to distinguish them clearly: drying, pyrolysis, oxidation/combustion, and gasification. Drying is necessary to remove biomass moisture when its content is too high. Pyrolysis occurs at temperatures around 400 °C, decomposing the thermally weak components of biomass and generating char, gases, and liquids. During the pyrolysis process, gases such as H_2, CO, CO_2, H_2O, and small molecular mass hydrocarbons like CH_4 are produced. Most of the liquid result is tar made of low molecular weight organic material. The reaction temperature, pressure, and heat rate conditions affect the composition of the products. The energy needed for gasification reactions is mostly derived from the oxidation and combustion of certain gas species as well as char. The gasification agent introduced into the gasifier reacts with combustible species, generating CO, CO_2, and H_2O, as well as the char created during the pyrolysis process. Through several gasification processes, the char formed during the pyrolysis stage is converted into CO, CH_4, and H_2. The factors that affect gasification are the processes temperature, gasification agent type, agent-biomass ratio, and pressure involved [83].

2.2.3 Hydrothermal carbonization

When the moisture content in a biomass is low, techniques like pyrolysis and gasification can give significant product yields with little energy waste. However, most biomass materials have significant moisture contents: therefore, a separate drying phase is necessary to produce high product yields and consume less energy during the process. Hydrothermal procedures are able to overcome this issue. In fact, water and biomass are mixed in a closed reactor and the temperature is increased to stabilize the process. Additionally, increased pressure is required to keep water in a liquid state over 100 °C. The primary byproducts of a hydrothermal method vary according to the employed temperature and include biochar [108] [109], bio-oil, and gaseous products (CO, CO_2, CH_4, and H_2 [110], respectively for processes below 250 °C, between 250-400 °C, and above 400 °C. The reaction temperature, pressure, residence time, and water content of the biomass are the primary factors controlling the properties of the products [111] [112]. Finally, the char produced by the hydrothermal carbonization method has a greater carbon content than the char produced by dry techniques [83] [113].

2.2.4 Torrefaction

Torrefaction is a thermal process that involves low temperatures and can be used to convert biomasses for energy purpose [114] . Long residence and processing times at temperatures between 200 and 350 °C induce the biomass to release both moisture and carbon dioxide. As a result, high yields of solid products with a lower O/C ratio are obtained [115] [116].

2.3 Properties

2.3.1 Density and porosity

Through the processes of pyrolysis and carbonization, biomass is converted into carbon-rich microporous materials with a highly developed porous structure [117]. The characteristics of the raw materials and carbonization techniques employed in this process are related to the properties of biochar [118]. The composition, inclusions, and cellulose and lignin content of the various biomasses

affect how the structure of the resulting BCs. The carbonization temperature has a significant impact on the structure of the biochar as well. It is commonly accepted that the biochar aromatic carbon structure and nanopore size both increase as the carbonization temperature rises. However, some microporous structures on the surface of biochar may be broken at temperatures above 700 °C, and the carbon skeleton structure of biochar will become unstable at temperatures above 800 °C [119]. Consequently, the BC bulk density decreases with treatment temperature. Indeed, during the pyrolysis process, a porous char is left behind as the gases devolatilize from the biomass structure [120].

2.3.2 Elemental composition

Biochar typically contains the following elements: C, H, O, N, S, P, K, Ca, Mg, Na, and Si. Among these, C has the highest content (usually above 60%), followed by H, O and N, while other elements are typically found in ashes [121]. Aromatic carbon, which is deposited in an irregular structure of stable aromatic rings, composes most of the carbon in biochar [117]. The accessible nitrogen content of biochar is quite low because most of the nitrogen is concentrated on the surface in a C-N heterocyclic structure [122]. Biochar has a considerably low P content. The P availability varies significantly, and the carbonization temperature has a negative correlation with it. The high pH of BC and phosphates with Ca and Mg created during carbonization may affect this variation [123] [124]. The concentrations of K, Ca, Mg, and Na vary depending on the kind of biochar, with livestock manure biochar having the greatest contents, followed by herbaceous and woody plant biochar. In biochar, low valence metal ions, like K and Na, are more readily available than high valence metal ions, such as Al, Ca, and Mg. Generally, raw materials, carbonization conditions and pH influence the elemental composition and activity of biochar [123] [125].

2.3.3 Specific surface area

The specific surface area of biochar varies from 1.5 to 500 m^2 g^{-1} [126] [127] and increases as the pyrolysis temperature increases in a specific range [128]. At low temperatures, the inner pore structure of biochar is filled with volatiles, tars, and other products derived from the thermal degradation of biomass, which

reduces the specific surface area. These compounds decompose and release volatile gases as the temperature rises, which causes the reduction of the pores in the biochar but an increase in their number, leading to more microporous structures and larger specific surface areas [129]. As the temperature rises, a plateau is reached in the specific surface area of the biochar. The specific surface area decreases with rising temperature when the temperature surpasses the critical value, most likely because of the collapse of the microporous structure and the expansion of the micropores [130].

For some applications, knowing the total surface area alone may not be sufficient. For instance, although having a huge surface area, some gases may not be able to easily access the biochar small pores, which would restrict the biochar capacity to adsorb a particular gas. Similarly, an abundance of pores in the order of nanometers has no effect on water accessible to plants, because they cannot overcome the capillary forces that keep water in these small pores [131].

2.3.4 Surface functional groups

Numerous functional groups, including carboxyl, carbonyl, and hydroxyl groups, are present in biochar. Many of these functional groups are either oxygen-containing or alkaline, giving biochar good hydrophilic or hydrophobic properties, and ion exchange capacity [132]. The amount of functional groups on the surface of biochar is directly correlated with the carbonization temperature. The C-O, C-H, and O-H bond amounts in biochar decrease as the carbonization temperature rises, along with the number of oxygen-containing functional groups like hydroxyl and carboxyl, as well as acid and acid-containing functional groups, while the number of alkaline functional groups increases. Overall, as the carbonization temperature rises, the density and quantity of functional groups decrease [133] [134].

2.3.5 Thermal conductivity and heat capacity

Due to the high degree of anisotropy in biomass, the thermal conductivity varies significantly depending on the direction of heat flow, reaching its maximum value when it is parallel to the direction of the grain. A higher density

is also typically correlated with a higher thermal conductivity. Therefore, the heat conductivity of biochars relative to their biomass decreases because of the development of a porous structure. The conductivities measured in various directions begin to converge with rising pyrolysis temperature, as a result of the degradation of biomass fibers and loss in morphology during carbonization. When char is produced at a very high temperature, the porosity may be reduced, increasing the density as a result (compared to chars produced at lower temperatures). In this range of temperatures, the thermal conductivity can rise once again. The results of thermal conductivity and heat capacity measurements are affected by the temperature, at which they are taken [120].

2.4 Biochar-polymer composites

The development of waste-derived materials that are also renewable is being pushed due to rising levels of pollution, greenhouse emissions, and trash production. These materials are intended to be designed in a way that simultaneously promotes the idea of sustainability and has acceptable performance characteristics (mechanical, chemical, thermal, etc.). It is essential that these materials have similar properties that could eventually replace those generated from synthetic or inorganic sources. On the other hand, the best is to prepare numerous application paths for a single material to assure its flexibility. The design of these novel, eco-friendly, and renewable materials needs to be planned so that they may adapt to various raw materials, be applicable to different production processes, and be flexible enough to meet a variety of market demands [135].

In this context, BC-polymer composites still need to be optimized to achieve performance equivalent to those observed for conventional carbon-based fillers like graphene and carbon nanotubes. Indeed, these materials can be employed to achieve excellent composite performances, but they are very expensive. Compared to a low-cost carbon filler like carbon black, BC is less expensive and is obtained from biomass. The recent years have seen a sharp increase in the number of studies looking at the formulation of BC-containing polymeric systems using either thermoplastic or thermosetting matrices. When compared to conventional carbonaceous fillers suitable for improving the mechanical, electrical, thermal, and fire-retardant properties of polymer-based composites, BC

represents an appealing option because of its interesting properties and the tailorability of its structure and functionalization [136].

2.4.1 State of the art

One of the first studies on polymeric composites containing BC obtained from organic matter through pyrolysis was carried out by Das et al. [137]. Different formulations were prepared mixing pine wood waste (30 wt.%) and the BC from the same wood (from 6 to 30 wt.%) used as filler in polypropylene-based composites. The mechanical characterization on these materials showed that the specimens containing 24 wt.% of BC maintain a similar tensile strength but present a higher flexural strength than traditional wood/polymer specimens, combined with a reduction in ductility. In addition, the thermal stability achieved the highest values when 18 wt.% of BC was added in polymer/wood composites. The same research group further proved the possibility to predict the hardness and elastic moduli of PP-BC wood composites using the nanoindentation technique. They applied theoretical model using the nanoindentation properties of particles, demonstrating a concordance between calculated values and experimental results. The increased hardness is due to the porosity of the biochar, which allows the molten polymer to infiltrate the pores during processing [138]. Further studies have demonstrated this theory, which is fundamental to the preparation of composite materials with superior mechanical properties [139] [140]. Paleri et al. [141] showed the effect of pyrolysis and torrefaction conditions, especially the temperatures involved, on the resulting BCs. Specifically, a co-product from corn ethanol industry was heat-treated for producing BCs at different temperatures (up to 1000°C) and used as a filler for PP based composites. The BC processed at 700 °C presented the best performance in terms of stiffness-toughness balance, due to its low polarity, with respect to lower temperatures treatments, and lower ash content and particle size compared to those treated at 1000 °C. This study highlights the importance to comprehend and optimize the heat treatment temperature for the BC production utilized as a filler in polymer composites depending on the particular characteristics to be achieved. Furthermore, the effect of pyrolysis temperature on crystallization behavior and thermal stability of BC/PP composites was studied [142]. It was demonstrated that the BC particles enhanced both the overall rate of crystallization process of the composites, acting as nucleating agents, as well as the thermal stability, due to the delay in onset temperature caused by the barrier effect of the BC particles. In details, the thermal

stability of PP/BC specimens was improved when both the pyrolysis temperature of BC used and its loading increased (Figure 9).

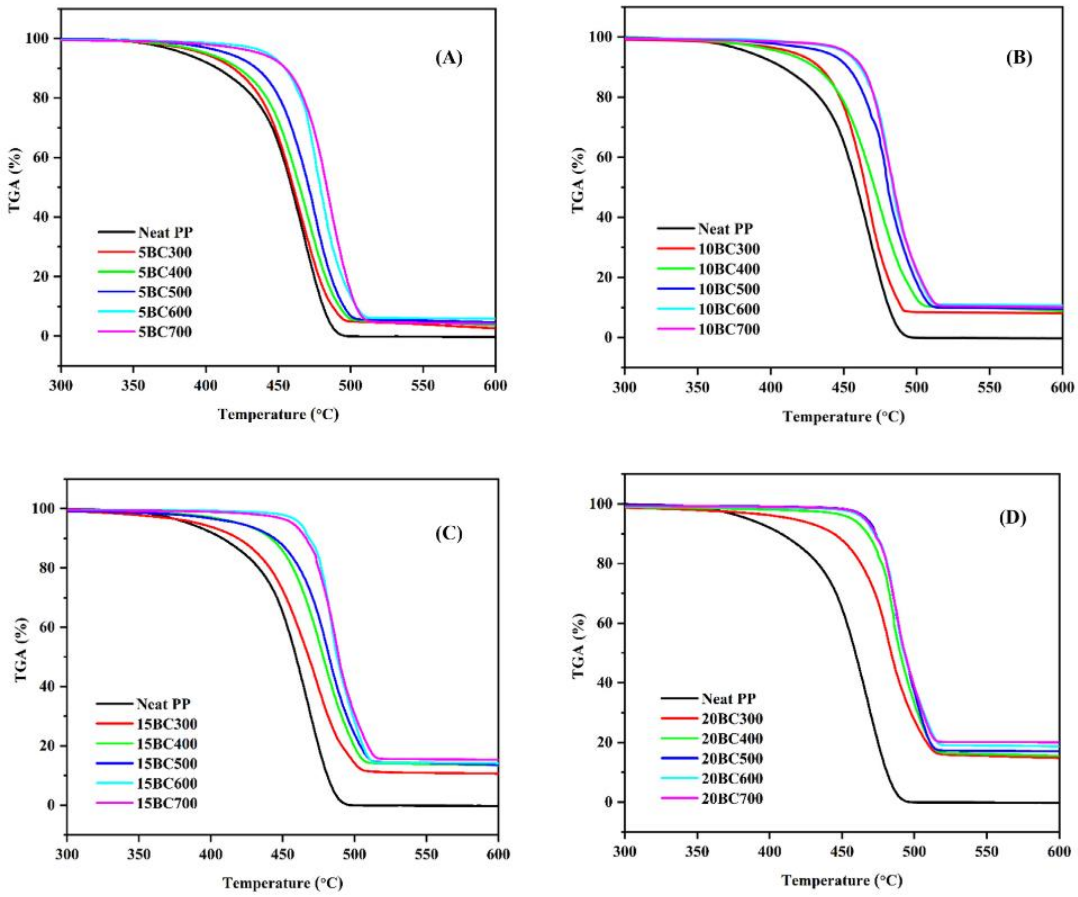

Figure 9. TGA curves of BC/PP composites at (A) 5%, (B) 10%, (C) 15% and (D) 20% loading of BCs treated from 300 to 700 °C. Reprinted with the permission from [142].

Polyethylene (PE) is the other extensively studied polyolefin for the preparation of BC composites. Among all types of PE, High Density Polyethylene (HDPE) and Ultra High Molecular Weight Polyethylene (UHMWPE) are the most common employed as a matrix for BC composites. Zhang et al. [143] prepared HDPE-based composites containing biochar ranging from 10 to 70 wt.% derived from rice husk as a feedstock. They demonstrate an improvement in flexural and tensile properties, in storage modulus, elasticity, creep resistance and anti-stress

relaxation ability of HDPE. Specifically, excellent mechanical properties were achieved for specimens containing 40 and 50 wt.% of BC due to the good dispersion of the particles and the structure shown in the interface. In addition, BC caused an improvement of thermal properties in BC/PP composites, as witnessed by the residues produced by TGA, and in flame retardant properties, due to the higher LOI values.

In a recent work, Zhang et al. [144] studied the effect of different pyrolysis temperature (up to 900 °C) on the properties of HDPE/BC composites. The highest tensile strength (26.25 MPa) and Young's modulus (1.87 GPa) were observed in composites containing BC produced at 500 and 600 °C, due to their good physical/mechanical interlocking structures shown in SEM. Indeed, the increment of pyrolysis temperatures led to a decrease of the number of polar functional groups located on BC surface, increasing the BC-HDPE compatibility. Furthermore, the thermal tests revealed an earlier crystallization temperature and an improvement of the thermal stability of HDPE.

The interactions between BC derived from waste coffee grounds and HDPE matrix were further investigated by Arrigo et al. [145] through rheological measurements. The restriction of the polymer chains onto the particles surface and/or within the BC porous structure caused the slowing down of the dynamics of PE macromolecules in composite materials. Additionally, by significantly raising the temperatures, at which PE decomposes, the BC particles were able to enhance the thermo-oxidative stability of composites.

From an overall point of view, UHMWPE/BC composites were designed for obtaining materials with a combination of high mechanical properties and high electrical conductivity [146] [147]. In this context, Li et al. [148] prepared UHMWPE based composites containing 3 different kinds of BCs (from pine, apple, and bamboo) via extrusion and hot-compression techniques. Due to the good dispersion of particles into the matrix and strong interfacial interactions assessed by SEM, the tensile strength increased up to 325 %, compared to unfilled UHMWPE. In addition, the composites containing 70 wt. % of BC showed good electrical conductivity, because of the formation of a conductive network by the BC particles. Then, it was also demonstrated the possibility of obtaining a segregated conductive network with a low BC amount. Indeed, the BC is distributed along specific paths and not incorporated in a uniform dispersion. This way, it was possible to achieve a high conductivity for composites: in particular,

1.1 x 10^{-2} S/cm was obtained for composites containing 7 vol% of BC from nano-bamboo, which is acceptable for many electrical applications [149].

The use of BC was also studied in polyamide matrices as a filler for increasing the strength and the elastic modulus but noticeably reducing ductility and toughness of the BC-polymer composites [150] [151]. As an example, Ogunsona et al. [152] prepared polyamide 6,10 (PA6.10)-based composites filled with a 20 wt. % of BC from miscanthus fibers. The reinforcing effects of BC of different particle size (i.e., crushed, <500, 500-426, 250-213, and <63mm) were studied. In details, a good interaction between BC and matrix was observed and resulting in considerable interfacial bonding. The impact strength increased with decreasing the particle size, while the tensile and flexural strengths were maximum enhanced with milled and unfractionated BC. From an overall point of view, the composites showed mechanical properties that were equal to or even better than those of the unfilled PA 6,10.

Aiming at improving the mechanical properties, BC was incorporated in PLA matrix [153] [154]. Arrigo et al. [155] reported the preparation of bio-composites by two different techniques (namely, melt mixing and solvent casting) containing BC from exhaust coffee grounds. The values of tensile modulus of the systems increase with increasing the BC amount due to the good dispersion of the particles into the polymer matrix. In addition, a decreased thermal stability was observed during thermogravimetric analyses as compared to unfilled PLA. Indeed, the catalytic effect of BC particles on the PLA degradation of PLA was suggested and reported also by other authors [156] [157].

Epoxy resins are one of the most researched thermosetting hosts because to their extensive variety of uses in numerous critical industrial processes, from the automotive to the aeronautical sectors [158]. These applications mainly focus on materials that have been reinforced with carbon, glass fibers, and CNTs [159] [160]. The use of BC as a filler in epoxy resins emerges as a low-cost alternative to improve specific properties of the matrix. As an example, Khan et al. [161] compared the mechanical properties of composites filled at 2 and 4 wt. % of CNTs and BC, showing an improvement in ultimate tensile strength and strain at break for BC composites. Similar works reported analogous results of reinforcement of the epoxy matrix by BC incorporation [162] [163] [164].

Other types of polymer matrices were employed for BC composites as example: polyvinyl alcohol (PVA) [165] [166] [167], unsaturated polyester resins [168] [169] [170], and polycarbonates (PC) [171] [172].

Only three additional works studied ethylene vinyl acetate copolymer (EVA) containing BC particles, not considering the publications of the PhD candidate. A first work [173] investigated PP/EVA composites filled with BC from pyrolysis of empty fruit bunches, varying the particles amount from 10 to 40 wt. %. The BC addition was beneficial for thermal stability and slightly increased the impact resistance of composites. In another work [174], EVA was filled with 50 wt. % of BC derived from recycled cotton fibres, obtaining composites that were characterized and compared with other composites with different matrices (namely TPU, ABS, PLA). The EVA/BC composites obtained the maximum elongation due to their softness and flexibility, with respect to the other composites. Finally, a last work [175] studied the properties of EVA based composites containing different amount (ranging from 5 to 40 wt. %) of BC from hemp fibers. DSC analyses showed that the presence of BC did not affect the thermal behavior of EVA (no remarkable changes in T_m, T_c and T_g); conversely, as assessed by TGA, an enhancement of the thermo-oxidative stability was observed, which increased with the BC loading. Furthermore, the composites showed higher stiffness and lower ductility than neat EVA (Figure 10), combined with a higher thermal conductivity and microwave electrical conductivity when a high concentration of BC was employed.

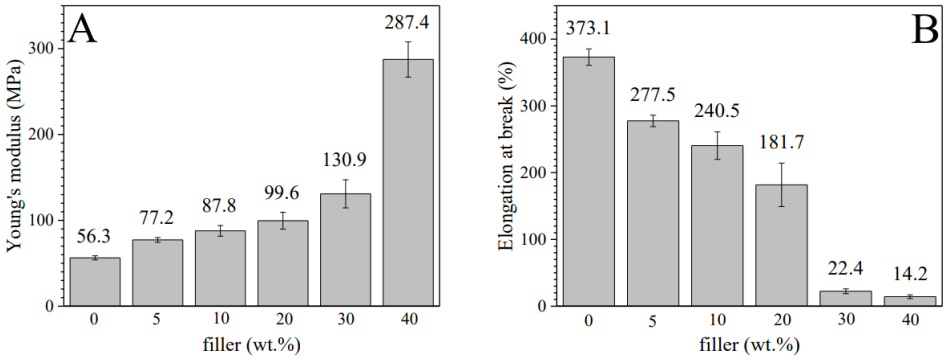

Figure 10. Tensile mechanical behavior of EVA/BC composites: (A) Young's modulus (MPa) and (B) elongation at break (%). Reprinted with the permission from [175].

2.4.2 Flame retardant systems containing BC

The first works on the use of biochar as a flame retardant in thermoplastic polymers were published in 2016. As an example, Das et al. [176] prepared polypropylene-BC composites using melt compounding and injection molding at different filler loadings, namely 15, 25, 30 and 35 wt.%. The pine wood feedstock used to produce the biochar was pyrolyzed at 500 °C and then activated at 900 °C. Cone calorimetry measurements revealed an interesting result: the carbon filler significantly reduced the peak heat release rate (from 1054 kW m^{-2} for the unfilled polymer to 477 kW m^{-2} for the 35 wt.% biochar-loaded composites). Additionally, thermogravimetric analyses revealed that neat PP started the degradation earlier (at 280 °C) with respect to composites and no residue was observed after the test. This result was more enhanced in samples that contained more biochar, indicating a better thermal stability of the BC-composites.

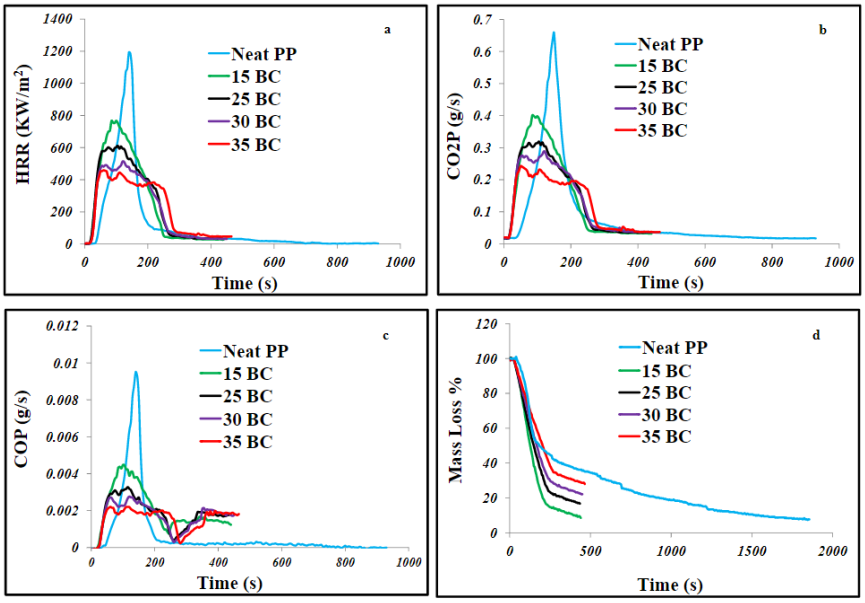

Figure 11. Cone calorimetry results of PP and its composites containing BC derived from pine wood. Reprinted with the permission from [176].

Ikram et al. [140] extended the results of this research to demonstrate the effectiveness of this carbon filler in PP. As determined by thermogravimetric analyses, the composites containing 36 wt.% of biochar showed improved thermal stability. Additionally, forced combustion tests revealed a significant decrease in the peak of heat release rate (by nearly 50% compared to unfilled PP),

demonstrating the flame retardancy provided by the filler. This result was attributed to the char layer formed on the surface of the composites after exposure to the heat flux. Indeed, this layer acted as a barrier, delaying the transmission of heat, oxygen, and flammable volatiles between the polymer and the radiant heat source. Following up on this study, Das et al. [177] demonstrated that when wool and biochar were combined with PP and an intumescent flame retardant (i.e., ammonium polyphosphate at 20 wt. % loading), synergistic benefits were achieved. The prepared composites exhibited improved flame-retardant properties as evidenced by the rise in limiting oxygen values from 18% for PP to 23% for the composite containing 25 wt.% of biochar and 10 wt.% of wool fibers, associated with a decrease in peak of HRR values, from 1054 to 318 kW m^{-2}. In another study [178], the same pine wood, used as a feedstock for BC, was added to BC-PP composites. The resulting formulations had similar FRs loadings but varied in terms biochar and wood composition. In details, the amount of wood and biochar was fixed at 34 wt.% (10, 20 or 30 wt. % of BC), with the polymer amount remaining constant at 42 wt.% and 4 wt.% of maleic anhydride grafted PP was incorporated as a compatibilizer. All the composites containing APP, regardless of their composition, showed peak of HRR values 60-65% lower than PP, as determined by cone calorimetry carried out at 50 kW m^{-2} irradiative heat flux. In addition, increasing the amount of biochar and decreasing the amount of wood in the composite formulation accounted for the lowest peak HRR (i.e., 376 kW m^{-2}). A similar behavior was observed for the composites containing magnesium hydroxide, although the fire performance was slightly worse than APP-containing composites due to the different flame retardant mechanisms. In fact, APP acts mainly through char formation and intumescence, while $Mg(OH)_2$ by flame dilution. However, the thermally stable biochar helped to produce a protective char layer that was able to prevent oxygen from reaching the burning polymer and volatile flammable gases derived from PP degradation from being released into the atmosphere. Finally, the presence of the FR particles, which are supposed to reduce the efficacy of the polymer's infiltration into the biochar pore due to their trapping inside the filler pores, did not significantly alter the mechanical behavior of the produced composites.

A variety of HDPE/biochar/wood flour composites was also designed by Zhang et al. [179] utilizing biochar produced by the pyrolysis of corn stalks at 500 °C. In particular, the polymer content was held at 40 wt.%, while the percentages of biochar and wood flour varied from 10 to 60 wt.%, keeping the overall filler loading at 60 wt.%. Additionally, $Mg(OH)_2$ or $Al(OH)_3$ fillers were added to the

composite, which contained high-density polyethylene, biochar, and wood flour at weight ratios of 40/30/30, respectively. According to limiting oxygen index measurements, the presence of $Mg(OH)_2$ at 40 wt. % provided the best flame retardant effects. In fact, this composition reached an LOI as high as 31.9 %, which is a substantial increase compared to the composite without flame retardant (equivalent to 23.9%). In another work, a series of HDPE/BC composites were developed by Zhang et al. [143] using rice husk as a feedstock to prepare BC at 600 °C. The BC loadings ranged from 10 to 70 wt.%. Although the tensile modulus increased with its content (up to 60 wt.% loading of BC), the filler was also capable of improving the flame retardancy of the polymer, as evidenced by the increased limiting oxygen index values (from 18.2 for the unfilled polymer matrix to 25.1% for the composite containing 70 weight percent of BC). Then, Barbalini et al. [73] reported on the use of BC as a component of a flame retardant treatment for cotton fabrics. They combined this carbon filler (made from used coffee grounds dried at 105 °C and then heated in a quartz reactor to 800 °C in argon) with phytic acid, a molecule containing six phosphate groups, extracted from many plant tissues, including the soy bean, grain, and oil seed. Aqueous dispersion of the two components was used to treat the cellulosic fabrics, maintaining a 1:1 weight ratio while obtaining a final dry add-on from 4 to 10 wt.%. As a point of comparison, the fabrics were also treated with single ingredients (final dry add-on achieved: 8%). Vertical and horizontal flame spread tests demonstrated that biochar was unable to suppress the flames by its own. Conversely, cotton experienced self-extinction when biochar and phytic acid were present together, at least at 6 wt.%. Additionally, in forced combustion tests, the self-extinguishing treated fabrics did not ignite when subjected to a 35 kW m^{-2} irradiative heat source, demonstrating the superior flame retardant properties provided by the specific treatment.

Chapter 3

EVA composites containing BC from Kraft Lignin

Increased consumption of fossil fuels, coupled with the depletion of some oil fractions, and growing concern about human impact on the environment have generated renewed interest in the use of sustainable resources for energy and materials. This growing interest in green and sustainable chemistry has also attracted attention to biomass, and particularly to lignocellulosic feedstocks, as a potential, renewable and abundant source of chemicals. The main components of lignocellulosic biomass are carbohydrate polymers (cellulose and hemicellulose) and aromatic polymers (lignin and tannin) [180]. Lignin is the second most prevalent polymer from biomass after cellulose [181] and the most abundant polymer in nature based on aromatic structure [182]. Three phenylpropane units (namely, p-hydroxyphenyl (H), guaicyl (G), and syringyl (S)) combine to form this intricate three-dimensional amorphous polymer. The lignocellulosic species mostly determines the variations in the monomer unit ratios [183]. For a long time, it was considered a waste product of the milling process; however, there is currently a lot of ongoing research to use lignin for industrial purposes [180]. It is thought to be a superior raw resource that can replace petroleum-based chemicals [184]. Lignin, in fact, is a by-product of chemical pulping processes and is produced in huge amounts. The creation of eco-friendly materials and the reduction of global warming problems are both regarded to be impacted by converting these numerous by-products into value-added resources, such as

materials, energy, chemicals, and fuel [185] [186]. Kraft lignin is derived from the most common pulping process, i.e., Kraft process [187].

In this chapter, the pyrolysis process of kraft lignin was set up and optimized to produce biochar, bio-oils, and gas at different temperatures. These products were then recovered and characterized with various techniques. Subsequently, the obtained biochars were used as filler for EVA copolymer in order to prepare composites with fire retardant properties.

3.1. Lignin characterization

Table 4 reports the obtained values, which were confirmed by those found in literature [188] [189] [190] [191]. Proximate analysis highlights an amount of fixed carbon (FC = 36.3 %) which is quite high if compared to other biomasses [192]. As an example, typical values of FC for cellulose and hemicellulose are around 4.96 and 13.1 %, respectively [193]. These findings suggest that the pyrolysis of lignin can result in the production of significant amounts of biochar. The remaining fraction detected by the analysis mostly refers to volatile matter, with a very low percentage of moisture (1.9 %). Ultimate analysis confirmed the high carbon fraction (56.1 %), followed by oxygen (36.4 %), and reports just traces of hydrogen and nitrogen. Finally, the Kraft Lignin presents a higher heating value (HHV) of 26.2 which is greater by about 15-65% if compared to other biomasses values found in literature [194] [195].

Table 4. Results of proximate analysis, ultimate analysis and higher heating values (HHV) for Kraft Lignin.

Proximate analysis [%]				HHV (MJ/kg)	Ultimate analysis [%]				
Moisture content	Volatile matter	Fixed carbon	Ash		C	H	N	S	O
1.9	60.1	36.3	1.7	26.2	56.1	5.5	0.3	-	36.4

3.2. BC production

The pyrolysis of Kraft Lignin was performed in a mechanically fluidized bed reactor (MFR) designed at ICFAR (Institute for Chemicals and Fuels from Alternative), Western University, London, Ontario, Canada [196], where the following experimental trials were performed by the author. The setup of MFR employed is schematized in Figure 12. The equipment consists of a cylindrical reactor 15 cm in diameter and 25 cm in height, heated by an induction system formed by a copper coil wrapping the reactor. The temperatures were measured by two K type thermocouples placed at the bottom and the top of the reactor and regulated by a controller. A vertical blade stirrer accounts for a high transfer rate to the biomass particles by vigorous continuous mixing, providing agitation close to the reactor wall. The biomass was inserted into the reactor after 24 hours of drying at 105 °C, and experiments were conducted with batch process. A pressure regulator was used to set the flow rate of nitrogen, which was injected through the reactor. The gases flowing out the reactor were collected with a condenser immersed in an ice bath; the non-condensable gases exiting the system could be collected using appropriated gas bags for further analysis and then discharged. The biomass was pyrolyzed at three different temperatures: from ambient temperature the reactor was heated at 500, 600, or 700 °C, with a heating rate of 20 °C min^{-1}. Once the target temperature was reached, that temperature was held for 25 minutes. Finally, after the reactor was cooled, the biochar was removed and collected.

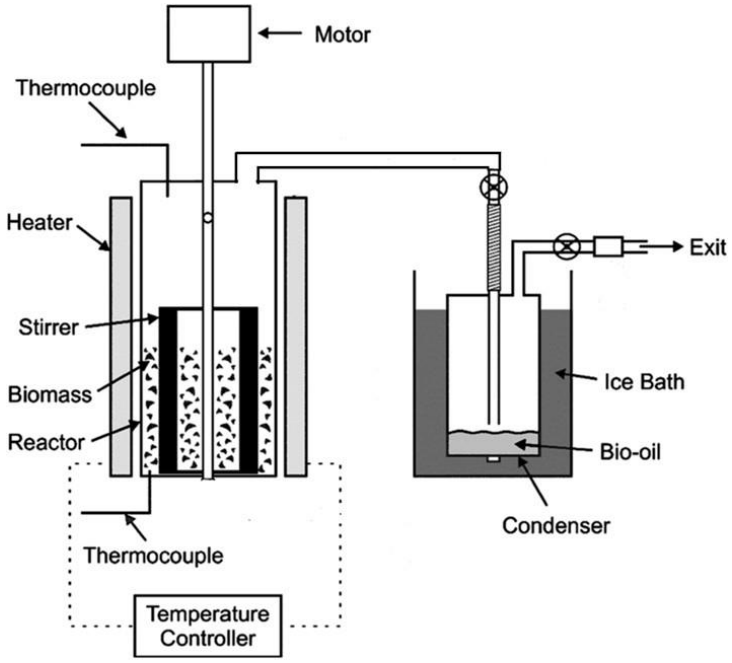

Figure 12. Setup of mechanically fluidized reactor used for pyrolysis of Kraft Lignin. Reprinted with the permission from [197].

The yields of the processes were calculated after pyrolysis, by weighting the biochar inside the reactor and the liquid phase obtained by gas condensation inside the condenser. The percentage of gas was calculated accordingly. Table 5 collects the yields obtained at different process temperatures. It is worth noting that the yield of each product remains almost constant regardless the temperature involved. The most abundant products were the solid (BC) and the gas phases with a yield around 40 %. The liquid phase accounted for only about 16 % of the total. These findings fall within the ranges found in the literature for lignin conversion, which are strictly dependent on the process parameters used [193] [198] [199] [200]. The high amount of char resulting after pyrolysis can be attributable to the aromatic rings present in the lignin, which are very stable [201]. These findings were in accordance with the high value of fixed carbon found in kraft lignin (Table 4) with respect to other biomasses with a low lignin content [194] [202].

Table 5. Product yield (%) values of Kraft Lignin processed by pyrolysis at different temperatures.

	500 °C	600 °C	700 °C
BC	40.7 ± 0.8	40.8 ± 1.4	42.0 ± 2.6
Liquid	16.1 ± 1.3	16.7 ± 1.9	16.2 ± 1.9
Gas	43.3 ± 1.2	42.5 ± 2.8	41.8 ± 4.3

Therefore, the pyrolysis of lignin resulted in higher char production compared with the other biomass [203]. As an example, Ma et al. [202] studied the different char content resulting from the pyrolysis of components of the lignocellulosic biomass: lignin, cellulose, and xylan (as a model compound for hemicelluloses). The study highlighted the effect of pyrolysis temperature on the biochar yield of the different biomasses. As shown in Figure 13, the char yield (expressed as mass yield %) of lignin (LC) was higher than that of cellulose (CC) and hemicellulose (HC) for each pyrolysis temperature above 300 °C. Interestingly, from a process carried out at 500 °C the char yield stabilizes around 40 % up to the maximum treatment temperature, in accordance with the results just obtained on kraft lignin.

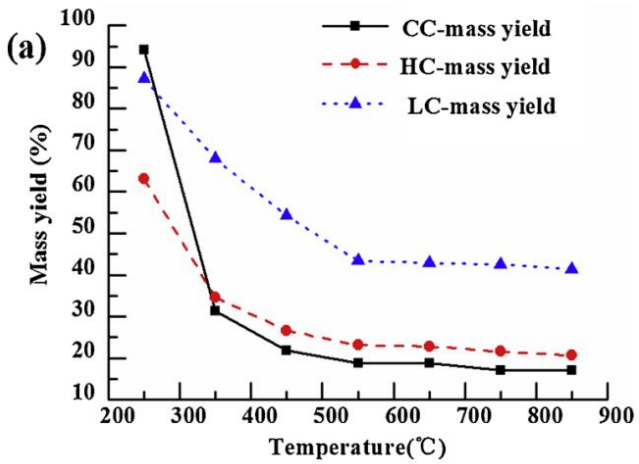

Figure 13. Effect of pyrolysis temperature on the yields (expressed as Mass yield) of biochar derived from pyrolysis of cellulose (CC), hemicellulose (HC) and lignin (LC). Reprinted with the permission from [202].

3.3. BC characterization

Table 6 lists the values obtained from the proximate and ultimate analysis of the biochars obtained at different temperatures. The value of fixed carbon content increased with the pyrolysis temperature due to the increasing amount of volatile matter released during process. This behavior can be attributed to the continuous degradation of organic matter, which promotes an increase in the concentration of inorganic compounds. The volatile matter found in BCs, as expected [204] [205] follows an inverse trend to fixed C, decreasing when the pyrolysis temperature increased. The ultimate analysis revealed no significant differences in the amount of C content, which appears to be about 80 % for each pyrolysis temperature. These obtained values were significantly higher than the respective C content found in the biomass before pyrolysis (Table 4, C = 56.1 %). These results can be attributed to the high level of graphitization due to the formation of polyaromatic carbon structures favoured by the high temperatures involved [202] [205].

Table 6. Results of proximate analysis and ultimate analysis biochar obtained from pyrolysis of Kraft Lignin at different temperatures (i.e., 500, 600 and 700 °C).

	Proximate analysis [%]				**Ultimate analysis [%]**				
Temperature [°C]	**Moisture content**	**Volatile matter**	**Fixed carbon**	**Ash**	**C**	**H**	**N**	**S**	**O**
500	0.4	10.2	72.7	16.7	80.3	2.0	0.6	-	0.4
600	0.5	6.3	78.3	14.9	79.5	1.6	0.7	-	3.3
700	0.6	4.6	81.4	13.4	80.0	1.3	0.9	-	4.4

The results of the surface area analyses on the various BCs are collected in Table 7: the values of average pore radius and surface area of BCs obtained at 500 and 600 °C were very similar. In contrast, BC at 700 °C shows a significantly lower average pore radius value, while its surface area is increased (more than

twice) compared to the other two. Pyrolysis temperature is considered the predominant parameter that influences the surface area and porosity of biochar [206]. In agreement with literature [207] [208], for the majority of biochars, the relationship between pyrolysis temperature and specific surface area is favorable as higher temperatures result in the formation of more pores, created by the volatile matters escaping from the char.

Table 7. Results obtained by surface analyses (BET method) of the BCs at different temperatures.

Temperature [°C]	Average pore radius [Å]	Surface area [m^2 g^{-1}]
500	9.87	248.446
600	11.42	255.075
700	5.06	633.805

3.4. Gas phase

The gas evolving profile from pyrolysis of the kraft lignin, tracked by Micro-GC every 100 °C, is shown in Figure 14; the volume percentages are collected in Table 8. The concentrations of H_2 and CH_4 follow opposite trends with increasing temperature: the former increases significantly from 15.5 vol.% at 300 °C to 63.5 vol.% at 700 °C; in contrast, methane release decreases from 32.6 vol.% at 300 °C to only 1.9 vol.% at 700 °C. The sum of these two gases provides the largest contribution to gas evolution during pyrolysis at any temperature, with the total amount ranging between 48 and 65 vol%. This behavior can be attributed to the high content of aromatic rings and O-CH_3 functional groups present in lignin. The H_2 produced by pyrolysis of organic matter, in fact, derives primarily from the cracking and deformation of aromatic C=C double bond and aromatic C-H, while the methane is formed by the cracking of methoxyl (-C-OH) groups [209]. Both carbon monoxide and carbon dioxide are typical gases released from lignin pyrolysis [210]. The evolution of carbon monoxide shows high amounts at 300 °C, and, with only one exception (600 °C), at subsequent temperatures it is below 30 vol.%. The total amount of CO_2 was about 6 - 8 vol.% until 600 °C, then its

value decreased to 3.2 vol.% at 700 °C. Finally, some hydrocarbons containing multiple carbon atoms were detected (Table 8) in low concentration. These findings suggest the potential use of valuable gases (H_2 and methane) for fuel and energy applications, as well as the use of CO/H_2 syngas as feedstock for converting the gases into liquid hydrocarbon fuel [211].

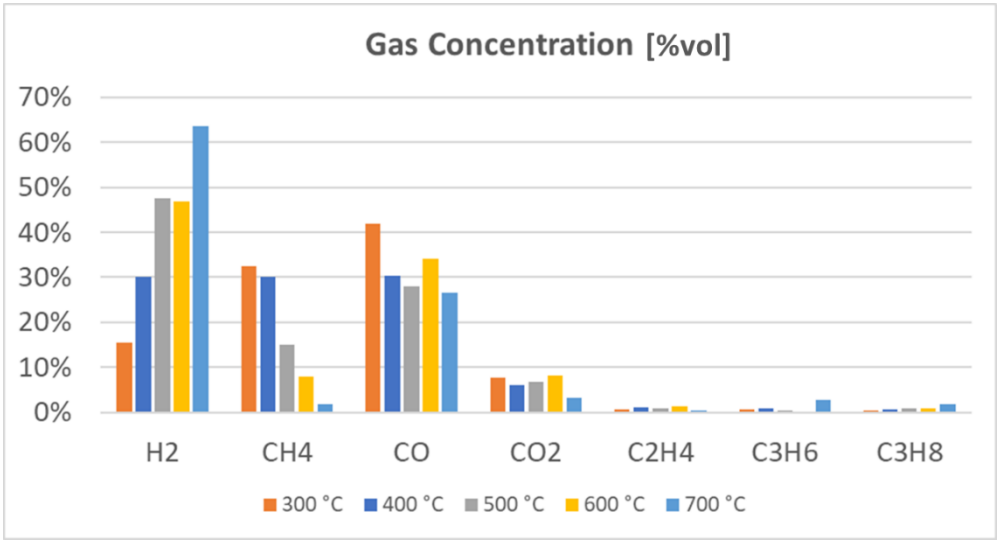

Figure 14. Gas evolution during pyrolysis process of Kraft lignin (gas collected every 100 °C from 300 to 700 °C).

Table 8. Values of gas concentration during pyrolysis process of Kraft lignin (gas collected every 100 °C from 300 to 700 °C).

Gases	Conc. [vol%] @ 300 °C	Conc. [vol%] @ 400 °C	Conc. [vol%] @ 500 °C	Conc. [vol%] @ 600 °C	Conc. [vol%] @ 700 °C
H_2	15.5	30.2	47.5	46.7	63.5
CH_4	32.6	30.1	15.1	8.0	2.0
CO	41.9	30.3	28.1	34.2	26.5
CO_2	7.7	6.0	6.8	8.2	3.2

C_2H_4	0.6	1.1	0.8	1.4	0.3
C_2H_6	0.4	0.4	0.3	0.3	0.1
C_3H_6	0.6	0.9	0.4	0.3	2.8
C_3H_8	0.5	0.7	0.8	0.8	1.7
C_4H_{10}	0.2	0.3	0.3	0.1	0.1
C_5H_{12}	0.1	0.0	0.1	0.0	0.0
C_6H_{14}	0.0	0.0	0.0	0.0	0.0

3.5. Liquid phase

The liquid phase derived from the pyrolysis of kraft lignin consists of the condensable gases that are collected in a condenser immersed in an ice bath at about 0 °C. Table 9 lists the most abundant compounds detected by HPLC at different temperatures of pyrolysis. Xylose and levoglucosan were typical compounds found in lignocellulosic materials [212] [213]. Most of the other components found are acid compounds. As previously reported in Table 5, the yield of the liquid phase was about 16 wt.% for the various processes. Due to the low yield obtained during these processes, the polyols were not considered further.

Table 9. Compounds detected by HPLC into the oil-phase of pyrolysis kraft lignin at different temperatures.

Compounds	Class	Conc. @ 500 °C [g/l]	Conc. @ 600 °C [g/l]	Conc. @ 700 °C [g/l]
Xylose	Aldehyde	0.03	-	-

Levoglucosan	Sugar	0.02	0.03	0.03
Formic acid	Acid	0.02	0.03	0.03
Acetic acid	Acid	0.19	0.09	0.11
Acetol	Alcohol	0.01	0.01	0.01
Propionic acid	Acid	0.03	0.02	0.02
Butyric acid	Acid	0.02	-	0.01
Iso-Valeric acid	Acid	0.41	-	-
Catechol	Phenol	0.21	0.21	0.24
Furfural	Aldehyde	0.06	0.02	0.02

3.6. Fire retardancy of EVA-BC composites

The fire retardant behavior of EVA and its composites containing BC (20 and 40 wt.%) from pyrolysis of kraft lignin at various temperatures was studied with cone calorimetry tests. The setup of the test and the detailed conditions employed are reported in the Appendix. The obtained curves of Heat Rate Release (HRR) vs. time are shown in Figure 15 and the values of the main parameters are collected in Table 10.

The unfilled EVA curve presents a rapid increase in the HRR values after the ignition of the specimen (TTI = 74 s). The HRR continues to rise after reaching a peak (pkHRR) at 178 s equal to 1803 kW/m^2; after this point, the flame decreases rapidly, and when the entire specimen has been consumed, the flame goes out without leaving any residue. This behavior is typical of the most unfilled thermoplastic polymer, which are not able to guarantee any protection to fire [214] [215] [216]. The introduction of the BC particles drastically changed the combustion behavior of the EVA and consequently the shapes of the HRR curves

of its composites. From a general point of view, the HRR curves of the composites show a significant decrease in peak of HRR (from 33 to 73 %) and varying TTIs depending on the type and loading of BC, compared with unfilled EVA. Regarding the specimens loaded at 20 wt.%, the use of BC 500 and BC 600 resulted in very similar TTI and pkHRR values (Table 10); these formulations are not able to protect the EVA matrix efficiently and their curves sharp as that of EVA. In contrast, the BC 700 acted better than the two latter in delaying TTI and decreasing pkHRR: this can also be seen from the HRR curves that change slope around 100 s, decreasing HRR. This result was attributed to the protection effect exerted by the BC particles. In fact, the BC particles tend to accumulate on the surface during combustion due to the recession of the polymer from surface by pyrolysis. As a result, a protective surface layer was formed and was able to act as a heat and mass transfer barrier and limiting the release of volatile compounds created during the material degradation. This effect is more pronounced in composites containing 40 wt.% of BC. Among them, BC 500 was the most ineffective in term of TTI, with a value similar to that of its counterpart at 20 wt.%. Conversely, BC 600 and BC 700 at 40 wt.% were able to slightly delay the TTI of EVA (+ 4 and + 7 s, respectively) and significantly reduce the pkHRR value (-71 and -73 %). Furthermore, these two composites delayed the time to peak compared with EVA by 34 and 42 s, respectively. Another feature that emphasizes the fire retardant effect exerted by the BC particles, was the decrease of the values of Total Heat Release (THR), Fire Performance Index (FPI, pkHRR/TTI ratio), and Fire Growth Rate Index (FIGRA, pkHRR/time to peak), compared with unfilled EVA. This decrease strictly depends on the type and loading of BC; BC 700 at 40 wt.% seems the most effective system. This latter was able to reduce THR by 38 %, FPI by 75 %, and FIGRA by 78 %. These results suggest that BC obtained by pyrolysis at 700 °C possesses the chemical and physical properties best suited for improved fire retardant behavior when incorporated into EVA, in comparison with the BC treated at lower temperatures.

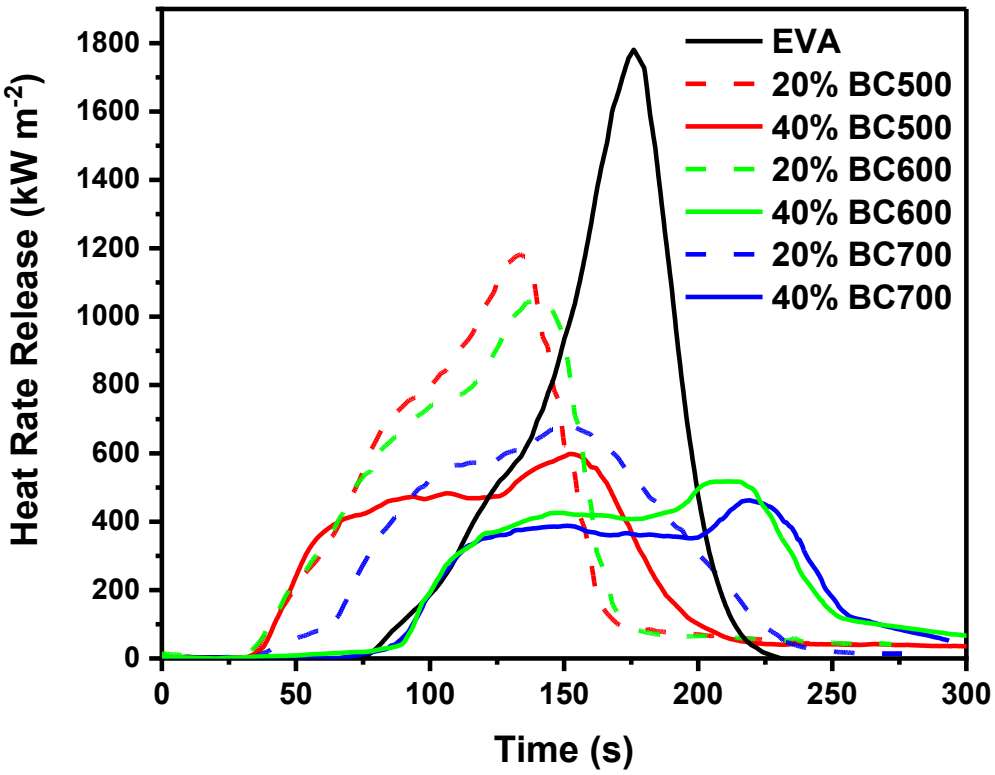

Figure 15. HRR vs. time curves for EVA and its composites containing BC from Kraft Lignin pyrolyzed at different temperatures (500, 600 and 700 °C).

Table 10. Main thermal parameters by cone calorimetry of specimens containing BC from kraft lignin at various temperatures.

Specimen	TTI [s]	pkHRR [kW m^{-2}]	pkHRR Reduction [%]	Time to peak [s]	THR [MJ m^{-2}]	Residue mass [%]	FPI $\left[\frac{(kW/m^2)}{s}\right]$	FIGRA $\left[\frac{(kW/m^2)}{s}\right]$
EVA	74	1803.0	-	178	96.6	0	24.8	10.1
20% 500BC	34	1206.6	33	135	89.6	12	35.7	9.0
40% 500BC	37	600.1	67	152	71.2	26	16.4	3.9
20% 600BC	32	1121.1	38	140	88.1	13	35.0	8.0
40% 600BC	78	522.1	71	212	66.0	27	9.1	2.5
20% 700BC	57	796.9	56	167	77.3	14	15.4	4.9

40% 700BC	81	481.8	73	220	59.5	29	6.1	2.2

Regarding smoke parameters, the introduction of BC particles significantly reduces the values of Total Smoke Release (TSR) and Specific Extinction Area (SEA), as shown in Table 11. Furthermore, the CO and CO_2 values decreased significantly compared with unfilled EVA, as evidenced by the increase in the CO/CO_2 ratio up to twice that of EVA. These results are due to the char layer, which not only lowers the combustion rate but also reduces the production of volatiles, smokes and other combustion products [217].

Table 11. Main smoke parameters by cone calorimetry tests of specimens containing BC from kraft lignin at various temperatures.

Specimen	TSR [$m^2\ m^{-2}$]	SEA [$m^2\ kg^{-1}$]	CO [%]	CO_2 [%]	CO/CO_2 ratio
EVA	1280.2	597.9	0,0383	3,25	0,0118
20% 500BC	499.5	196.1	0,0043	0,19	0,0230
40% 500BC	171.8	83.6	0,0028	0,14	0,0202
20% 600BC	462.2	186.1	0,0040	0,18	0,0220
40% 600BC	44.7	26.6	0,0027	0,12	0,0219
20% 700BC	634.9	244.9	0,0034	0,14	0,0249
40% 700BC	109.7	54.9	0,0027	0,11	0,0256

Chapter 4

EVA composites containing BC from various biomasses

Part of the work described in the Chapter 4 has been previously published in:

"Matta S., Bartoli M., Frache A. and Malucelli G. Investigation of Different Types of Biochar on the Thermal Stability and Fire Retardance of Ethylene-Vinyl Acetate Copolymers. Polymers. 2021" [218]

The purpose of this chapter is to discuss the flame retardant properties of BCs derived from various biomasses in an EVA copolymer. Three different kinds of biochar with varying ash contents were selected for this use. They were produced from various bioproducts, namely softwood, rapeseed, and rice husk. Depending on the ash concentration, these BCs were referred to in the text as "low," "medium," and "high", respectively. A twin co-rotating extruder was used for the incorporation of fillers into the EVA matrix at different loadings. The equipment and operating conditions employed (screw profile, temperatures, etc.) are reported in the appendix. These process conditions were designed to maximize the effectiveness of the flame-retardant properties of the polymer-BC systems by targeting good particle distribution in the EVA matrix. 15 and 20 wt.% of BCs were chosen to evaluate the behavior of the samples at low loadings with a slight variation in the amount of BC; in addition, a 25 wt.% formulation was prepared using BC from rapeseed. Then, the BC content was increased to obtain 40 wt.%

loaded samples. The obtained systems were thoroughly studied in terms of their thermal, mechanical, and flame retardant properties. Furthermore, a surface approach was used to coat specimens of unfilled EVA with a 0.5- or 1.0-mm-thick layer of composite containing various amounts of BC from rapeseed, which emerged as the most promising. In particular, specimens with a total amount of BC of 3 or 6 wt.% were prepared and tested by cone calorimetry.

4.1 BC characterization

4.1.1 Morphological investigations

The SEM observation of biochar powders represents an effective tool for assessing the morphology and dimensions of the fillers. Knowing this information, it will then be possible to determine from the SEM images of the composites whether the particles have been distributed homogeneously in the polymer matrix. Additionally, the energy dispersive X-ray (EDX) micro-analyses were useful to study the chemical elements present in the various BCs to establish a correlation with the properties conferred by the fillers to EVA.

Figure 16 shows the SEM images of the powders of BC low, BC medium and BC high at 3000X magnification and their corresponding EDX spectra. The morphologies of the fillers appear similar for the three types of BC. The particles have irregular shapes and are found in the micron-size. In particular, the size of the largest aggregates ranges from about 30 to 40 μm. Table 12 collects the main elements detected by EDX micro-spectroscopy in the various types of BC, given as wt.%. From a general point of view, the most abundant element found is C, ranging from 70.9 to 92.7 wt.% depending on BC. These values are quite remarkable considering that the materials were treated at 1000 °C. Oxygen is the second most abundant element found, followed by a smaller quantity of other elements. In details, the BC low samples contain the highest amount of carbon (i.e., 92.7 wt.%) and the lowest inorganic content, consisting of 0.5 wt.% of Calcium and 0.5% of Potassium. Conversely, BC medium and BC high show a smaller amount of C (76.6 and 70.9 wt.%, respectively), which, summed to O, reaches 90.5 wt.% and 87.4 wt.%, respectively. The remaining inorganic content of BC medium consisted mainly of K (4.4 wt.%), Si (2.5 wt.%) and Ca (1.3

wt.%), while BC high included phosphorus (3.1 wt.%) in addition to K and Si (3.9 and 4.2 wt.%, respectively). A low amount of Mg and other various elements was found in BC medium and BC high.

Table 12. List of the chemical elements identified by EDX analyses of BC low, medium, and high.

Material	C [%]	O [%]	Ca [%]	K [%]	Si [%]	P [%]	Mg [%]	Other [%]
BC low	92.7	6.2	0.5	0.5	-	-	-	0.1
BC med	76.6	13.9	1.3	4.4	2.5	-	0.4	0.9
BC high	70.9	16.5	-	3.9	4.2	3.1	1.1	0.3

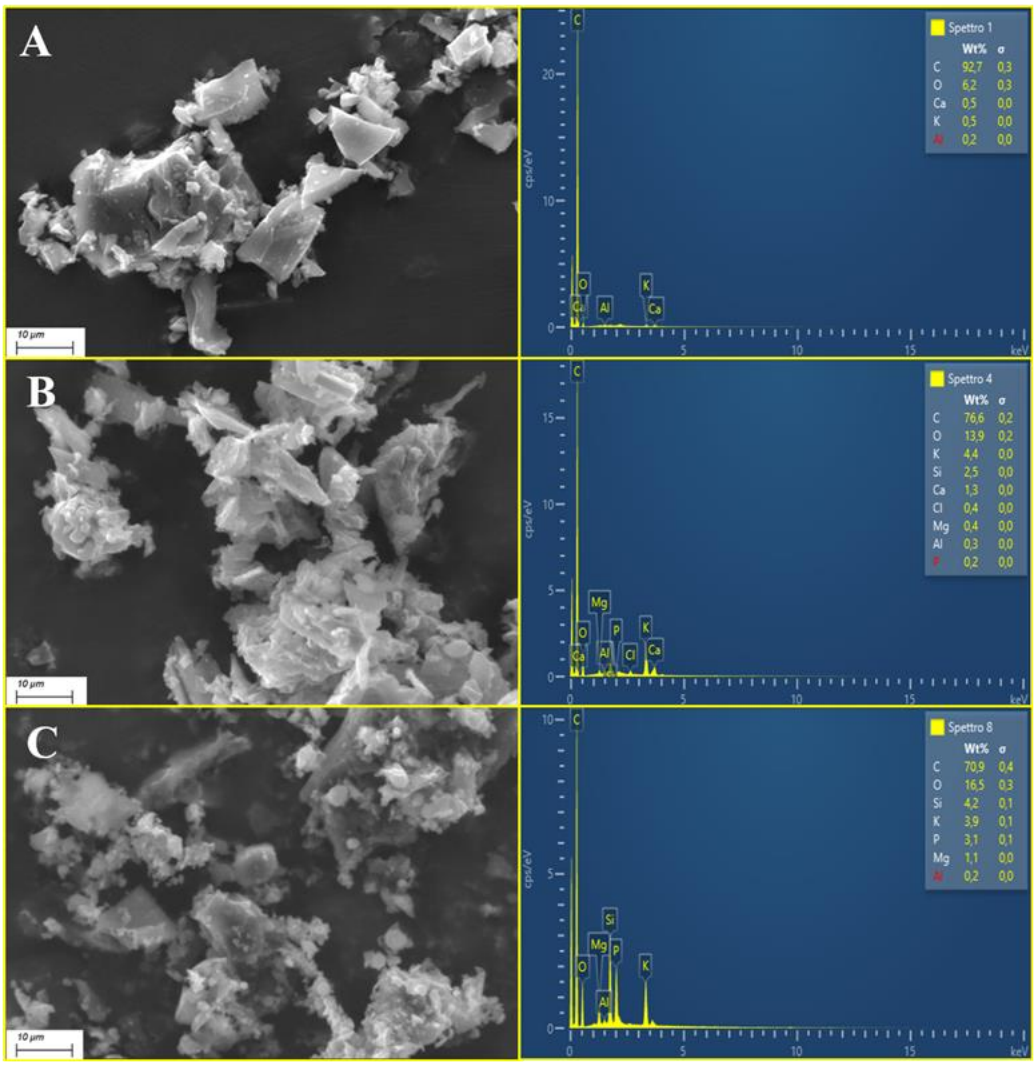

Figure 16. SEM images at 3000 X magnification with the corresponding EDX spectra of BC low (A), BC medium (B) and BC high (C).

4.2.2 Raman

The Raman spectra of three biochars are shown in Figure 17. The typical curves of BCs show sharp double peaks that dominate the spectra and a band in the range 2500 to 3500 cm^{-1}. The two main peaks are attributed to the D band and G band, at 1350 cm^{-1} and 1580 cm^{-1}, respectively, and the last band is identified as the 2D region [219]. The D band (defect band) cannot occur in perfect graphite structure and is activated only when a defect is found. This is characteristic of sp^3 carbon networks and was associated to defects and disorder in graphite structures.

Contrary, the G band (Graphite band) is attributed to the bond-stretching movement of pairs of C sp^2 atoms, so this mode reveals graphitic networks [220] [221]. To obtain information on the structure of the BC, it is possible to calculate I_D/I_G the ratio of the intensity of the peaks D and G. This parameter is crucial for the study of carbonaceous structures and is used to estimate the degree of carbon order [222]. BC low, BC medium, and BC high showed I_D/I_G values of 1.3, 1.5, and 1.7 respectively. These results are typical of materials that have a high degree of disorder but are in the transition phase to graphitic carbon [220], as already confirmed in the scientific literature [223]. Additionally, they demonstrate how BC low, which has a reduced inorganic content, promoted the development of highly organized carbon structures. They also demonstrate that low BC, which has a lower value of I_D/I_G, promoted the development of highly organized carbon structures. This finding may be associated with the reduced inorganic content compared with medium BC and high BC (as seen in the previous section). Finally, the shape of the 2D region confirms the presence of materials rich of sp^3 sites with a low order in aromatic structures and far from complete reorganization in graphitic structures. For obtaining narrow bands in this region, which are typical of more ordered structure, a treatment at temperatures above 1300°C is required [223] [224].

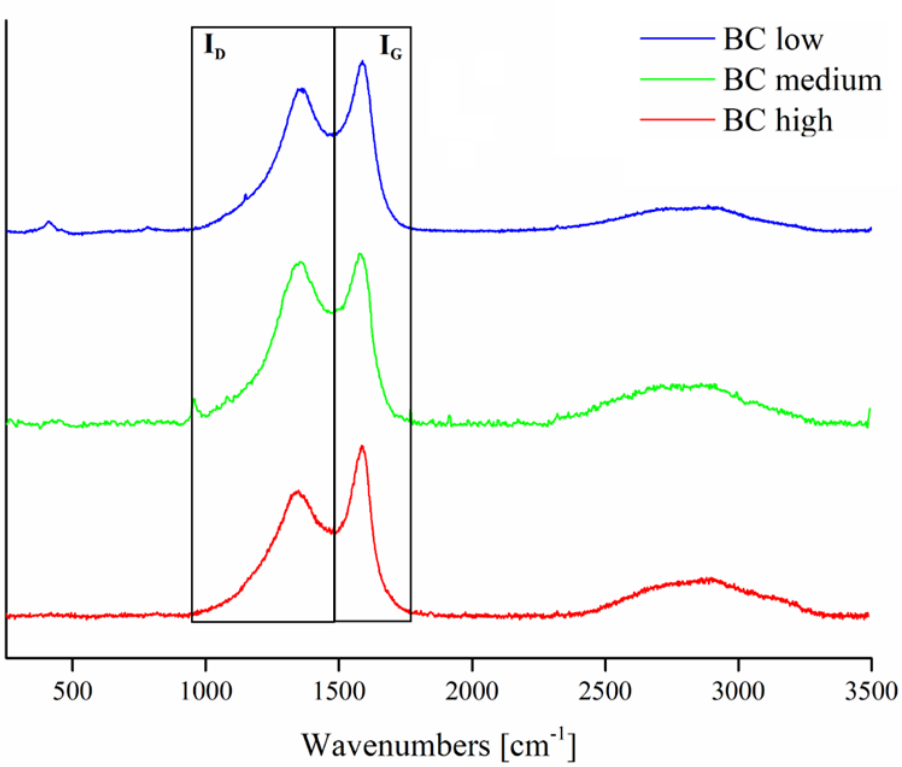

Figure 17. Raman spectra of BC low (blue), BC medium (green) and BC high (red) in the range from 250 cm^{-1} to 3500 cm^{-1}.

4.2.3 Thermogravimetric analyses

The thermogravimetric analyses (TGA) were carried out to assess the thermal and thermo-oxidative stability of the different types of BC. For this purpose, BC samples were analyzed in both nitrogen and air, following the conditions described in the Appendix. The thermograms of these materials are reported in Figure 18 and the collected data are listed in Table 13.

The curves obtained in nitrogen atmosphere (Figure 18A) show very stable materials with very low weight loss at the final temperature of 700 °C. In particular, the final residues varied from 86.0 to 90.9 wt.% depending on the BCs. The scenario changes very noticeably in air atmosphere, as expected, due to the oxygen interaction with the BCs. In this case, the different BCs follow a single degradation step that begins at very different temperatures, indicated by the T_{onset} (Table 13). In details, the highest T_{onset} was found in BC low (513 °C), followed by BC high (487 °C); the BC medium sample starts degrading at remarkably

lower temperatures (i.e., at about 365 °C). Consequently, the temperatures at maximum rate of degradation (T_{max}) of the different BCs, follow the same trend as the T_{onset}. Furthermore, a large difference in sample weights was found at 700 °C, depending on the BCs. The BC with the lowest inorganic content, namely BC low, showed the lowest residue at the end of the test (about 7.4 wt.%). In contrast, BC medium and BC high, due to a higher inorganic content (Table 12), displayed a residue of 24.6 and 39.6, respectively.

Table 13. Results from thermogravimetric analyses in nitrogen and in air for BC powders (T_{max} in nitrogen atmosphere were not identified due to the limited mass loss; these values were not reported and consequentely neither were the values of Residue at T_{max}).

Atmosphere: nitrogen				
Material	T_{onset} [°C]	T_{max} [°C]	Residue @ T_{max} [°C]	Residue @ 700°C [%]
BC low	548	-	-	90.9
BC medium	400	-	-	88.3
BC high	540	-	-	86.0
Atmosphere: air				
Material	T_{onset} [°C]	T_{max} [°C]	Residue @ T_{max} [°C]	Residue @ 700°C [%]
BC low	513	597.8	37.0	7.4
BC medium	365	430.4	61.9	24.6
BC high	487	576.9	60.3	39.6

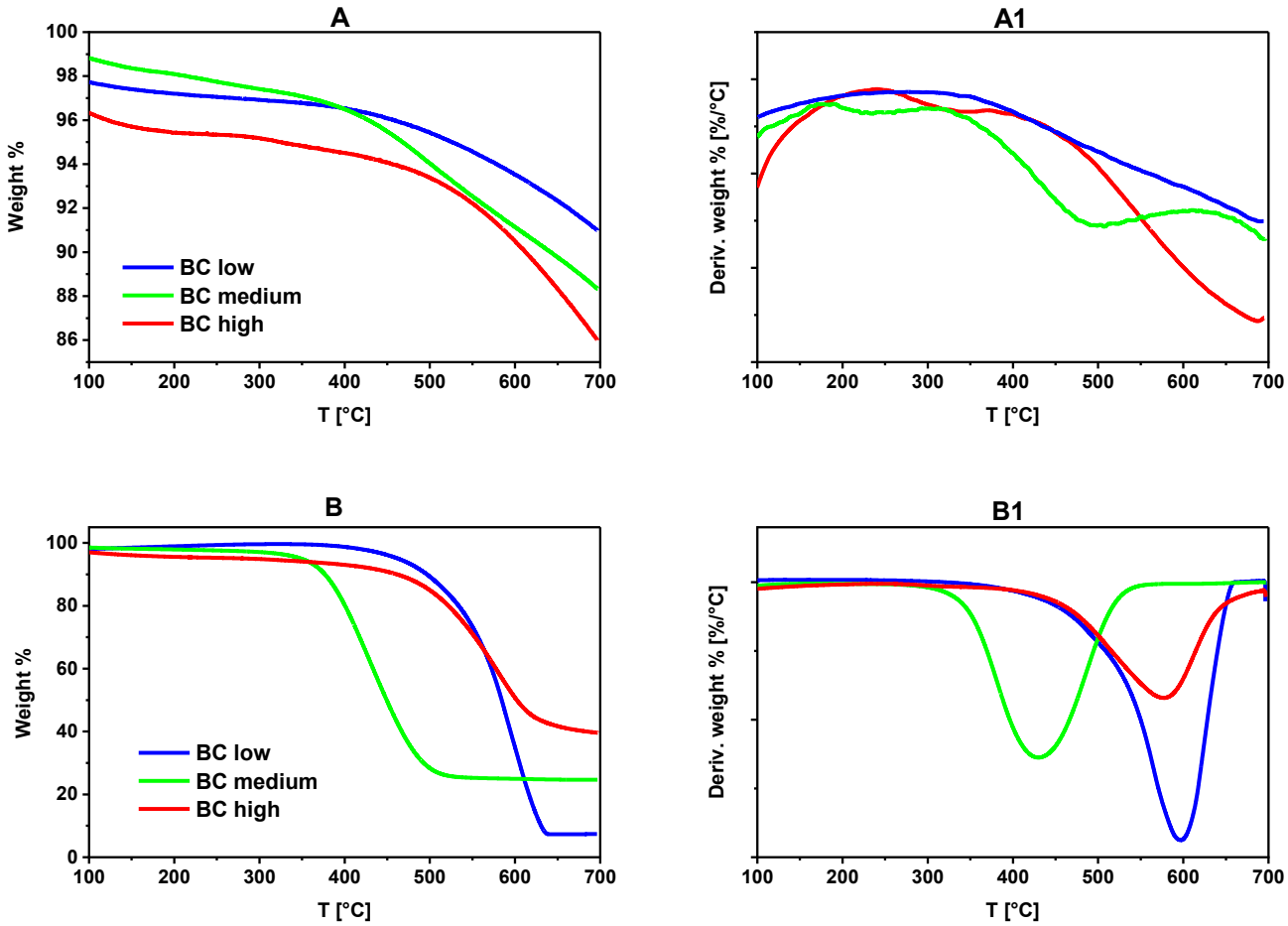

Figure 18. Thermogravimetric and dTG curves in nitrogen (A, A1) and air (B, B1) of BC low, medium and high.

4.2 Composites characterization

4.2.1 Morphological investigations

The EVA/BC composites were analyzed by SEM to assess the distribution and the dispersion of BC particles within the EVA. The SEM images of the fractured surface of composites containing 20 wt.% of the three biochars in bulk are shown in Figure 19. As it is clearly visible, the BC particles are well distributed into polymer matrix, regardless of the BC used. Furthermore, particle sizes are in the micrometer range, and the largest aggregates do not exceed 100 microns. These results suggest that the extrusion process carried out with the

adopted operating conditions described in the Appendix was successful. In fact, it was possible to obtain a homogenous dispersion of the particles, irrespective of the type of BC.

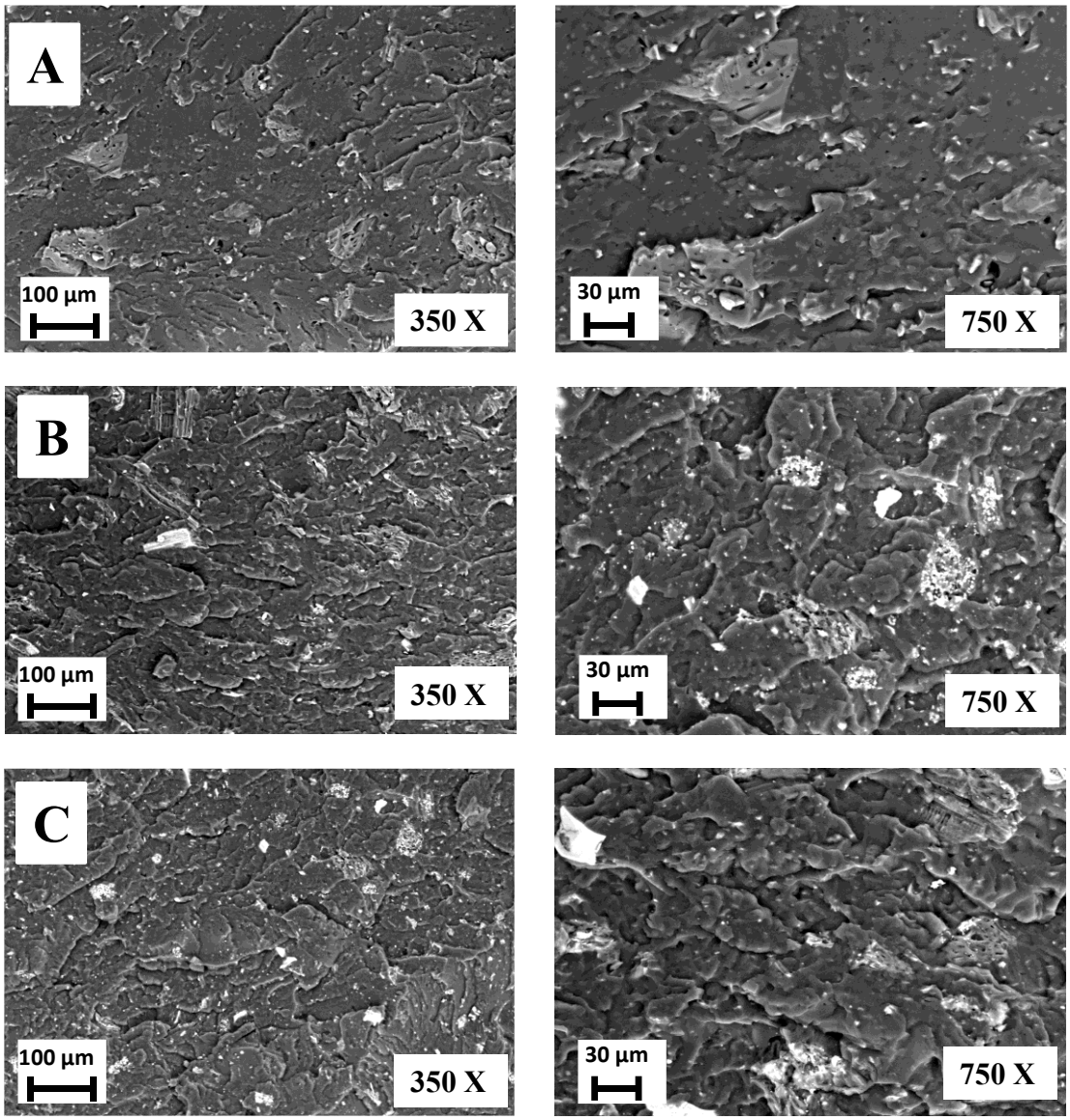

Figure 19. SEM images at different magnification (350 X and 750 X) of EVA + 20 wt.% of: BC low (A), BC medium (B) and BC high (C).

SEM observations were also performed on specimens with BC dispersed only on the surface of neat EVA. The total thickness of the specimens was set at 3 mm, and the BC-rich surface layer was 0.5 to 1.0 mm thick, with different amounts of

BC. Figure 20 shows specimen containing 6 wt. % of BC dispersed in 1 mm thick coating. The particles were well distributed in the matrix, and their sizes are in the micrometer range, with some larger aggregates not exceeding 100 µm.

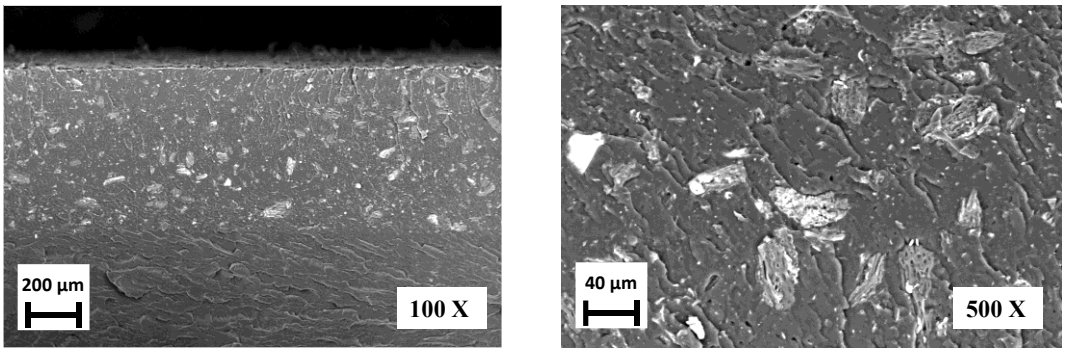

Figure 20. SEM images of specimen containing 6 wt. % of BC dispersed in 1 mm coating at different magnifications.

Similar specimens prepared with a 500 µm thick coating with two different amounts of BC, namely, 3 and 6 wt. %, were investigated by SEM (Figure 21). The difference in the amount of BC particles between the two systems is clearly visible with a higher concentration of particles in the sample at 6 wt. %, leading to the formation of larger aggregates. Even in this case, the size of 100 microns is not exceeded.

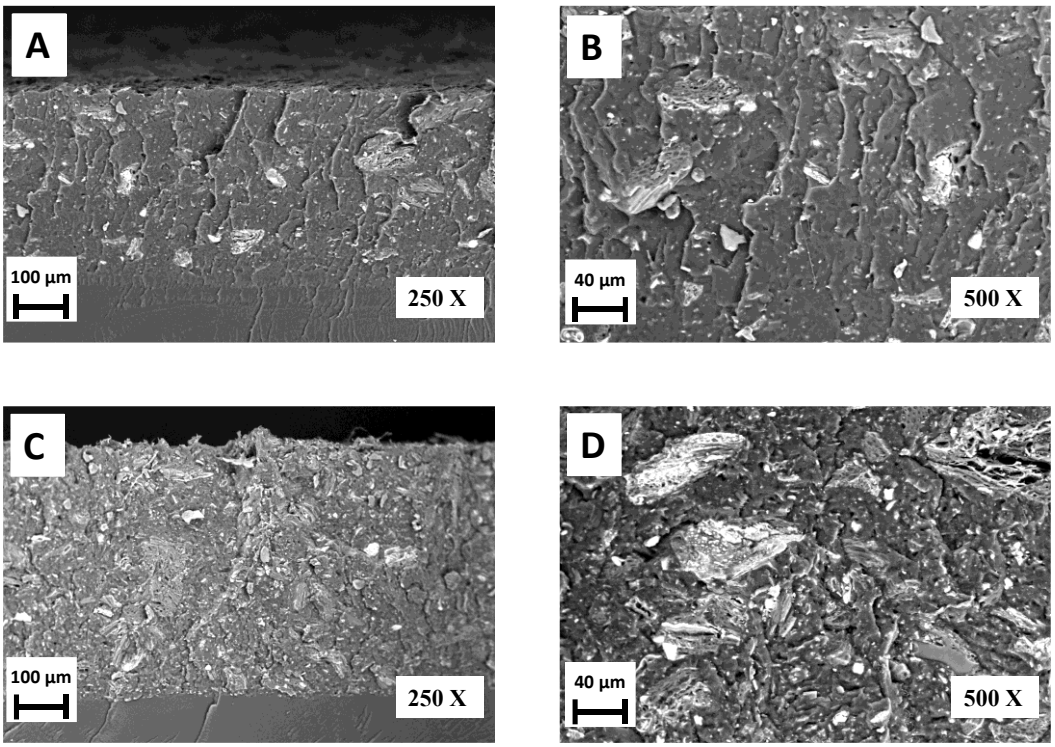

Figure 21. SEM images of specimen containing 3 wt.% (A, B) and 6 wt.% (C, D) of BC dispersed in 500 µm coating at different magnifications.

4.2.2 Differential scanning calorimetry analyses

Differential scanning calorimetry (DSC) analyses were performed on EVA and its composites to investigate the characteristic temperatures of the samples. The results obtained during the selected thermal cycle for EVA and EVA-BC samples are reported in Table 14. The melting temperature (T_m) of unfilled EVA is about 85 °C, and this value is substantially not affected by BC incorporation, irrespective of type and loading. In addition, the crystallization temperature (T_c) of EVA is about 62 °C and the incorporation of the filler increases this value by about 3 °C for every type and loading of BC. Otherwise, the degree of crystallinity of EVA (X_c about 4.5 %) tends to decrease when BC is incorporated to the polymer. This effect was shown for all formulations and is more pronounced as the total amount of filler increases. This result can be explained by a slowing effect of the crystallization process caused by the BC.

Table 14. Results from DSC analysis for ethylene vinyl acetate (EVA) and its composites.

Sample	Tc (°C)	ΔHc (J/g)	Tm (°C)	ΔHm (J/g)	Xc (%)
EVA	62.71	27.58	85.28	13.20	4.5
15% BC low	65.32	19.63	85.50	9.01	3.7
20% BC low	65.01	17.12	85.32	8.40	3.6
40% BC low	66.12	12.95	84.41	5.62	3.2
15% BC med	65.42	20.51	85.04	8.82	3.6
20% BC med	65.13	19.10	85.03	8.23	3.5
25% BC med	65.15	17.27	85.56	7.54	3.5
40% BC med	65.93	13.94	84.89	5.17	3.0
15% BC high	65.52	17.11	85.59	7.89	3.2
20% BC high	65.50	15.82	85.24	7.17	3.1
40% BC high	65.47	14.61	85.12	4.16	2.4

4.2.3 Thermogravimetric analyses

The typical thermogravimetric curves for EVA and its composites containing BC in nitrogen and in air, were reported in Figure 22 and Figure 23, respectively. The data obtained from the tests are listed in Table 15. In nitrogen atmosphere, EVA degradation occurs according to two steps. The first step is ascribed to acetic acid release, which takes place between 300 and 390 °C; as a result, the mass loss is proportional to the number of acetate groups that were initially present in the EVA. The chain scission phenomenon is responsible for the second decomposition step, which takes place between 405 and 500 °C [225].

In general, the incorporation of different BCs appears to have no significant influence on T_{max} values compared with unfilled EVA, with a variation of ± 5 °C. Contrary, a slight increase in T_{onset} results was observed due to the protective behavior carried out by the fillers. In particular, this increase reaches 12°C for the composite containing 40 wt.% of BC medium. Finally, it is worth noting that the residues at the end of the test were higher than unfilled EVA and in good agreement with the amount of BC used for preparing the composites.

In air atmosphere, EVA follows a three-step degradation pathway. The oxidation of the products created during the previous steps is the mechanism responsible for the third decomposition step [226]. From a general point of view,

the incorporation of BC into the EVA matrix is responsible for a shift toward higher values of T_{onset}, T_{max1}, and T_{max2}. In particular, the highest values of these temperatures were obtained with BC medium composites. In fact, the T_{onset} of unfilled EVA increased from about 304 to 328 °C, T_{max1} from 337 to 354 °C, and T_{max2} from 431 to 476 °C when 40 wt.% of BC was employed. These results highlight the protective effect of BC particles on oxygen diffusion in the EVA, which can slow down the degradation of the polymer [227]. Rice husk (BC high) accumulates more silicon than oil seed rape (BC medium) in its tissues [228] in the form of silica structures known as phytoliths [229]. Many Si-OH sites are present in these structures, making them ideal for interacting with polysaccharides and glycoproteins [230] that might persist even after the pyrolysis. These acidic silica structures could accelerate the thermo-oxidative degradation of EVA-BC high samples [231], resulting in a reduced stability. Finally, the residues at the end of the tests were in good agreement with the weight loss identified from BC powders in air (Table 13). Consequently, it appears that the nature of the inorganic components and their concentration in the chosen biochars are factors that affect the thermal and thermo-oxidative stability of the obtained composites.

Table 15. Results from thermogravimetric analyses in nitrogen and in air for EVA and its composites.

Atmosphere: nitrogen						
Sample	Tonset [°C]	Tmax1 [°C]	Residue @ Tmax1 [%]	Tmax2 [°C]	Residue @ Tmax2 [%]	Residue @ 700°C [%]
EVA	323	353	92	472	32	0
15% BC low	328	351	94	472	27	13
20% BC low	329	353	92	473	43	16
40% BC low	328	355	93	468	60	35
15% BC med	325	354	92	475	42	11
20% BC med	326	353	92	465	52	12
25% BC med	327	354	92	466	50	10
40% BC med	334	346	93	477	50	36
15% BC high	326	356	93	472	42	12
20% BC high	328	354	92	472	43	15
40% BC high	333	355	92	476	48	30

Atmosphere: air

Sample	Tonset [°C]	Tmax1 [°C]	Residue @ Tmax1 [%]	Tmax2 [°C]	Residue @ Tmax2 [%]	Residue @ 700°C [%]
EVA	304	337	89	431	47	0
15% BC low	308	337	89	433	60	0
20% BC low	311	344	88	439	59	0
40% BC low	322	349	91	453	63	1
15% BC med	320	354	87	475	26	3
20% BC med	320	341	92	475	33	4
25% BC med	324	341	91	474	29	4
40% BC med	328	354	90	476	39	8
15% BC high	309	347	88	431	58	5
20% BC high	312	344	89	453	37	7
40%BC high	319	346	90	467	43	14

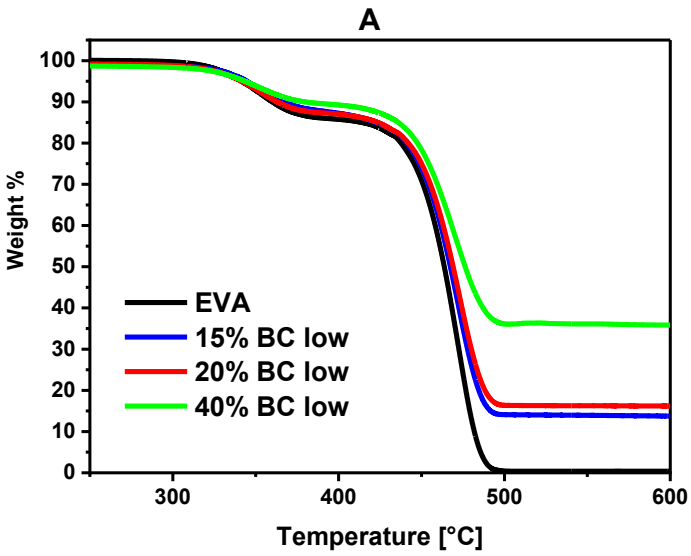
A
Weight %
Temperature [°C]
EVA
15% BC low
20% BC low
40% BC low

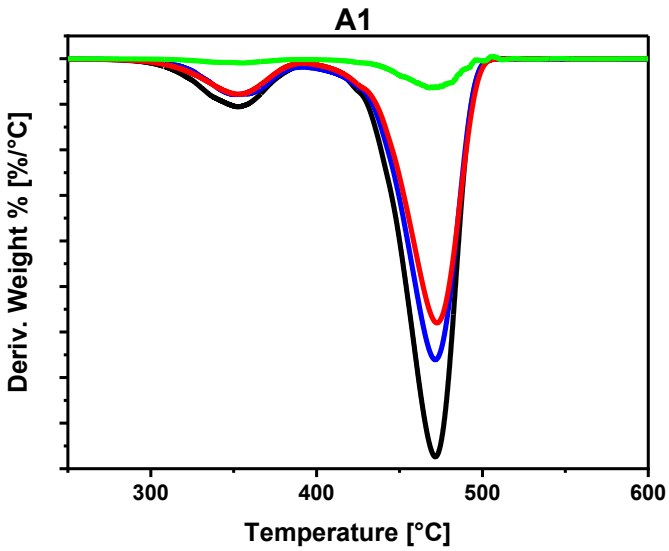
A1
Deriv. Weight % [%/°C]
Temperature [°C]

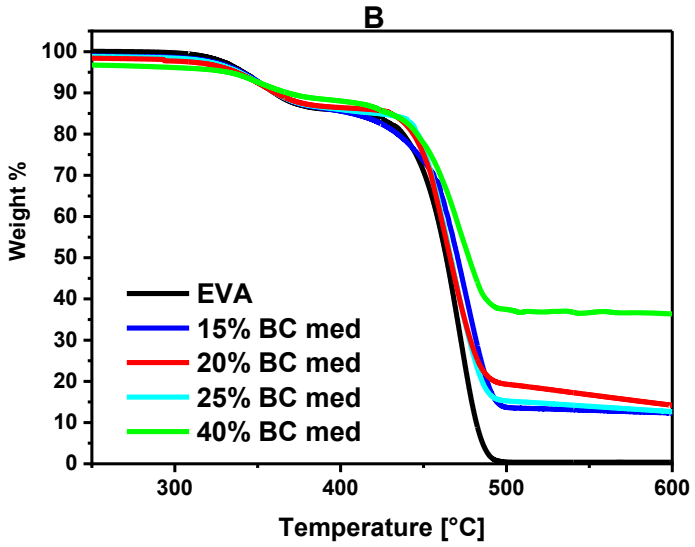
B
Weight %
Temperature [°C]
EVA
15% BC med
20% BC med
25% BC med
40% BC med

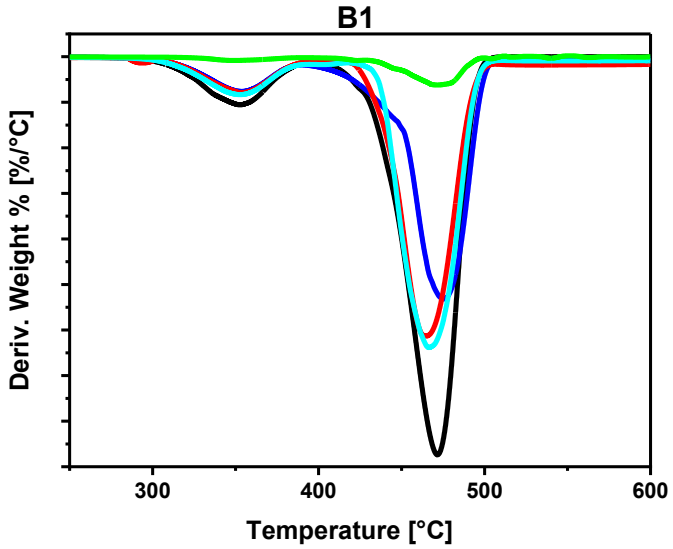
B1
Deriv. Weight % [%/°C]
Temperature [°C]

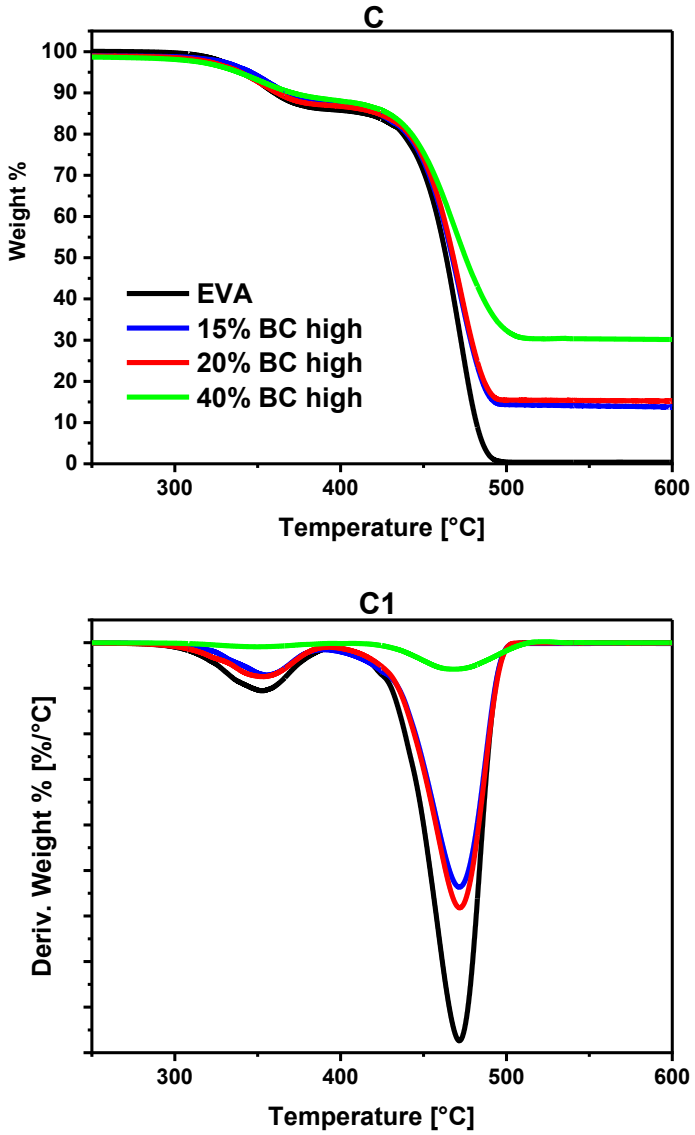

Figure 22. TG (A, B, C) and dTG (A1, B1, C1) curves of EVA and its composites containing BC low, medium and high in nitrogen.

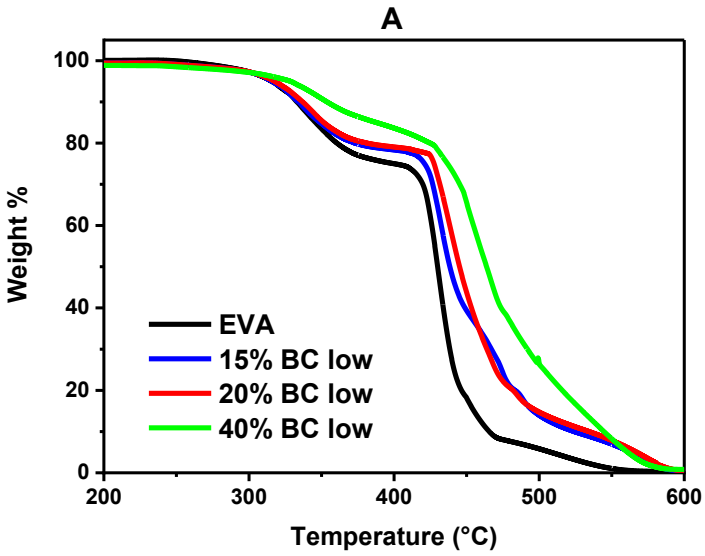
A
Weight %
100
80
60
40
20
0
200
300
400
500
600
Temperature (°C)
EVA
15% BC low
20% BC low
40% BC low

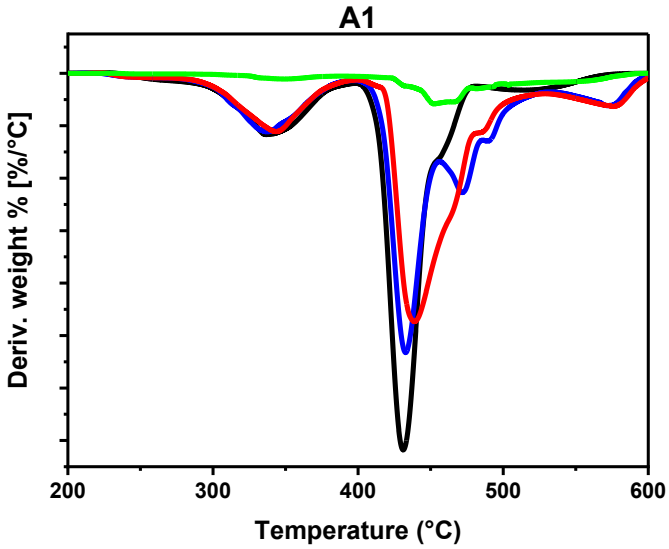
A1
Deriv. weight % [%/°C]
200
300
400
500
600
Temperature (°C)

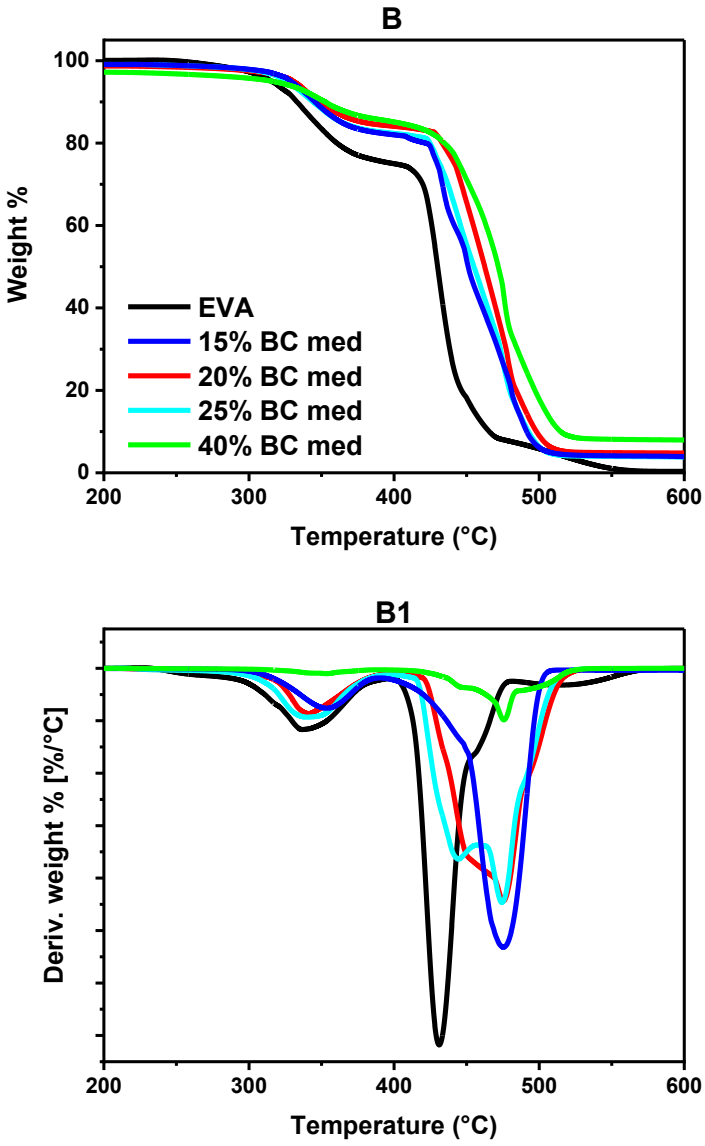
B
Weight %
Temperature (°C)
EVA
15% BC med
20% BC med
25% BC med
40% BC med
B1
Deriv. weight % [%/°C]
Temperature (°C)

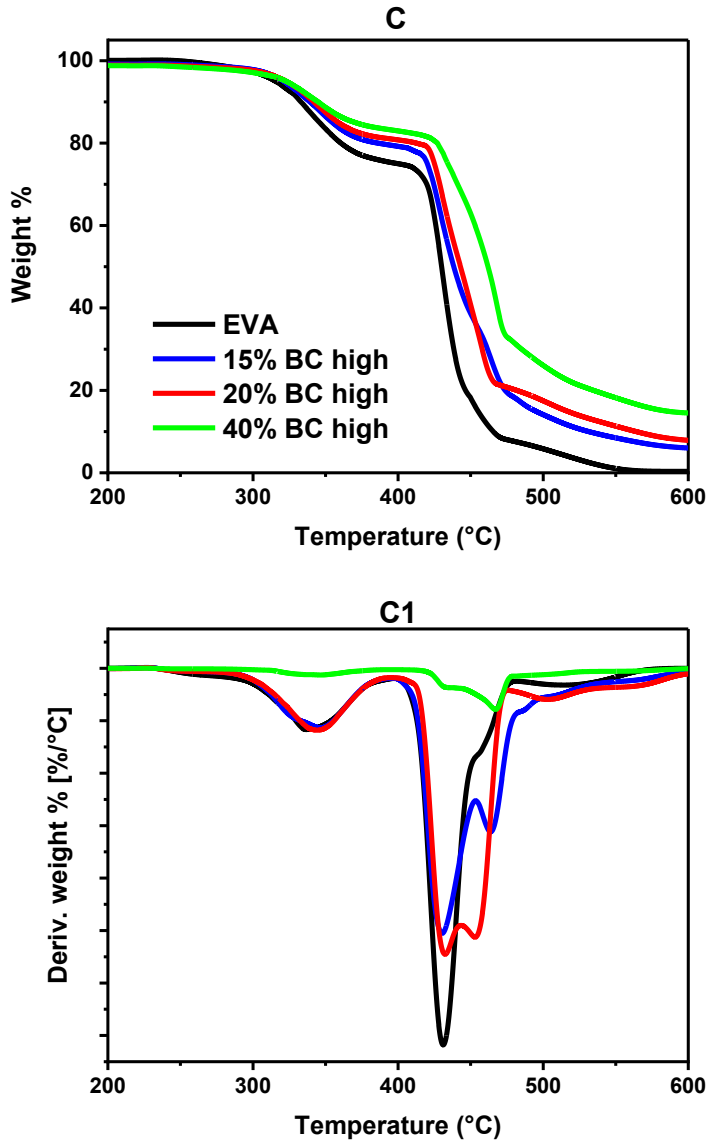

Figure 23. TG (A, B, C) and dTG (A1, B1, C1) curves of EVA and its composites containing BC low, medium and high in air.

4.2.4 Flammability

The flammability behavior of EVA and its composites was evaluated using vertical flame spread tests (UL-94 V). Table 16 lists the results obtained using the setup and the conditions described in the Appendix. Unfilled EVA passed the test with a V-2 rating. The same result was obtained by the specimens filled with 15,

20 and 25 wt.% of BC, regardless of the type of particles used. All the specimens showed abundant melt dripping, which was able to force the flame out of the specimen. The composites, unlike EVA, showed a decrease in after flame times (t_1 and t_2); however, due to the dripping of the melt igniting the cotton, a higher rating was not obtained. In contrast, specimens containing 40 wt.% BC failed the tests, showing a not classified (NC) rating. In fact, after the second application of the flame, the specimens failed to extinguish it and the flame reached the metal clamps, invalidating the test. This finding can be ascribed to the high thermal conductivity provided by the higher amount of BC, which facilitates the propagation of the flame.

Table 16. Average results of vertical burning tests for EVA and EVA/BC specimens.

Sample	t_1 [s]	t_2 [s]	Classification
EVA	12	24	V-2
15% BC low	4	4	V-2
20% BC low	6	10	V-2
40% BC low	12	-	NC
15% BC med	7	2	V-2
20% BC med	10	8	V-2
25% BC med	10	9	V-2
40% BC med	10	-	NC
15% BC high	8	4	V-2
20% BC high	8	9	V-2
40% BC high	14	-	NC

4.2.5 Forced-combustion tests

4.2.5.1 Bulk systems

The combustion behavior of EVA and its composites exposed to an irradiative heat flux was thoroughly studied through cone calorimetry. The setup of the test and the detailed conditions employed are reported in the Appendix. The thermal and the smoke values obtained from the tests were listed in Table 17 and Table

18, respectively. The curves of heat release rate over time are displayed in Figure 24. Each graph shows the set of composites prepared with one type of BC and compares them with unfilled EVA.

In general, the incorporation of BC particles is responsible for the earlier ignition times of the composites compared with unfilled EVA (TTI = 76 s). This behavior, already observed in the scientific literature [232] [67] could be attributed to the higher thermal conductivity of composites. In fact, it implies a high heat diffusion through the specimen which can rise faster the temperatures on the specimen surface, leading to anticipated TTIs. Consequently, the times of peak HRR of the composites were shifted to lower values.

The most relevant effect of flame retardancy carried by the BC was seen in the decrease of the HRR peaks, as well as a variation in the HRR curves, depending on the type and loading of BC. The HRR curve of EVA shows the typical behavior of an unfilled polymer, displaying a single sharp peak. After reaching the maximum HRR value (i.e., the peak of HRR), the curve begins to decrease until all the material is consumed, and then reaches the flame out without leaving any residue.

The introduction of BC particles modifies considerably the HRR curves, more significantly with the increase of the BC content. The samples containing 15, 20, and 25 wt.% of BC show HRR curves that reach a plateau and then decrease much more gradually than unfilled EVA. In particular, the values of pkHRR are lower than those of EVA from 44 to 63 %. These findings highlight the protection effect exerted by the BC particles that are able to create a surface protective layer during combustion. This effect was more pronounced in the curves of specimens containing 40 wt.% of BC. This amount of BC was capable of lowering the pkHRR of EVA from 65 to 74%, depending on the type of filler used. Furthermore, the obtained HRR curves present two distinct peaks: the first one is referred to the formation of char structure. After this peak, the increase in HRR is suppressed and the curve tends to decrease, because of the presence of the effective protective shield. The formed char resists continuous exposure to heat for some time, then cracks form on the surface of the char, which break it down and decrease the thermal barrier effect. As a result, the curve begins to rise, reaching a second peak [233]. In particular, the composites containing BC medium exhibited in the greatest decrease in peak HRR compared with those filled with BC low and BC high. Consequently, BC medium composites presented remarkably decreased FPI (pkHRR/TTI ratio) and FIGRA (pkHRR/time to peak)

values. In addition, the presence of BC decreased the THR values of EVA, especially for specimens containing BC low and BC medium, indicating the formation of a stable carbon layer that protects the polymer matrix from heat exposure. Finally, Table 18 demonstrates that, in general, the addition of BC encourages a decrease in TSR and SEA values.

Table 17. Main thermal parameters by cone calorimetry tests at 35 kw m^{-2}.

Specimen	TTI [s]	pkHRR [kW m^{-2}]	pkHRR Reduction [%]	Time to peak [s]	THR [MJ m^{-2}]	Residue mass [%]	FPI $\left[\frac{(kW/m^2)}{s}\right]$	FIGRA $\left[\frac{(kW/m^2)}{s}\right]$
EVA	74	1803	-	178	97	0	25	10
15% BC low	24	884	51	104	86	7	38	9
20% BC low	27	863	52	112	80	8	33	8
40% BC low	35	624	65	111	77	27	18	6
15% BC med	34	742	59	131	91	8	22	6
20% BC med	36	661	63	117	84	10	19	6
25% BC med	41	706	61	136	89	10	17	5
40% BC med	45	478	74	113	70	18	11	4
15% BC high	37	1008	44	114	96	10	27	9
20% BC high	39	1030	43	139	91	8	27	7
40% BC high	39	534	70	87	72	21	14	6

Table 18. Main smoke parameters by cone calorimetry tests at 35 kw m^{-2}.

Specimen	TSR [m² m^{-2}]	SEA [m² kg^{-1}]	CO yield [kg kg^{-1}]	CO2 yield [kg kg^{-1}]	CO/CO2 ratio
EVA	1280	598	0.0383	3.25	0.0118
15%BC low	955	383	0.0292	2.63	0.0111
20%BC low	870	330	0.0309	2.62	0.0498
40% BC low	996	407	0.0613	2.44	0.0251
15%BC med	1276	517	0.0332	2.72	0.0122
20%BC med	1240	441	0.0316	2.39	0.0132
25% BC med	1248	503	0.0329	2.58	0.0127

40%BC med	1076	508	0.0376	2.52	0.0149
15%BC high	1141	481	0.0445	3.03	0.0147
20%BC high	967	374	0.0363	2.62	0.0139
40% BC high	989	424	0.0322	2.39	0.0135

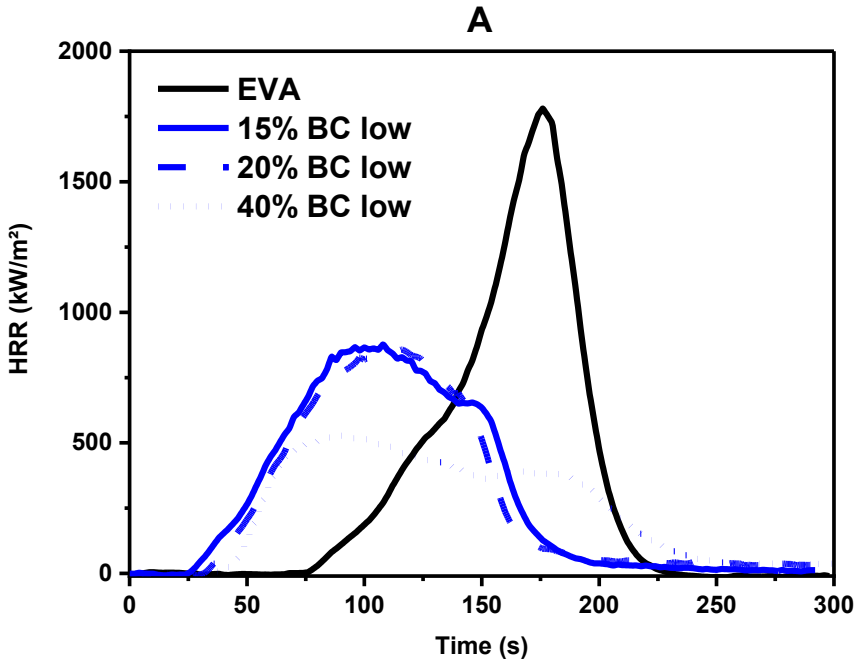

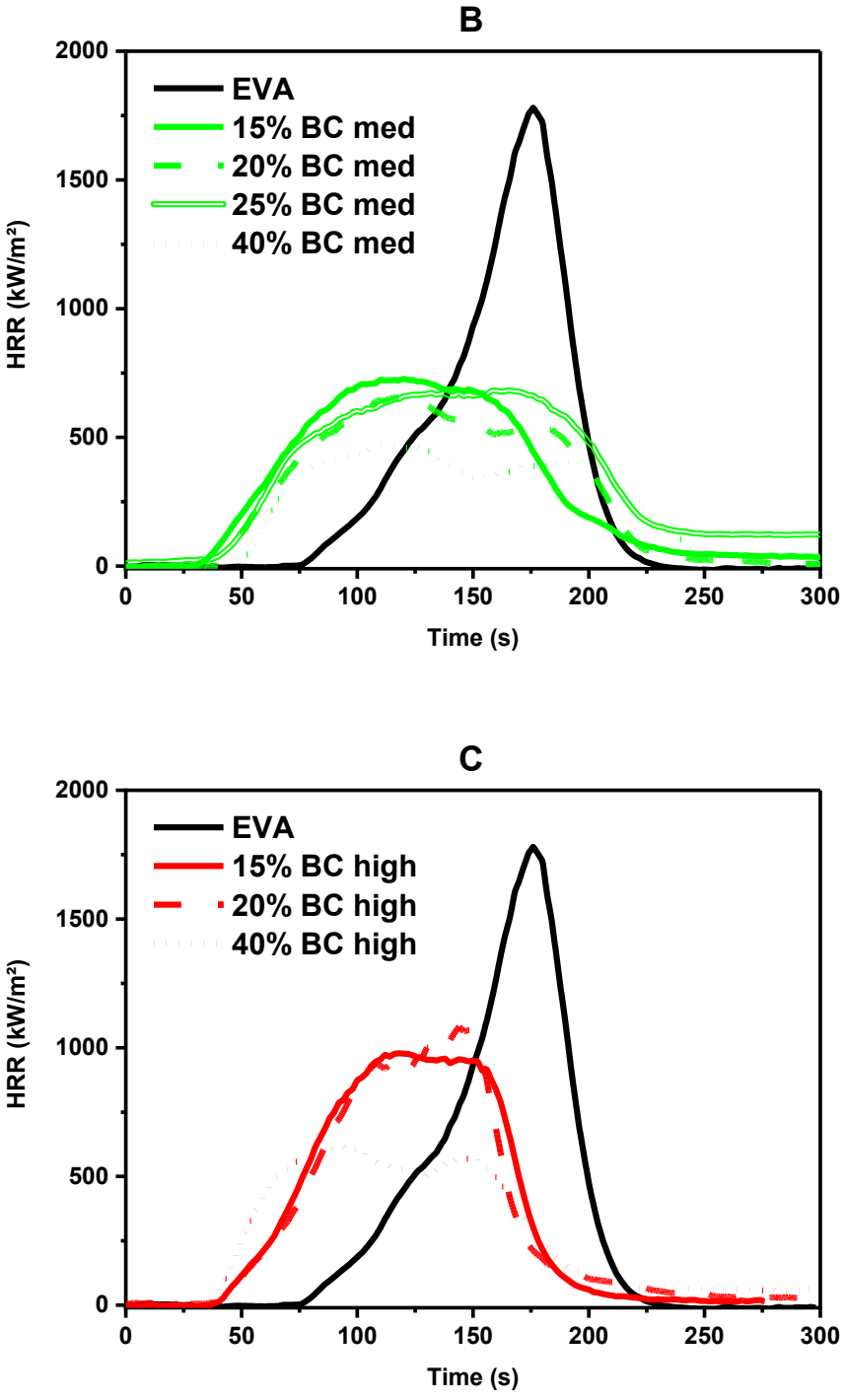

Figure 24. HRR vs. time cone calorimetry curves at 35 kW m^{-2} of EVA and its composites: EVA/BC low (A), EVA/BC medium (B), and EVA/BC high (C).

4.2.5.2 Surface approach

Specimens were prepared using BC from rapeseed, which proved to be the best compromise for pkHRR reduction and TTI delay of EVA in bulk systems (Table 17). The test conditions used were the same as for cone calorimetry of bulk specimens. Table 19 and Figure 25 show, respectively, the results and the HRR vs. time curves of specimens with BC-rich surface layer. From a general point of view, it is worth noting that, compared with EVA, pkHRR is reduced by BC incorporation. This behavior is more pronounced when the 1 mm layer is applied to EVA; in fact, these systems are able to reduce pkHRR by up to 43% compared with that of EVA. In contrast, the TTIs of the 1 mm systems decrease to 38 and 46 s (for 3 and 6 wt. % BC, respectively), while the 0.5 mm layer can reach the ignition at 70 s. This value is very close to that of EVA, which presents a TTI at 74 s. For comparison, the bulk specimens (Table 17) presented lower values of TTI, approximately half in the best cases, compared to unfilled EVA. These results reveal a better fire retardant effect in terms of TTI compared with bulk systems, associated with a decrease in pkHRR of EVA, but with the use of significantly less BC loadings. This behavior can be attributed to a better particle distribution in the surface layer (Figure 20 and Figure 21), which has fewer particle aggregates than bulk systems. In fact, these aggregates act as surface defects, which promote crack propagation within the initial char layer, releasing gases that facilitate specimen ignition [234]. In addition, the surface approach is able to considerably delay pkHRR time compared to EVA samples: as a result, FIGRA values decrease from 31 to 54 %.

Table 19. Main thermal parameters of EVA and surface-confined BC specimens by cone calorimetry test at 35 kw m^{-2}.

Specimen	TTI [s]	pkHRR [kW m^{-2}]	ΔpkHRR [%]	Time to peak [s]	THR [MJ m^{-2}]	Residue mass [%]	FPI $\left[\frac{(kW/m^2)}{s}\right]$	FIGRA $\left[\frac{(kW/m^2)}{s}\right]$
EVA	74	1803	-	178	97	0	25	10
3% BC med (1 mm)	38	1176	35	186	100	2	31	6
6% BC med (1 mm)	46	1036	43	219	95	3	23	5
3% BC med (0.5 mm)	70	1570	13	225	109	1	23	7

6% BC med (0.5 mm)	69	1440	20	230	110	3	21	6

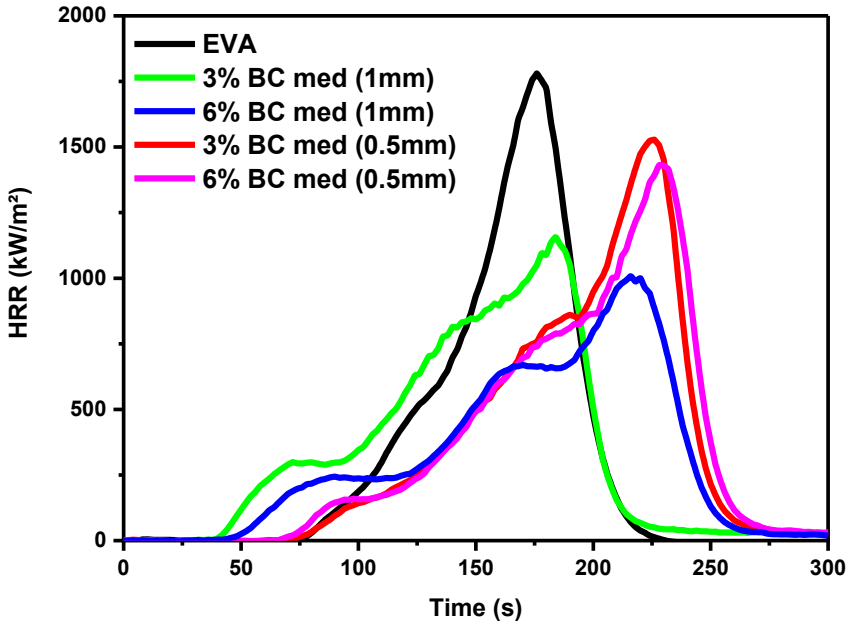

Figure 25. HRR vs. time cone calorimetry curves at 35 kw m^{-2} of EVA specimens containing various amounts of BC from rapeseed confined in a 0.5 or 1 mm thick surface layer.

4.2.6 Tensile tests

Tensile tests on EVA and its composites were performed to determine the impact of the BC particles on the mechanical behavior of EVA. Table 20 summarizes the values in terms of tensile modulus, elongation at break and tensile strength; the typical stress-strain curves as shown in Figure 26. The addition of BC, regardless of its kind and amount, enhances the stiffness of EVA and decreases its ductility. However, elongation at break undergoes a significant drop only with the maximum amount of BC is used: in particular, values between 24 and 26 % for specimens containing 40 wt.% of BC were obtained, compared with

123 % for unfilled EVA. The tensile modulus enhancement is also strong evidence of the BC particles reinforcing effect. In detail, the tensile moduli of 40 wt.% BC specimens reach more than quadruplicate the value of EVA (E = 49.8 MPa), with the highest value using BC high (E = 221.4 MPa). These findings are in agreement with those obtained with EVA filled with traditional flame retardants such as, for example, hydroxides, hydroxycarbonate, ammonium polyphosphate, aluminum trihydrate [23] [235]. In conclusion, BC incorporated into the EVA, is very effective in terms of the overall fire behavior but is also responsible for an important toughness loss, which must be taken into consideration when the flame retarded should undergo mechanical stresses, depending on the final application.

Table 20. Tensile properties of EVA and EVA/BC composites.

Material	Tensile Modulus (E) [MPa]	Std. Dev. [MPa]	Elongation at Break (ε) [%]	Std. Dev. [%]	Tensile Strength (σ_y) [MPa]	Std. Dev. [MPa]
EVA	49.8	2.5	123.1	6.1	6.1	0.1
15% BC low	85.2	3.7	76.7	7.2	5.1	0.2
20% BC low	99.6	2.9	58.2	5.5	5.3	0.3
40% BC low	211.2	10.9	26.0	2.4	8.8	0.4
15% BC med	103.6	3.2	102.4	4.1	9.2	0.1
20% BC med	120.4	1.6	74.7	3.9	7.9	0.3
25% BC med	119.6	1.7	87.5	5.7	8.0	0.1
40% BC med	212.1	28.1	24.2	5.5	7.9	0.7
15% BC high	72.7	2.6	91.8	8.3	5.2	0.1
20% BC high	72.7	3.6	86.9	3.0	5.1	0.2
40% BC high	221.4	23.8	24.3	1.3	8.5	0.6

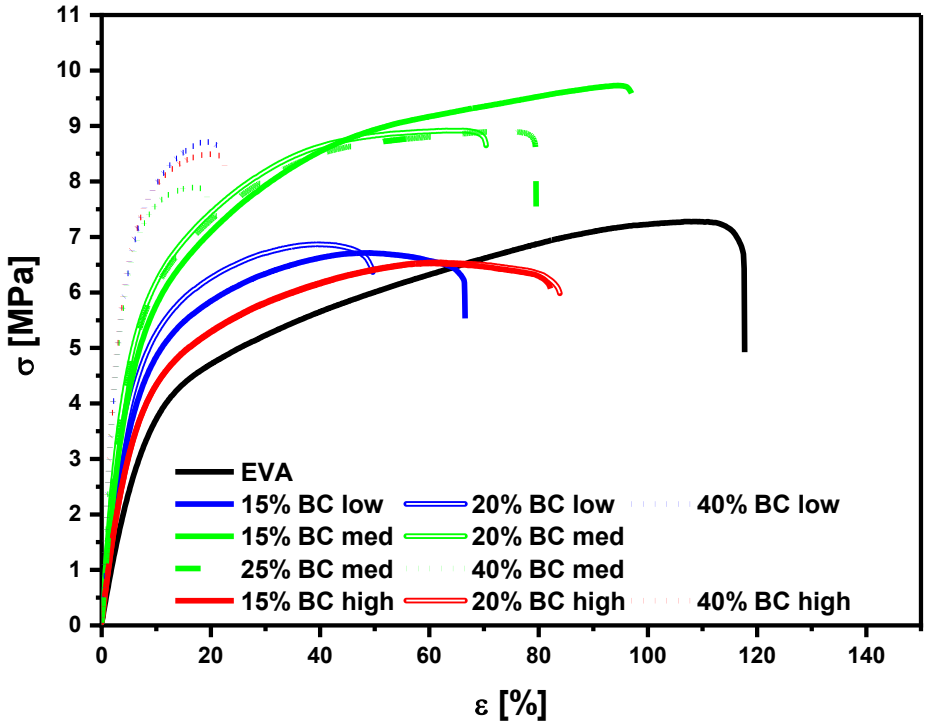

Figure 26. Stress-strain curves for EVA and EVA/BC composites.

Chapter 5

EVA composites containing BC and humic acid

Humic acid (HA) is natural substance with high functionality, which is omnipresent in water, soil, and sediments [236] [237]. Humic acid, as it has been conventionally isolated, is a complex condensed combination of monomers that contains organic acids (from the alkaline or anaerobic digestion of carbohydrates), phenolic groups (from lignin), as well as a significant fraction of hydrocarbons, originating from waxes and fatty acids, and low residues of amino acids [236]. This material is derived from the degradation of both vegetal and animal biomasses present in the soil through biological, physical, and chemical transformation processes [237]. HA is regarded as a potential and affordable source of new materials and high-value goods [238]. Its carbon-rich nature and its skeleton of aliphatic and aromatic units, largely cross-linked by various oxygen-containing functional groups, suggest that humic acid may behave as a new type of charring agent [239]. Consequently, HA has the potential as promising flame retardant for polymers. In this chapter, HA was used in combination with rapeseed-derived biochar, due to its best performance in fire retardancy studied in the previous chapter, as a filler for EVA. In detail, three formulations were prepared by compounding with a total filler amount (BC + HA) of 40 wt. % with various HA/BC ratios, as reported in Table 21. The thermal stability, flame retardancy, and mechanical properties of these materials were investigated.

Table 21. Label and compositions of the prepared formulations containing biochar from rapeseed (BC) and humic acid (HA).

Name	BC (wt. %)	HA (wt. %)
25BC_15HA	25	15
20BC_20HA	20	20
15BC_25HA	15	25

5.1. Characterization of the composites

5.1.1. TGA analyses

Table 22 and Figure 27 report the results and curves of thermogravimetric analysis of EVA and its composites containing biochar and humic acid, respectively. In nitrogen atmosphere, the sample containing the largest amount of BC shows an increased thermal stability in terms of increased $T_{onset,}$ and T_{max2}, compared with unfilled EVA and the other formulations. In addition, the residue at the end of the test was remarkably higher than other formulations (39 vs 25 wt.%), demonstrating an improved barrier effect provided by the BC-HA particles. The TGA results of the formulations with 20 and 15 wt.% BC show similar values and lower thermal stability than the sample with 25-15 wt.% BC-HA.

In air atmosphere, the incorporation of BC and HA into EVA is responsible for a shift toward higher values of T_{onset}, T_{max1}, and T_{max2}. In detail, also in this scenario, the sample containing 25 wt.% of BC and 15 wt.% of HA showed a higher T_{onset} (325.9 °C) compared with EVA and the other formulations. These findings account for an improved thermal and thermo-oxidative behavior for the 25 BC_15HA formulation.

Table 22. Results from thermogravimetric analyses in nitrogen and air for EVA and its composites containing biochar and humic acid.

Atmosphere: nitrogen

Sample	Tonset [°C]	Tmax1 [°C]	Residue @ Tmax1 [%]	Tmax2 [°C]	Residue @ Tmax2 [%]	Residue @ 700°C [%]
EVA	322.5	352.8	91.9	471.6	32.1	0.4
25BC_15HA	335.8	360.3	91.8	475.9	56.6	39.3
20BC_20HA	332.0	350.2	91.6	469.7	54.6	25.4
15BC_25HA	333.4	352.9	90.8	473.6	49.5	24.8
Atmosphere: air						
Sample	**Tonset [°C]**	**Tmax1 [°C]**	**Residue @ Tmax1 [%]**	**Tmax2 [°C]**	**Residue @ Tmax2 [%]**	**Residue @ 700°C [%]**
EVA	304.1	336.9	88.5	431.2	46.9	0.4
25BC_15HA	325.9	348.9	90.8	471.3	48.3	9.7
20BC_20HA	312.4	356.5	86.9	478.9	47.6	8.3
15BC_25HA	319.4	345.7	88.9	478.9	45.7	8.2

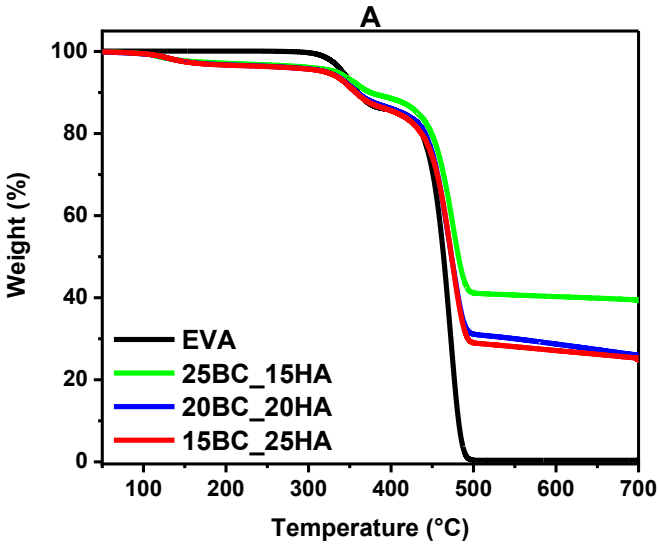
A
Weight (%)
Temperature (°C)
EVA
25BC_15HA
20BC_20HA
15BC_25HA

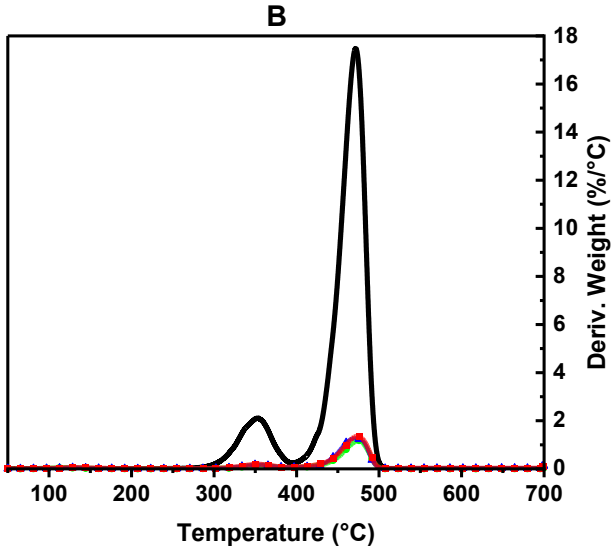
B
Deriv. Weight (%/°C)
Temperature (°C)

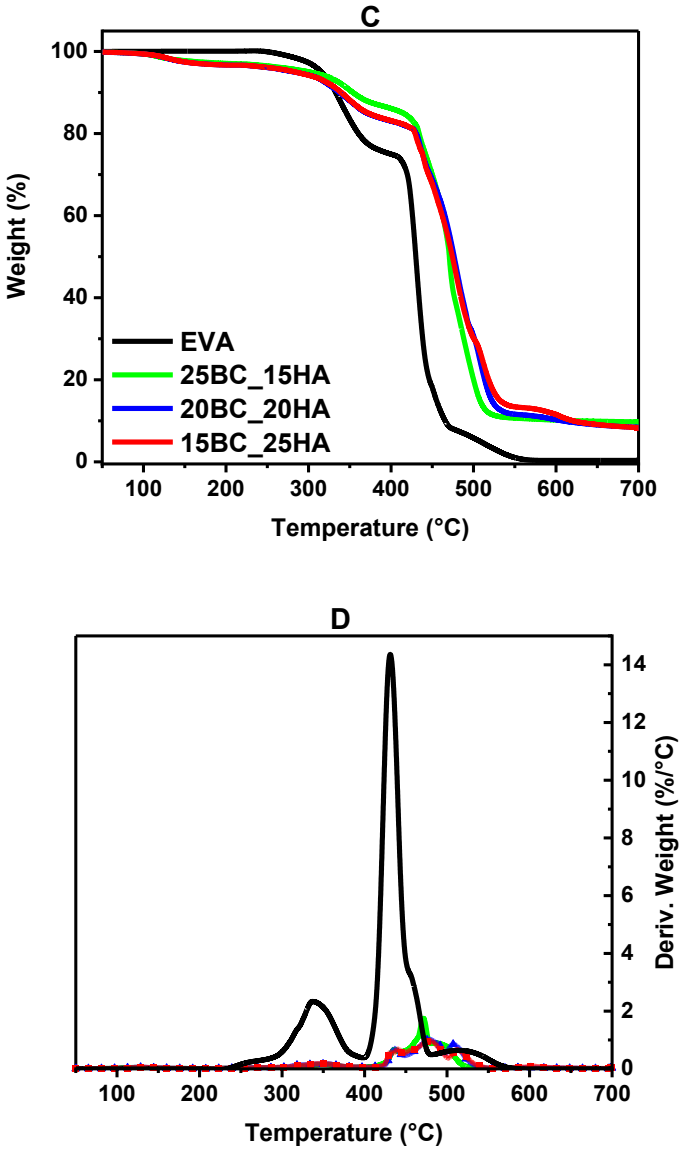

Figure 27. TG and dTG curves of EVA and its composites containing biochar and humic acid in nitrogen (A, B) and in air (C, D).

5.1.2. Cone calorimetry

Table 23 reports the main results from cone calorimetry for EVA and EVA-BC-HA composites, while Figure 28 compares their respective HRR vs. time curves. From a general point of view, the presence of humic acid together with

biochar is effective in increasing the time to ignition and to peak values compared with specimens containing just BC, as shown in the previous chapter (Table 17). In the latter case, the TTI and the time to peak of EVA/BC specimens containing 40 wt.% of BC from rapeseed were recorded at 45 s and 113 s, respectively. In addition, FPI and FIGRA values were significantly lower than unfilled EVA and the other composites containing BC only. Furthermore, composites containing HA presented HRR curves with very low HRR values with respect to unfilled EVA. By comparing these curves each other, the maximum peak decrease is associated with specimens with 25 and 20 wt.% of BC (- 74 and -75 %, respectively). The third specimen, which contained the highest amount of HA (namely 25 wt.%), showed a slightly decreased peak (- 70 %). In this case, it is worth noting that the TTI was higher than that of unfilled EVA (95 vs 83 s), as well as the time to peak (191 vs 168 s). The BC-HA ratio employed was critical for this purpose; it was shown that a predominant amount of BC was beneficial in lowering peak of HRR. In contrast, higher HA loading were able to increase the ignition time of the specimens. This is because HA acts as a charring agent and can promote char formation. By acting as a barrier to the escape of volatile degradation products and the heat and oxygen transfer, the generated char layers can prevent further pyrolysis of the EVA matrix, as already observed in the scientific literature [239].

Table 23. Results from cone calorimetry tests performed on EVA and its composites containing biochar (BC) and humic acid (HA).

Specimen	TTI [s]	pkHRR [kW m^{-2}]	pkHRR Reduction [%]	Time to peak [s]	THR [MJ m^{-2}]	Residue mass [%]	FPI $\left[\frac{(kW/m^2)}{s}\right]$	FIGRA $\left[\frac{(kW/m^2)}{s}\right]$
EVA	83	1737	-	168	91	0.0	21	10
25BC_15HA	69	447	74	191	71	1	7	2
20BC_20HA	65	430	75	142	67	1	6	3
15BC_25HA	95	507	70	180	80	1	5	3

Figure 28. HRR vs. time cone calorimetry curves of EVA and its composites containing biochar

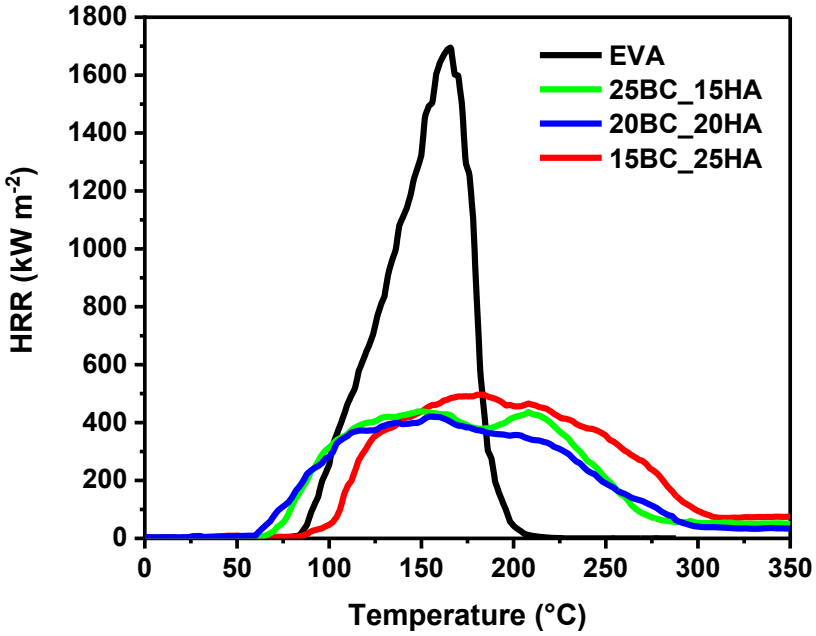

(BC) and humic acid (HA).

5.1.3. Tensile tests

Table 24 reports the results obtained from the tensile tests of EVA and its composites containing BC and HA. From a general point of view, the composites showed increased tensile modulus (2 to 3 times) and lower values of elongation at break than unfilled EVA, as expected. In contrast to the previously tested specimens that showed a tensile modulus above 200 MPa, in this case lower results were gathered, in the range of 97 to 154 MPa. Elongation at break is also variable and decreases when the elastic modulus increases. These results show that the introduction of HA significantly changes the mechanical properties of the EVA polymer compared with that observed with the use of BC alone.

Table 24. Results of tensile tests of EVA and its composites containing BC and HA.

Sample	Tensile modulus (E) [MPa]	Elongation at break (ε) [%]
EVA	50 ± 2	123 ± 6
25BC_15HA	97 ± 20	44 ± 9
20BC_20HA	154 ± 5	29 ± 1
15BC_25HA	103 ± 21	48 ± 5

Chapter 6

EVA composites containing char from Tetra Pak®

Part of the work described in the Chapter 4 has been previously published in:

"Matta S., Bartoli M., Arrigo A., Frache A., Malucelli G. Flame retardant potential of Tetra Pak®-derived biochar for ethylene-vinyl-acetate copolymers. Composites Part C: Open Access. 2022" [240]

Due to the variability of the waste streams, recycling composite materials is a very challenging task in the field of waste management [241]. Tetra Pak® is the most popular multilayered packaging composite because of excellent mechano-chemical resistance [242] and compatibility with several foods and beverages [243]. Tetra Pak® is difficult to dispose of as it contains paper, aluminum foils, and polyethylene, all at once. Since Tetra Pak® was introduced to the market, industrial and academic research have paid close attention to what would happen to its end of use [244]. Tetra Pak® waste streams have been the subject of many attempts to valorize them and prevent them from landfill confinement. Tetra Pak® waste streams can be specifically controlled by reusing the material after grinding as filler for cementitious matrices [245] [246] and wood laminates [247], by isolating the various constituents [248] [249], or by undergoing conversion processes. According to the literature [250] [251], hydrolytic procedures for the

recovery of cellulose nanocrystals from the paper layers constitute a potential Tetra Pak® waste-stream conversion route. However, this approach has a high cost for product isolation and is unable to effectively handle the poly(ethylene) and aluminum fractions. In contrast, pyrolysis offers a more durable option for the generation of fuels and chemicals [252] [253] as well as a highly energy-efficient [254] [255] method for the long-term disposal of Tetra Pak®. Using various reactors and processing methods, a few studies showed that BC may be produced from the pyrolysis of Tetra Pak® wastes [256] [257] [258] [259] [260]. Huo et al. [257], using a pyrolysis process at 550 °C, succeeded in separating aluminum foil from char derived from paper and from polyethylene. Then, they obtained porous carbons using different processing steps, including carbonization at 850 °C. Tetra Pak®-derived BC is distinguished from pure biomass-derived BC by a high inorganic percentage caused by the aluminum foils, which is undesirable for soil usage but may be advantageous for the design of composites with improved flame retardancy [261] [262] [263].

This chapter describes the pyrolysis process of Tetra Pak® to obtain alumina-rich biochar. The BC achieved was used as a filler for EVA copolymer and the flame retardant behavior of the resulting composites was investigated. In detail, two different systems were prepared. In the first method, the BC was incorporated in bulk EVA using the compound technique. In the second method, the obtained composite was applied onto the surface of unfilled EVA specimens. Then, the two systems were studied, and the flame retardants properties were evaluated.

6.1 BC characterization

The waste multilayers packaging was treated by pyrolysis, following the different steps schematized in Figure 29.

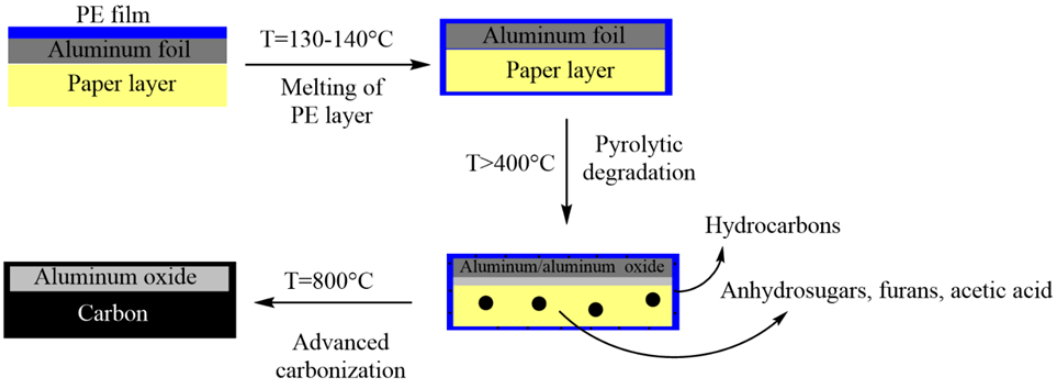

Figure 29. Schematic pathway of Tetra Pak® pyrolysis for BC production.

In the first step, carried out at temperatures of 130-140 °C, the poly(ethylene) layers are subjected to melting, creating a homogeneous environment for the subsequent pyrolytic degradation that happens above 400 °C. Under these conditions, cellulose degrades with the release of anhydrosugars and furans, which go through additional degradative processes and result in a significant amount of acetic acid formation [264]. The presence of inorganic oxides in the aluminum foil of Tetra Pak® can enhance this last mechanism [265]. The last step, occuring at high temperatures (i.e., T = 800 °C) combined with the acidic atmosphere, can lead to the oxidation of the aluminium layer with consequent formation of alumina, as shown by XPS analysis (Figure 30). Figure 30b clearly shows that the alumina (Al2p signal, 75.4 eV), reaching 74% of abundance, accounts for the majority of aluminum compounds. In addition, the O1s component (peak at 531.1 eV) also indicates its presence. The presence of further aluminum species, for example $Al_2(CO_3)_3$, can be excluded because of the instability of such compounds [266] and the absence of peaks ascribed to AlOOH or $Al(OH)_3$ [267]. The XPS spectra of biochar carbon composites (Figure 30a) show the large amount of sp^2 carbon (284.7 eV) tailored with hydroxyl (C1s 285.8 eV, O2p 532.1 eV) and carboxylic (C1s 289.2 eV, O2p 533.2 eV) functionalities and the absence of sp^3 species.

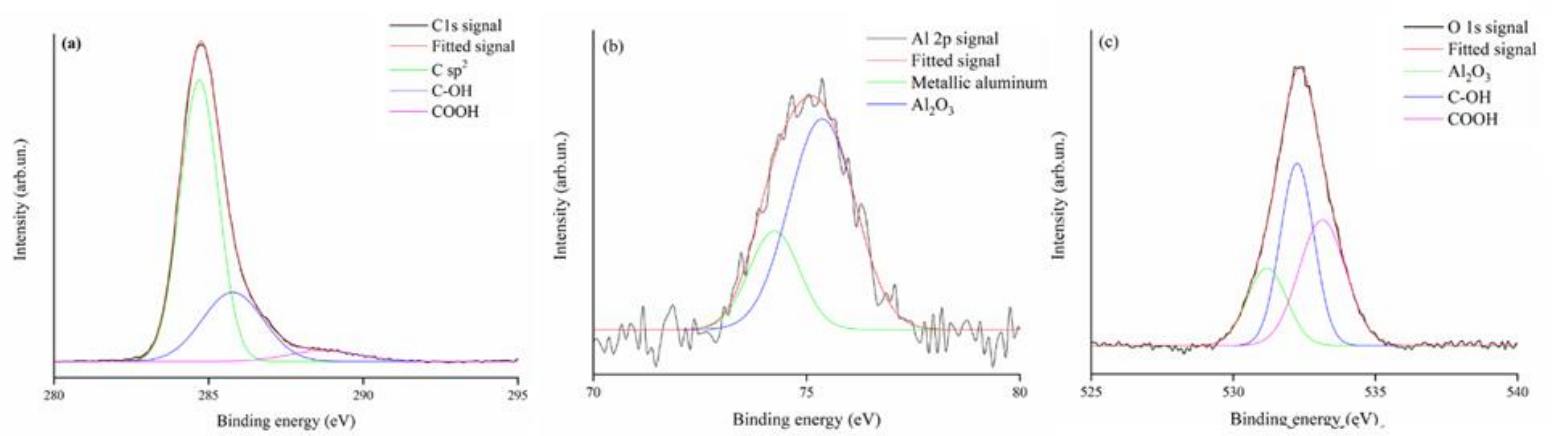

Figure 30. XPS spectra of a) carbon, b) aluminum and c) oxygen of BC.

Raman spectra in Figure 31 demonstrate how the significant amount of sp^2 carbon led to the formation of quite organized carbonaceous materials. BC from Tetra Pak® shows sharper D and G peaks with respect to that obtained at temperatures between 700 and 1000 °C [268], and presents a partially structured 2D region and I_D/I_G ratio value of 1.1. These results can be ascribed to the advanced carbonization process supported by the synergistic effect of the homogenous pyrolytic environment given by the poly(ethylene) melted together with the aluminum compounds.

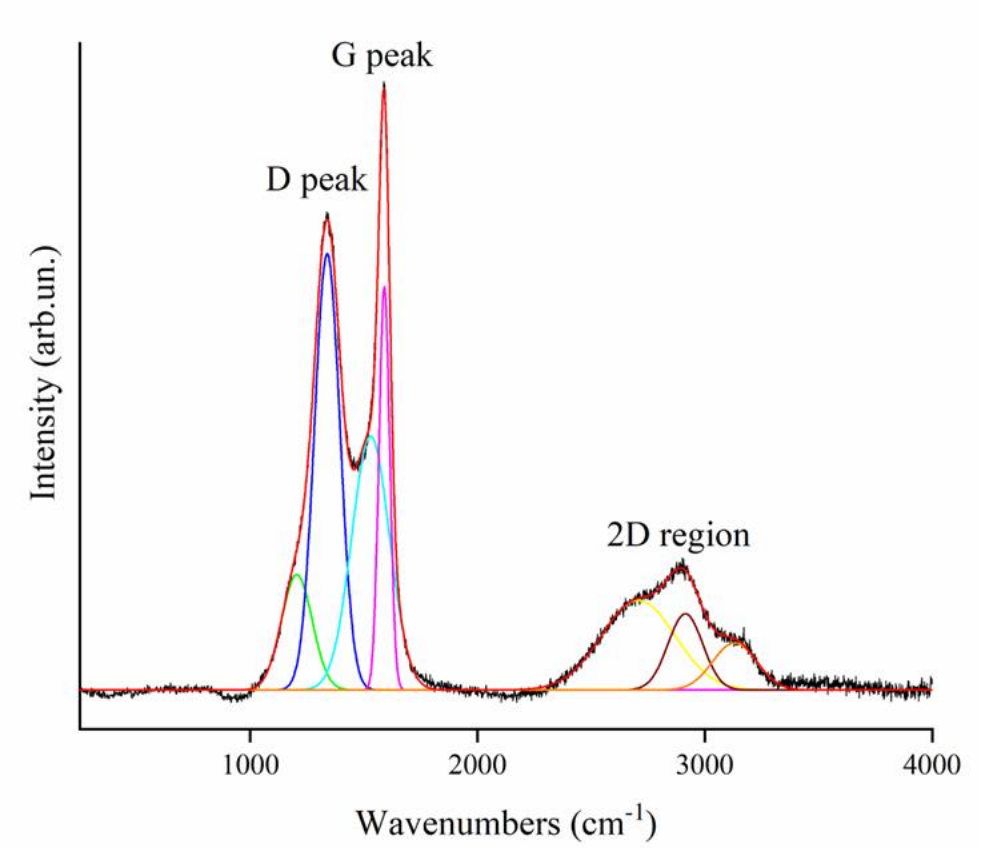

Figure 31. Raman spectra of BC in the range from 500 cm^{-1} up to 4000 cm^{-1}.

The FESEM images in Figure 32 further help to understand the distinctive properties of BC derived from Tetra Pak®. BC exhibits a morphology made up of micrometric and sub-micrometric carbon particles with an average radius of 1.2 ± 0.2 mm, arranged in structures between 1 and 10 mm in size. Figure 32a displays aluminum-rich flakes that are quite uniformly dispersed. Nevertheless, EDX analysis performed in areas 1 and 2 of Figure 32 demonstrates that great differences are visible at a sub-micrometric scale. Table 25 lists the chemical elements found in these two areas, highlighting an aluminum-rich zone (Region 1) and a carbon-rich zone (Region 2). Region 1 presents a carbon content of 24 wt.%, which supports the hypothesis that in this scenario a carbon layer is mixed with the aluminum flakes. There, the aluminum amount reaches 51.4 wt. %, while in region 2 the Al found was negligible (i.e., 0.5 wt. %). Among other elements found, the presence of Calcium and Silicon can be attributed to the paper layer of Tetra Pak®, as these elements are commonly present during paper processing [269].

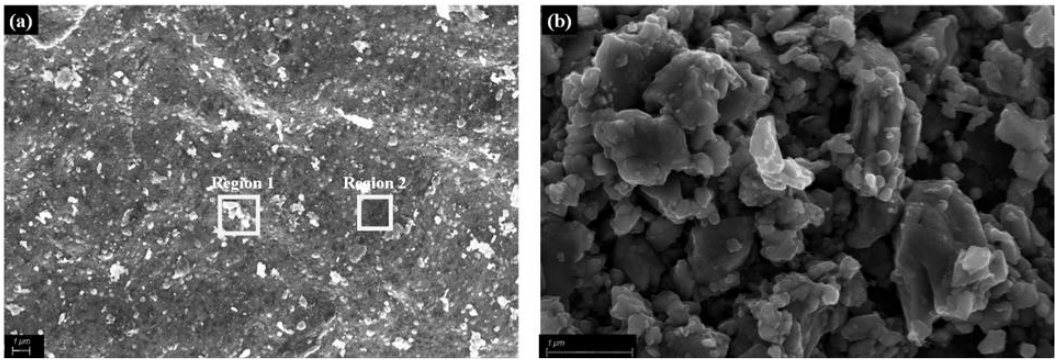

Figure 32. FESEM capture of BC with magnification of a) 0.5K and b) 20K. Aluminum- (region 1) and carbon-rich (region 2) regions are highlighted in white.

Table 25. Elemental composition obtained through EDX analysis of region 1 and region 2 of BC.

Element	Weight (%)	
	Region 1	Region 2
Carbon	24.5	60.4
Oxygen	22.3	27.9
Aluminum	51.4	0.5
Silicon	0.2	1.3
Calcium	0.2	8.8
Sodium	1.3	1.1

Figure 33 presents the typical thermogravimetric curves for BC in both nitrogen and air atmospheres. In inert environment (Figure 33a), the BC showed highly stable behavior, exhibiting about 2 % of mass loss during the heating up to 800 °C. In air atmosphere, the thermo-oxidative degradation takes place in two different phases. The first step occurs in the range of temperature between 350 and 570 °C, while the second one takes place at temperatures between 630 and 700 °C. Above 700 °C, BC is thermally stable, which account for a final residue of about 35 wt.% at 800 °C.

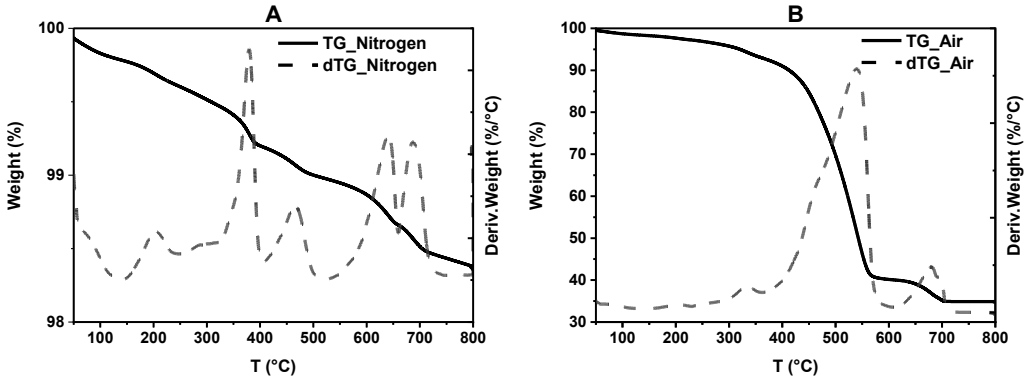

Figure 33. TG and dTG curves of BC from Tetrapak in nitrogen (A) and in air (B).

6.2 Composites characterization

6.2.1 Morphological investigations

SEM analysis were performed on EVA-BC composites in order to assess the particle morphology and their distribution within EVA. EDX micro-analyses were performed on the composites to further study the dispersion of the particles into EVA. Figure 34 displays the SEM images at different magnifications of the composites containing 20 and 40 wt.% of BC. The BC is well distributed within the EVA and its size is basically micrometric and submicrometric, according to the average particle size of BC, though some aggregates up to 100 μm can be identified. These results show that the conditions of compounding process were appropriate for achieving a fairly homogeneous dispersion of the BC within EVA. The EDX maps of the main elements contained in the BC were exploited to support the good distribution of BC in EVA (Figure 35).

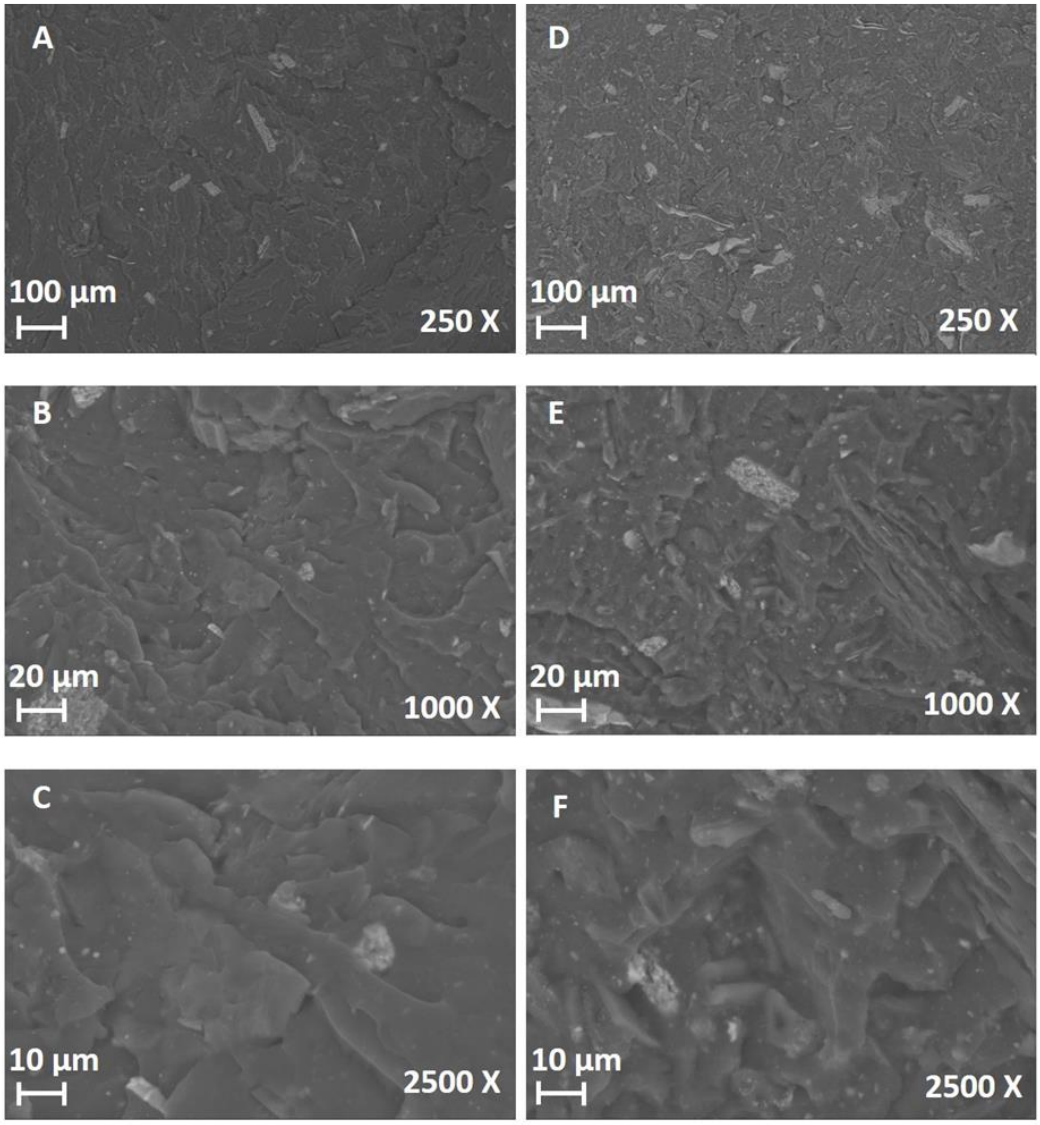

Figure 34. SEM images at different magnification of the bulk composites containing 20 wt.% (A, B, C) and 40 wt.% (D, E, F) of BC.

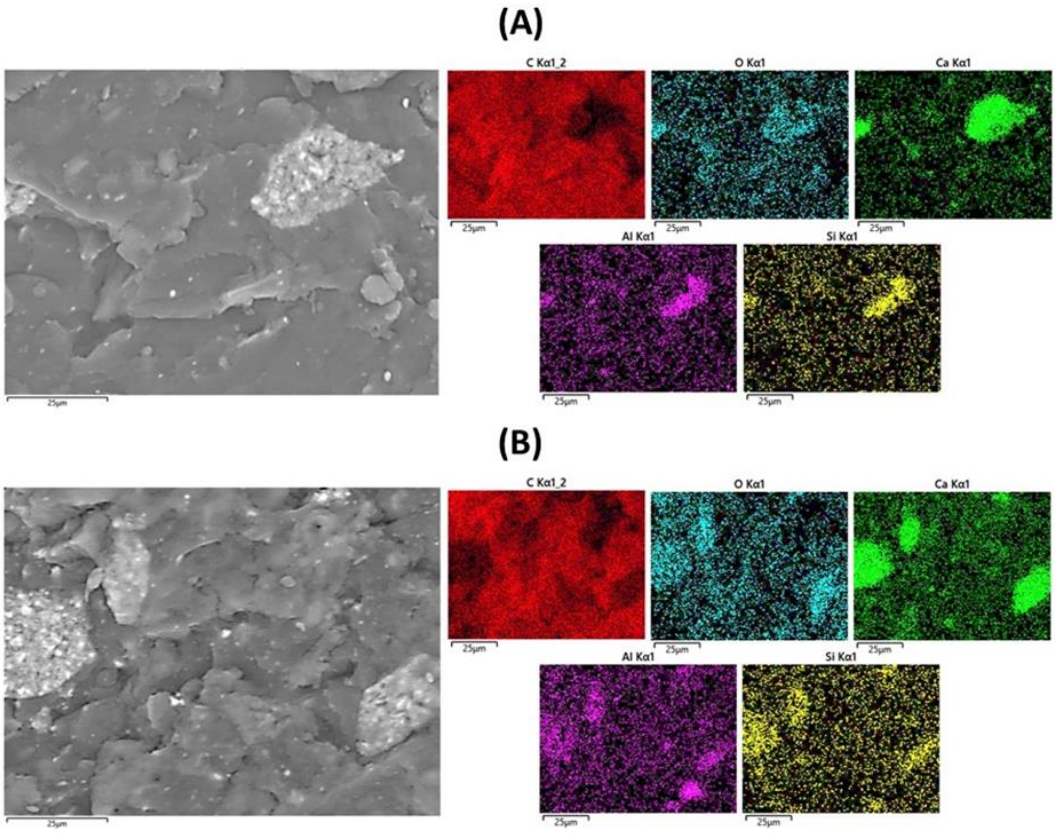

Figure 35. EDX maps of the elements included in biochar for the bulk composites containing 20 wt.% (A) and 40 wt.% (B) of BC.

Furthermore, the SEM analyses were carried out on the cross-sections of the specimens with BC dispersed on their surface (Figure 36). Regardless of the amount of BC, which was 3 and 6 wt.%, the coatings presented a thickness of about 500 µm. Furthermore, the images show a marked separation between the coating and the underlying polymer. Finally, the particle distribution in these samples was also homogeneous, except for some larger aggregates up to 100 µm.

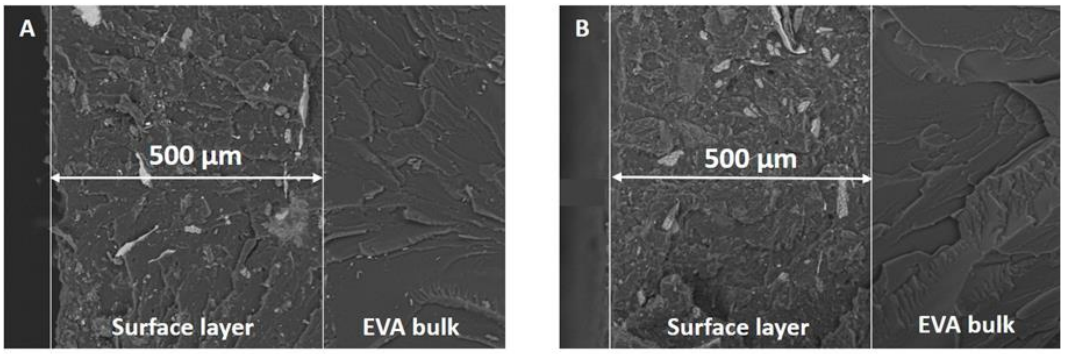

Figure 36. EVA coated with EVA layers containing 3 wt.% (A) and 6 wt.% (B) of BC.

6.2.2 Rheological analyses

The complex viscosity curves of EVA and its composites containing BC are reported in Figure 37. Unfilled EVA shows the typical viscosity behavior of the thermoplastic polymers: a Newtonian trend was observed in the low-frequency region, followed by the shear-tinning zone that results in a rapid decrease in complex viscosity values with respect to frequency. In the low-frequency range, the addition of 20 wt.% of BC results in a slight improvement of the complex viscosity values compared to the EVA matrix but has a limited effect on the rheological response of the material at high frequencies. Higher complex viscosity values are observed throughout the whole tested frequency range for 40 wt.% BC composites, although the frequency dependence of the viscosity curve corresponds quite closely to that of an unfilled matrix. According to scientific literature for polymers containing micrometric BC particles [155], these findings indicate a modest impact of the filler on the relaxation dynamics of EVA. In conclusion, the rheological performance of these materials seems principally governed by the viscoelastic response of matrix macromolecules.

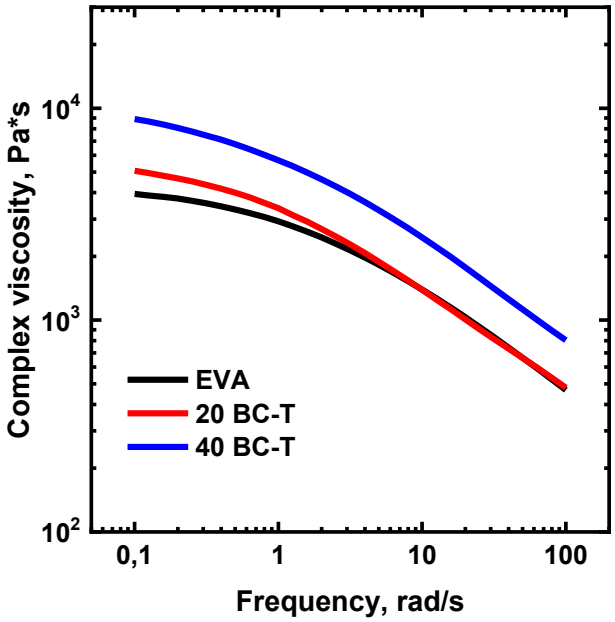

Figure 37. Complex viscosity curves for EVA and BC-containing composites.

6.2.3 DSC analyses

Table 26 collects the main DSC data from each selected thermal cycle for EVA and its composites. The melting peak at 85.3 °C as well as the crystallization temperature at 62.7 °C were substantially not influenced by the presence of BC, regardless its amount. In contrast, the crystallinity of unfilled EVA showed a slight decrease due to the BC incorporation. These results agreed with the values obtained in the previous chapter from BCs derived from different biomasses.

Table 26. Results from DSC analyses for EVA and its composites with BC.

Sample	Tc (°C)	ΔHc (J/g)	Tm (°C)	ΔHm (J/g)	Xc (%)
EVA	62.7	27.6	85.3	13.2	4.5
20 BC-T	64.6	22.3	85.4	7.2	3.1
40 BC-T	64.9	11.9	85.0	5.3	3.0

6.2.4 Thermogravimetric analyses

The typical TG and DTG curves for EVA and for its composites containing BC are shown in Figure 38. The main results obtained in nitrogen and air atmosphere are listed in Table 27.

In nitrogen, the presence of BC accounted for a slight increase in the T_{onset} values, implying limited protection exerted by the filler. In addition, the amount of final residue increased significantly for the BC composites due to the high inorganic content introduced by BC. However, as displayed in paragraph 6.1, the TGA of BC in inert atmosphere highlighted a weight loss about 2 wt.% at 800 °C, so the obtained residue values do not correspond to the initial amount of filler incorporated into EVA (i.e., 20 and 40 wt.%). This finding can be explained by interactions with the polymer that cause the BC to lose thermal stability.

In air atmosphere, the inclusion of BC results in increased values of T_{onset}, T_{max1} and T_{max2}, highlighting the protective effect exerted by the filler. The sample containing 40 wt.% of BC was more effective in raising T_{onset} and T_{max1} than its counterpart filled at 20 wt.%, reaching values similar to EVA in inert atmosphere. This behavior emphasizes the barrier effect of the particles on oxygen diffusion in the polymer, which has already been documented in the scientific literature [227]. The interactions occurring between EVA and BC particles were studied by calculating the theoretical TG curves of samples at 20 and 40 wt.% of BC and comparing the obtained curves with their respective experimental curves (Figure 39). For the 20 wt.% BC sample, the first phase associated with acetic acid release follows the same trend for both experimental and calculated curves. In contrast, the second phase of weight loss due to the degradation of the unsaturated chains (from 405 to 480 °C) was observed at higher temperatures for the experimental curve. This delay emphasizes again the barrier effect created by the filler. The 40 wt.% BC samples demonstrate a higher interaction between EVA and BC particles as the experimental curve showed a higher thermo-oxidative stability since the starting of degradation. The barrier effect toward oxygen is reduced at higher temperatures ($T > 450$ °C), probably because of the presence of particle aggregates, as shown in SEM images. The calculated final residues were in agreement with those obtained from TG analysis, confirming the amount of BC contained in the samples.

Table 27. Results from thermogravimetric analyses in nitrogen and air for EVA and its composites.

Atmosphere: nitrogen

Sample	Tonset [°C]	Tmax1 [°C]	Residue @ Tmax1 [%]	Tmax2 [°C]	Residue @ Tmax2 [%]	Residue @ 800°C [%]
EVA	322.5	352.8	91.9	471.6	32.1	0.3
20 BC-T	325.2	347.7	93.1	471.5	42.0	13.6
40 BC-T	333.7	354.0	92.8	472.8	51.5	27.1

Atmosphere: air

Sample	Tonset [°C]	Tmax1 [°C]	Residue @ Tmax1 [%]	Tmax2 [°C]	Residue @ Tmax2 [%]	Residue @ 800°C [%]
EVA	304.1	336.9	88.5	431.2	46.9	0.2
20 BC-T	310.0	338.5	89.4	471.5	29.2	5.8
40 BC-T	322.3	347.5	91.7	459.1	45.6	15.7

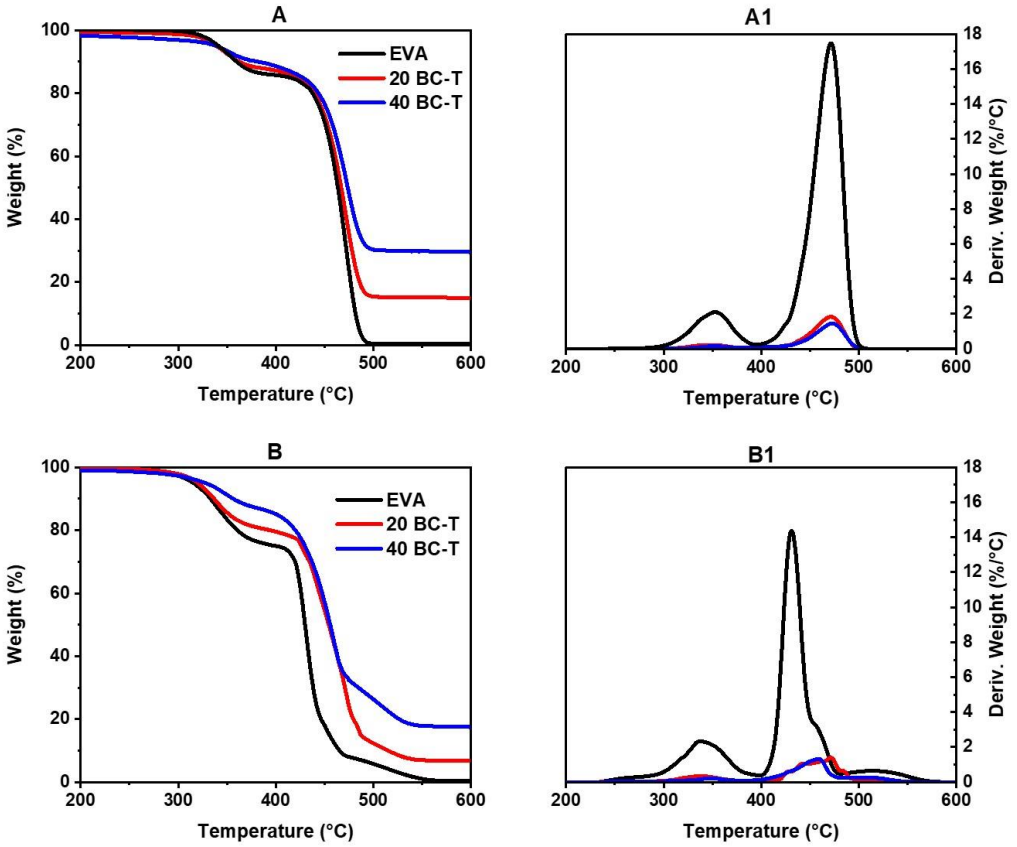

Figure 38. TG and dTG curves of EVA and its composites in nitrogen (A, A1) and in air (B, B1).

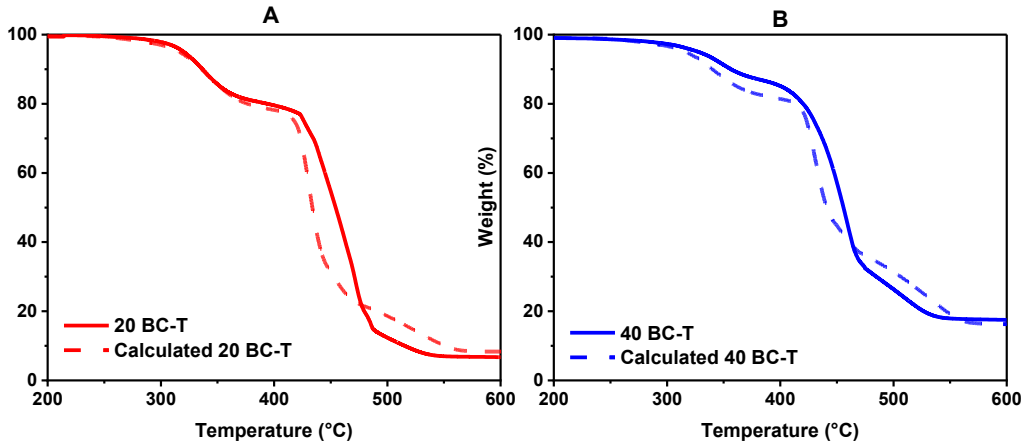

Figure 39. Comparison between the experimental and calculated TG curves in air for 20 BC-T and 40 BC-T composites.

6.2.5 Cone calorimetry

Table 28 shows the main parameters provided by cone calorimetry on EVA and its composites; Figure 40 shows their HRR vs. time curves. The most noticeable effect of incorporating BC into EVA is the decrease in pkHRR compared to the unfilled copolymer. In detail, this behavior was more pronounced with the increase of BC from 20 to 40 wt.%: the reduction observed was, respectively, by 45 and 65 % compared with unfilled EVA. As a consequence, also FPI (pkHRR/TTI ratio) and FIGRA (pkHRR/time to peak) values were also significantly lowered with respect to EVA. In addition, the protection provided by BC was confirmed by the decrease of THR values of composites. Indeed, as already discussed in the previous chapters, the BC creates a protective surface layer during combustion which is able to slow down the degradation, acting as a thermal and mass transfer barrier. This effect was clearly visible in the shape of HRR curves of composites: the typical two-peaks curves, due to char formation, can be seen both in 20 and 40 wt.% specimens. Among them, the specimen with the highest BC loading shows a curve with two peaks that are sharper and more separated from each other, indicating enhanced charring ability.

Table 28. Results from cone calorimetry tests performed on EVA and its composites.

Specimen	TTI [s]	pkHRR [kW m^{-2}]	pkHRR Reduction [%]	Time to peak [s]	THR [MJ m^{-2}]	Residue mass [%]	FPI $\left[\frac{(kW/m^2)}{s}\right]$	FIGRA $\left[\frac{(kW/m^2)}{s}\right]$	FRI
EVA	74	1803	-	178	96.6	0	24.8	10.1	-
20 BC-T	44	993	45	142	92.9	6	22.6	7.0	1.12
40 BC-T	43	635	65	105	80.3	20	14.8	6.0	1.98
3 BC-T_sup	112	1405	22	226	111.1	1	12.5	6.2	1.69
6 BC-T_sup	66	1194	34	208	112.5	3	18.1	5.7	1.16

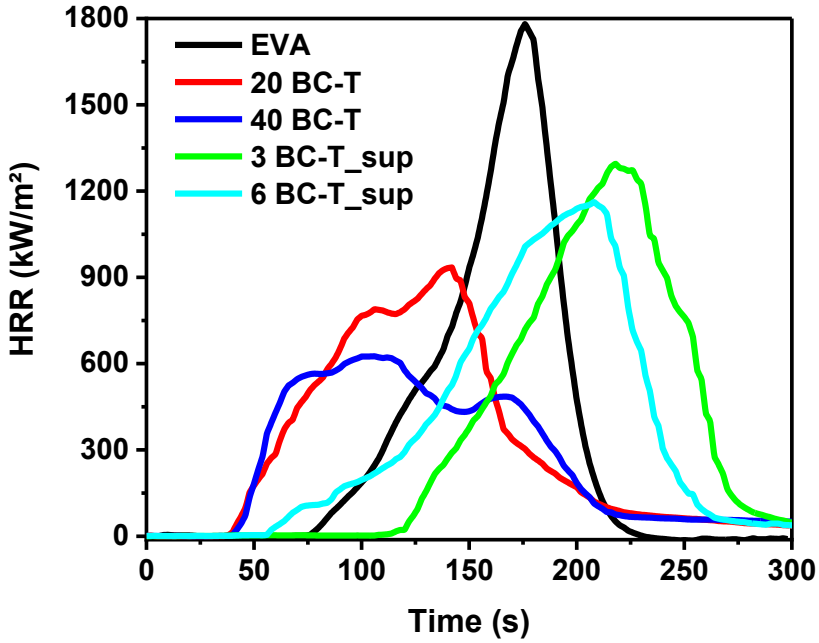

Figure 40. HRR vs. time cone calorimetry curves of EVA, its bulk composites and its surface-coated samples.

The cone calorimetry analyses were also carried out on the surface-coated specimens: the obtained data were reported in Table 28 and the HRR curves are shown in Figure 40. From an overall point of view, it is worth noting that the results between bulk incorporation and surface dispersion of BC are noticeably different when comparing the times to ignition of the specimens. In bulk systems, both TTIs and times to peak were anticipated by the presence of BC with respect to unfilled EVA, with similar TTI values for 20 and 40 wt.% of BC composites, as already reported in the scientific literature [218] [232]. Otherwise, the specimens with BC distributed as a surface coating showed delayed TTIs. The specimen with 3 wt.% of BC surface-distributed exhibited better performance in retarding the ignition than the counterpart containing 6 wt.% of filler. In fact, the lower BC content was able to increase the TTI up to 112 s, probably due to the better BC dispersion caused by a lower loading. Therefore, a larger amount of BC can lead to the easy formation of particle aggregates on the specimen surface. These aggregates act as defects that promote the breaking of the initial char skin and cause the release of the gases needed to ignite the specimen [234]. This hypothesis was supported by the analysis of the particle distribution on the surface of the

coated samples. On specimens with 3 and 6 wt.% of BC-coating, the BC particle distribution was detected by software and their total occupied areas were calculated. Figure 41 shows the obtained images of the particles on the specimen surface. The calculated total occupied area by BC for 3 and 6 wt.% of BC showed values of 2.14 and 4.86 %, respectively. However, the presence of numerous particle aggregates was clearly visible in the specimen containing 6 wt.% of BC, compared to the 3 wt.% specimens, in line with the previous hypothesis. Furthermore, the reduction of TTI from 112 to 66 s with the increase in biochar amount can also be ascribed to the increase in thermal conductivity, because of the accumulation of not-oxidized metal particles on the surface. As a consequence of the ignition delay, also the times to peak for both coated specimens show remarkably higher values compared to unfilled EVA and bulk specimens. Furthermore, each flame retardant system investigated exhibits a Flame Retardancy Index (FRI, Table 28) value that is in the range 1 – 10, so it was classified as "good" [270]. Finally, the cracks formation during the combustion test on the exposed surface of coated specimens limits the protection provided to the underlying unfilled polymer. As result, the HRR peak values recorded for these systems were higher than for specimens with bulk incorporation of BC, indicating a better performance for the latter.

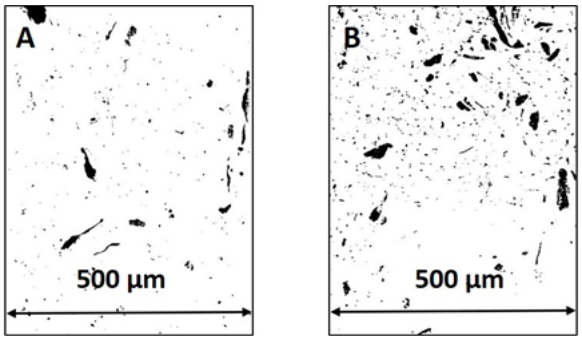

Figure 41. Detected particles of BC from SEM images of EVA specimens of Figure 36(a) and Figure 36 (b).

6.2.6 Temperature profiles during combustion tests

Further investigation of the heat shield effect given by BC particles was performed by recording the temperature profiles during forced-combustion tests on the surface and back of the EVA and its composites. The obtained curves are displayed in Figure 42: the curve labeled “T surface” refers to the temperature of

the surface directly exposed to heat flux; the other curves represent the temperatures on the backside of the various specimens. From a general point of view, the surface temperature of the specimens rapidly increases during the test due to its proximity to the irradiative heater, reaching about 600 °C at the end of the test. The specimens containing BC result in a decrease in the temperature measured on their backside, proving the thermal shielding effect provided by the particles. In particular, these temperatures decreased by about 100 - 140 °C compared with the unfilled EVA specimen, regardless of the type of system and filler loading. These results may pave the way toward a remarkable reduction in the amount of BC used while still achieving the same thermal shielding performance.

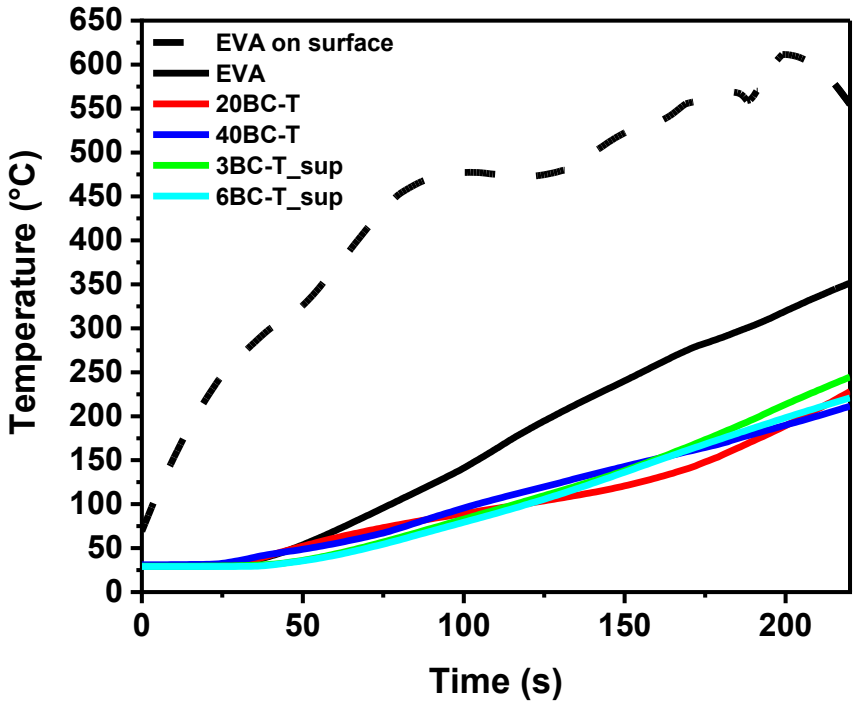

Figure 42. Temperature profiles recorded on the surface (dotted line) exposed to the irradiative heat flux (35 kW m^{-2}) and on the backside of the samples during forced-combustion tests.

6.2.7 Tensile tests

Figure 43 shows the characteristic stress-strain curves of EVA and its bulk composites. Table 29 lists the obtained values of tensile modulus and elongation at break. The specimens containing BC exhibited an increase in stiffness, which was greater as the amount of filler increased to 40 wt.%. In particular, the latter reached a value of 246 MPa, more than four times higher than that of the unfilled copolymer (E = 50 MPa). In contrast, the ductility of EVA significantly deteriorated in the presence of BC.

Table 29. Results of tensile tests of EVA and its composites containing BC from Tetra Pak.

Sample	Tensile modulus (E) [MPa]	Elongation at break (ε) [%]
EVA	50 ± 2	123 ± 6
20 BC-T	117 ± 6	90 ± 10
40 BC-T	246 ± 34	31 ± 7

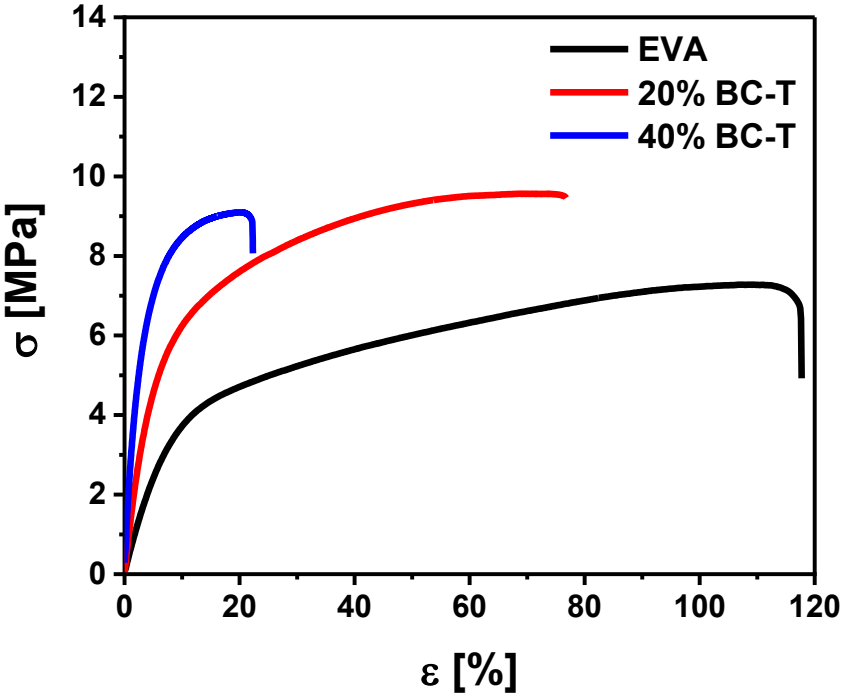

Figure 43. Stress-strain curves for EVA and EVA/BC-T composites.

Chapter 7

HDPE composites containing char from Tetra Pak®

In this chapter, the effect of biochar obtained from the pyrolysis of Tetra Pak used as a filler was further investigated. BC was incorporated in two polyethylene matrices with different properties: HPDE_HV with high viscosity and HDPE_LV with a lower viscosity (more details are provided in the Appendix). Composites with 20 wt.% of BC were prepared via compounding, and their thermal, combustion and mechanical properties evaluated.

7.1. Morphological investigations

Figure 44 shows the SEM magnifications of the two HDPE-based composites containing BC from Tetra Pak. A good filler distribution was observed for both materials; some aggregates of larger size, ranging from 100 to 200 μm, were observed in both samples, while other smaller particles were distributed throughout the matrix. The EDX analyses of the composites reported in Figure 44 and Figure 45, show the chemical composition of the BC particles. These maps show that the lamellar particles consisted mainly of aluminum. In contrast, the porous-shaped particles contained mainly Ca, O and Si. These results showed that the different viscosities of the two matrices slightly influenced the dispersion and distribution of the particles.

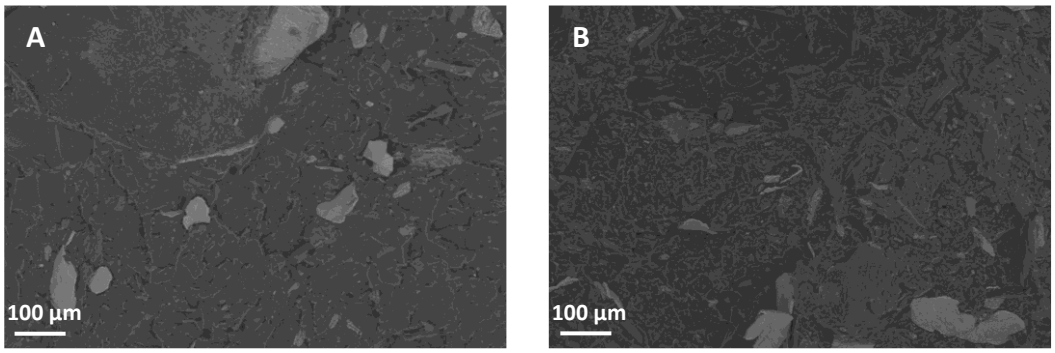

Figure 44. SEM magnifications (250 X) of HDPE_HV (A) and HDPE_LV (B) composites containing 20 wt.% of BC from pyrolysis of Tetra Pak.

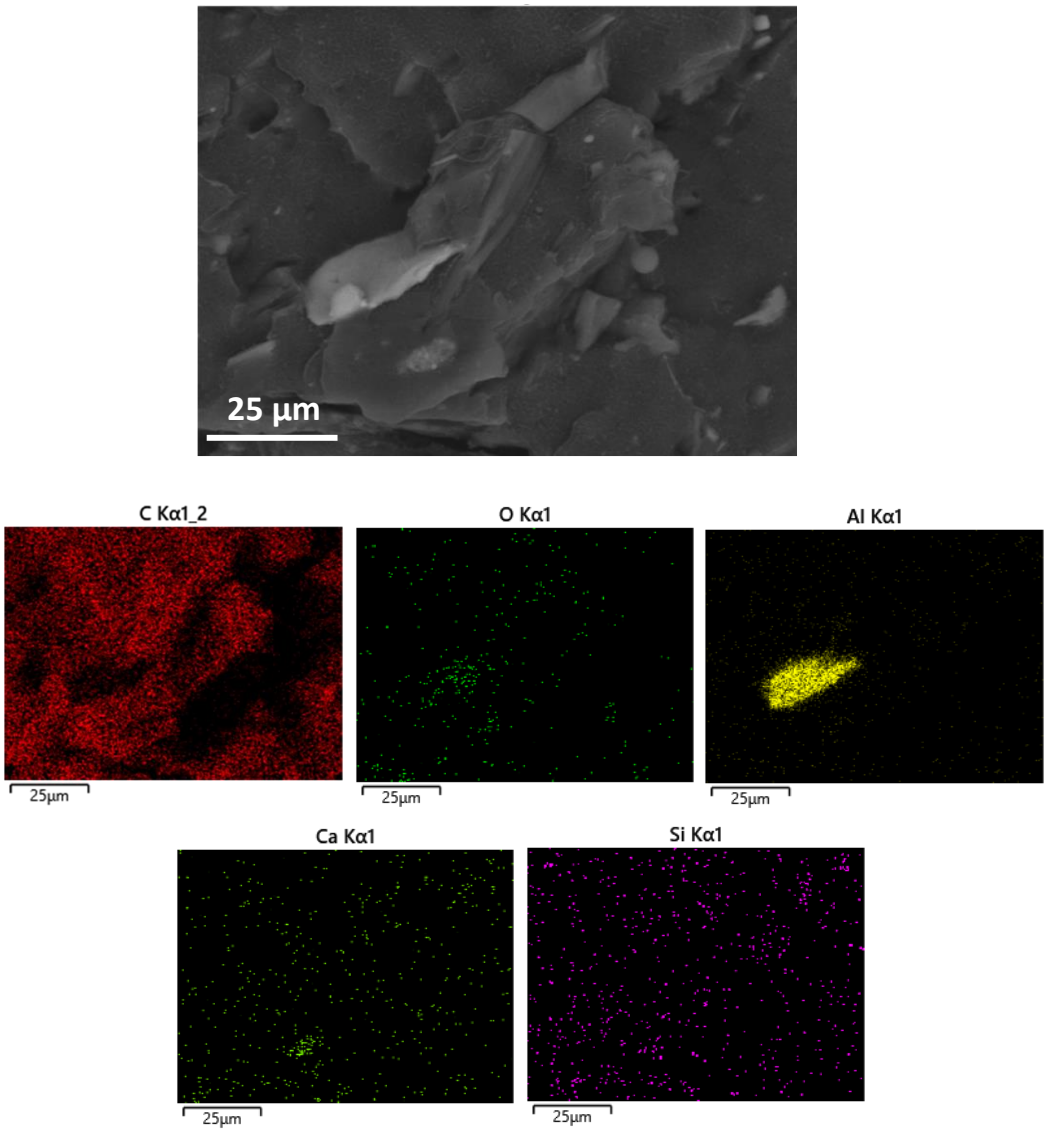

Figure 45. SEM image of the HDPE_HV-BC composites and its EDX maps of the elements included in biochar.

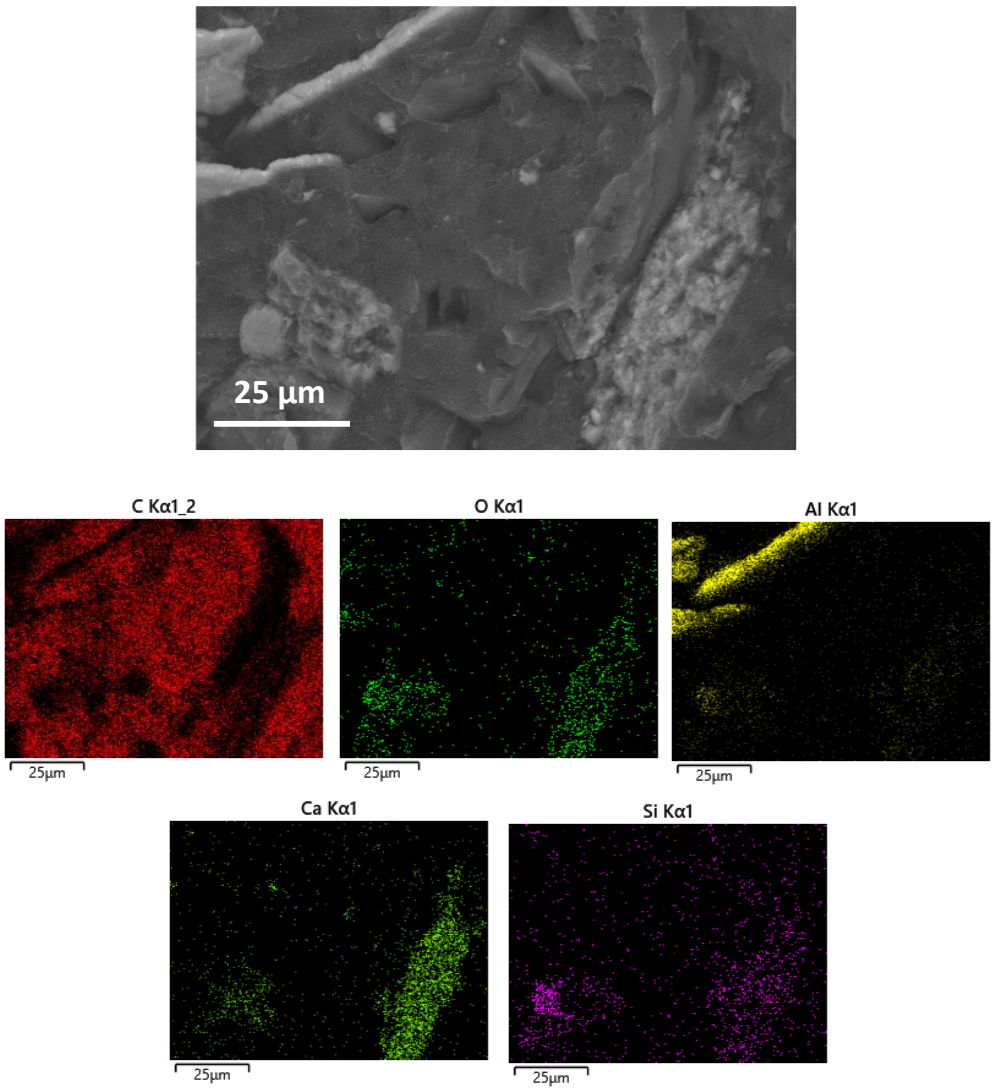

Figure 46. SEM image of the HDPE_LV-BC composites and its EDX maps of the elements included in biochar.

7.2. DSC analyses

Table 30 collects the results of DSC analyses performed on HDPE_HV, HDPE_LV, and their respective composites containing 20 wt.% of BC. Both crystallization and melting temperatures show similar results for neat PE and composites, highlighting that the presence of BC does not influence the these parameters. In addition, BC particles do not affect crystallization processes, as the variation in crystallinity between pure PE and its composites is only about 1%.

These findings demonstrate how the composites can be processed using the same conditions employed for their unfilled polymers.

Table 30. Results from DSC analyses for HDPEs and their composites.

Sample	Tc (°C)	ΔHc (J/g)	Tm (°C)	ΔHm (J/g)	Xc (%)
HDPE_HV	115.4	162.7	131.5	180.9	61.7
20 HDPE_HV	113.5	143.2	132.9	140.8	60.1
HDPE_LV	116.0	214.5	135.2	223.3	76.2
20 HDPE_LV	116.4	170.6	135.4	177.1	75.5

7.3. Thermogravimetric analyses

The thermogravimetric results for HDPEs and their composites are reported in Table 31; Figure 47 shows the TG and DTG curves obtained in nitrogen and in air. In nitrogen atmosphere, the degradation of the samples occurs in a single degradation step, starting at T_{onset} and ending at about 500 °C. From a general point of view, the analyzed samples show negligible variations in their characteristic degradation temperatures. In contrast, the final residue at the end of the test increases from zero (unfilled polymer) to 15 and 17 wt.% (HDPE_HV and HDPE_LV, respectively). These values, close to the amount of BC incorporated (i.e., 20 wt.%), indicate an interaction taking place between polymer and BC particles. In fact, the high thermal stability of BC, shown in Figure 33(A), was slightly reduced by the radicals formed during HDPE degradation.

The values of characteristic temperatures of TGA in air show an improvement in the thermo-oxidative stability of BC-containing specimens. This effect is particularly evident in the T_{onset} value of HDPE_HV-based composite, which is delayed by 53 °C compared to the unfilled counterpart, while the HDPE_LV-based composite presents a delay in T_{max1} of 79 °C compared to the unfilled matrix. These findings can be observed in the TGA curves (Figure 47B), which show better stability of HDPE_HV composite up to 450 °C and, after that temperature, a higher stability of HDPE_LV composite until the end of the test. Finally, the final residues were in agreement with the TG analysis of BC in air, which lost about 65% of its initial weight. Again, these findings highlight the

barrier effect of BC particles on oxygen diffusion in the polymer, already discussed in previous chapters.

Table 31. Results from thermogravimetric analyses in nitrogen and in air for HDPEs and their composites.

Atmosphere: nitrogen						
Sample	Tonset [°C]	Tmax1 [°C]	Tmax2 [°C]	$T_{10\%}$ [°C]	$T_{50\%}$ [°C]	Residue @ 800°C [%]
HDPE_HV	438	484	-	457	481	0
20 HDPE_HV	445	484	-	458	484	15
HDPE_LV	434	481	-	456	480	0
20 HDPE_LV	442	485	-	458	485	17
Atmosphere: air						
Sample	Tonset [°C]	Tmax1 [°C]	Tmax2 [°C]	$T_{10\%}$ [°C]	$T_{50\%}$ [°C]	Residue @ 800°C [%]
HDPE_HV	270	413	443	367	413	0
20 HDPE_HV	323	443	-	390	450	6
HDPE_LV	316	402	458	343	405	0
20 HDPE_LV	315	481	-	368	465	7

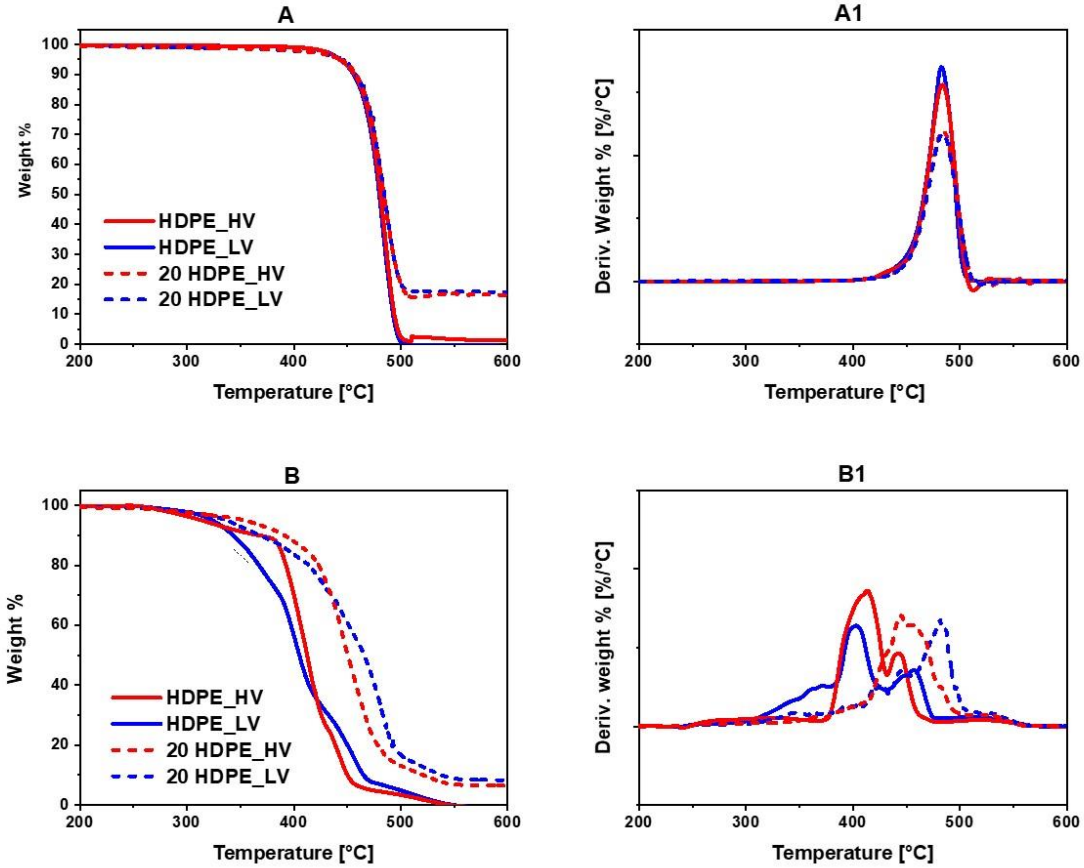

Figure 47. TG and dTG curves of HDPEs and their composites in nitrogen (A, A1) and in air (B, B1).

7.4. Cone calorimetry

7.4.1. HDPE High Viscosity

Table 32 and Table 33 list the main thermal and smoke parameters, respectively, of HDPE high viscosity and its composites containing 20 wt.% of BC, tested at 25, 35, and 50 kW m^{-2}. The related HRR vs. time curves are reported in Figure 48. From an overall point of view, the composites show anticipation in TTIs and a decrease of the peak HRR, as expected. The latter exhibited a strong decrease when tested at 25 kW m^{-2}, with a value reduced by 30 % compared to the unfilled polymer. At higher heat fluxes, the reduction was 27 and 22 % (at 35 and 50 kW m^{-2}, respectively). In the latter cases, the specimens were heated faster, quickly reaching high temperatures that do not allow an effective surface barrier to be created, as observed at a lower heating flow. This finding is witnessed by the

shapes of the HRR curves (Figure 48): the curve at 25 kW m^{-2} after a very sharp initial slope shows a change in slope, reflecting the formation of a thermal barrier layer; at higher heat fluxes, this change in slope is not so evident, with the overall shape of the curves similar to that of the unfilled polymer. Despite these differences the area under the curves, namely the total heat release (THR), remains the same for both the polymer and its composites. The TTIs of the specimens decrease significantly when the heat flux increases, as already reported by several studies [271] [272].

Regarding the smoke parameter values (Table 33), the level of CO and CO_2 remains similar for the polymer and its composite at the specific heat flux. The THR and SEA, on the other hand, were significantly reduced, as the incorporation of BC is responsible for a smoke suppression effect. BC particles promote carbonization while decreasing aromatization and volatilization of aromatics, which produce dense smokes [273].

Table 32. Main thermal parameters of HDPE_HV and its composite containing 20 wt.% of BC by cone calorimetry test at different heat fluxes.

Specimen	TTI [s]	pkHRR [kW m^{-2}]	pkHRR Reduction [%]	Time to peak [s]	THR [MJ m^{-2}]	Residue mass [%]	FPI $\left[\frac{(kW/m^2)}{s}\right]$	FIGRA $\left[\frac{(kW/m^2)}{s}\right]$
25 kW m^{-2}								
HDPE_HV	148	1222	-	265	108	0	8.3	4.6
20 HDPE_HV	130	853	30	227	105	10	6.6	3.8
35 kW m^{-2}								
HDPE_HV	87	1515	-	187	105	0	17.4	8.1
20 HDPE_HV	78	1103	27	179	103	9	14.1	6.2
50 kW m^{-2}								
HDPE_HV	51	2039	-	127	99	0	39.9	16.1
20 HDPE_HV	32	1587	22	116	96	8	49.6	13.7

Table 33. Main smoke parameters of HDPE_HV and its composite containing 20 wt.% of BC by cone calorimetry test at different heat fluxes.

Specimen	TSR [m² m^{-2}]	SEA [m² kg^{-1}]	CO [%]	CO2 [%]	CO/CO_2 ratio
25 kW m^{-2}					
HDPE_HV	1024	384	0.0030	0.15	0.0200
20 HDPE_HV	933	380	0.0036	0.15	0.0240
35 kW m^{-2}					
HDPE_HV	798	304	0.0037	0.17	0.0218
20 HDPE_HV	537	208	0.0034	0.17	0.0200
50 kW m^{-2}					
HDPE_HV	1063	369	0.0045	0.22	0.0205
20 HDPE_HV	465	187	0.0047	0.25	0.0188

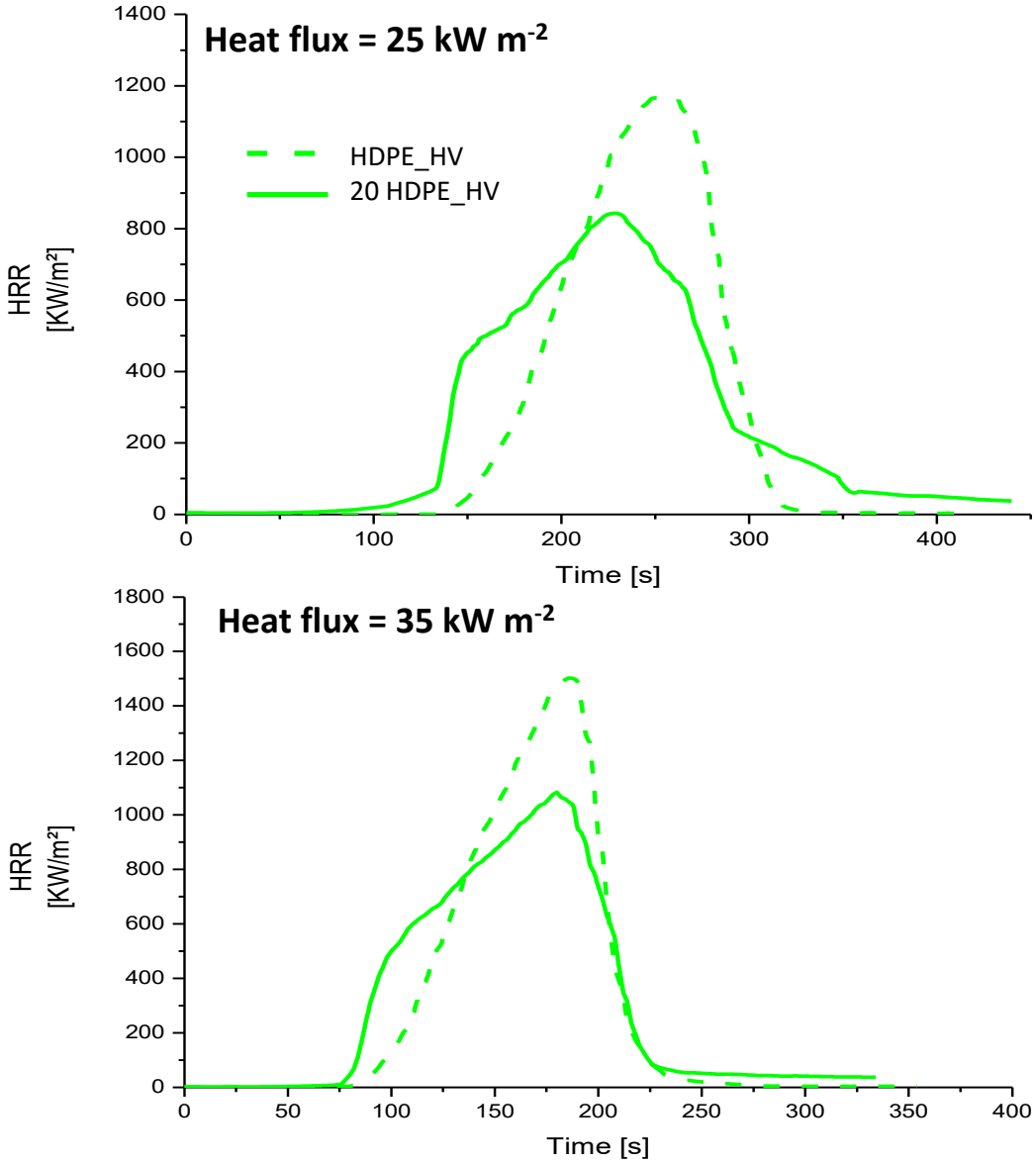
Heat flux = 25 kW m-2
HDPE_HV
20 HDPE_HV
HRR [KW/m²]
Time [s]
Heat flux = 35 kW m-2
HRR [KW/m²]
Time [s]

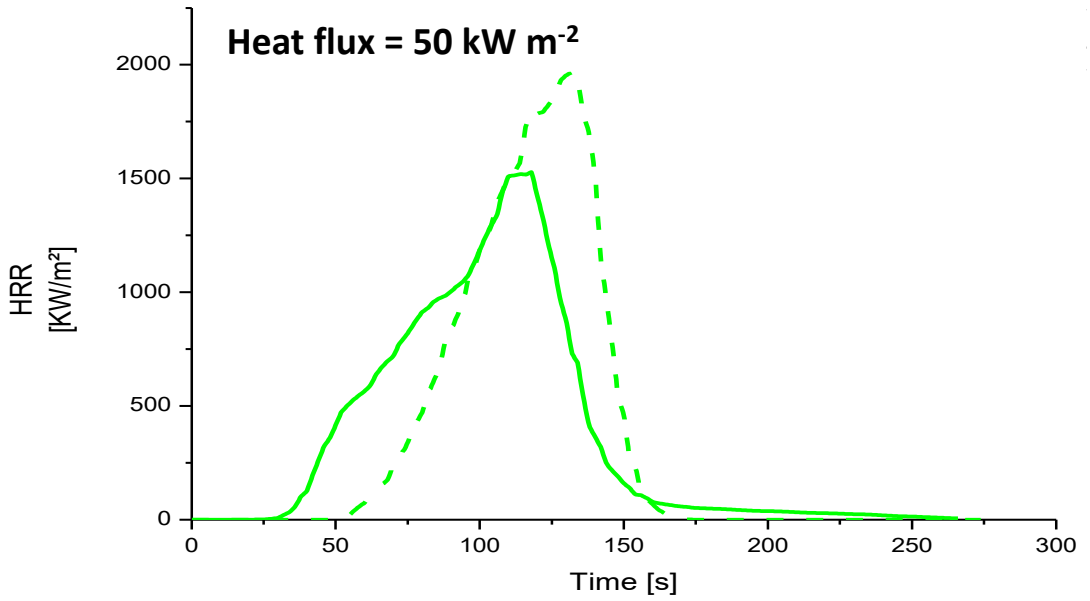

Figure 48. HRR vs time curves for HDPE_HV and its composite containing 20 wt.% of BC at different heat fluxes (i.e. 25, 35, and 50 kW m^{-2}).

7.4.2. HDPE Low Viscosity

Table 34 and Table 35 list the main thermal and smoke parameters, respectively, of HDPE low viscosity and its composites with 20 wt.% of BC, tested at 25, 35, and 50 kW m^{-2}. The respective HRR vs time curves are reported in Figure 49. In the cases of low and medium heat flux (i.e., 25 and 35 kW m^{-2}), the curves of HRR show a double peak, due to the stability of the thermal barrier layer provided by biochar, as already reported in the previous chapters. The curve of composite tested at a higher heat flux did not exhibit such pronounced behavior: this latter shows a slope inversion at about 50 s. The reduction in peak of HRR caused by BC incorporation compared with unfilled polymer was between 34 and 46%. For each heat flux considered, the TTIs of the filled specimens were anticipated compared to the unfilled polymer, as well as the time to peaks. THR values were not significantly affected by the presence of BC, with a slight decrease in their values. As well as for High Viscosity HDPE, the smoke parameters of TSR and SEA were greatly reduced by the BC presence while the CO and CO_2 maintained about the same values.

Table 34. Main thermal parameters of HDPE_LV and its composite containing 20 wt.% of BC by cone calorimetry test at different heat fluxes.

Specimen	TTI [s]	pkHRR [kW m^{-2}]	pkHRR Reduction [%]	Time to peak [s]	THR [MJ m^{-2}]	Residue mass [%]	FPI $\left[\frac{(kW/m^2)}{s}\right]$	FIGRA $\left[\frac{(kW/m^2)}{s}\right]$
25 kW m^{-2}								
HDPE_LV	146	1141	-	267	96	0	7.8	4.3
20 HDPE_LV	90	682	41	219	85	9	7.6	3.1
35 kW m^{-2}								
HDPE_LV	86	1396	-	183	98	0	16.2	7.6
20 HDPE_LV	51	923	34	179	96	10	18.1	5.2
50 kW m^{-2}								
HDPE_LV	55	2046	-	134	98	0	37.2	15.3
20 HDPE_LV	21	1097	46	121	92	9	52.2	9.0

Table 35. Main smoke parameters of HDPE_HV and its composite containing 20 wt.% of BC by cone calorimetry test at different heat fluxes.

Specimen	TSR [m² m^{-2}]	SEA [m² kg^{-1}]	CO [%]	CO2 [%]	CO/CO_2 ratio
25 kW m^{-2}					
HDPE_LV	847	309	0.0030	0.15	0.0200
20 HDPE_LV	239	108	0.0032	0.14	0.0229
35 kW m^{-2}					
HDPE_LV	910	321	0.0038	0.16	0.0238
20 HDPE_LV	492	198	0.0028	0.16	0.0175
50 kW m^{-2}					
HDPE_LV	1072	434	0.0044	0.22	0.0200
20 HDPE_LV	706	301	0.0045	0.20	0.0225

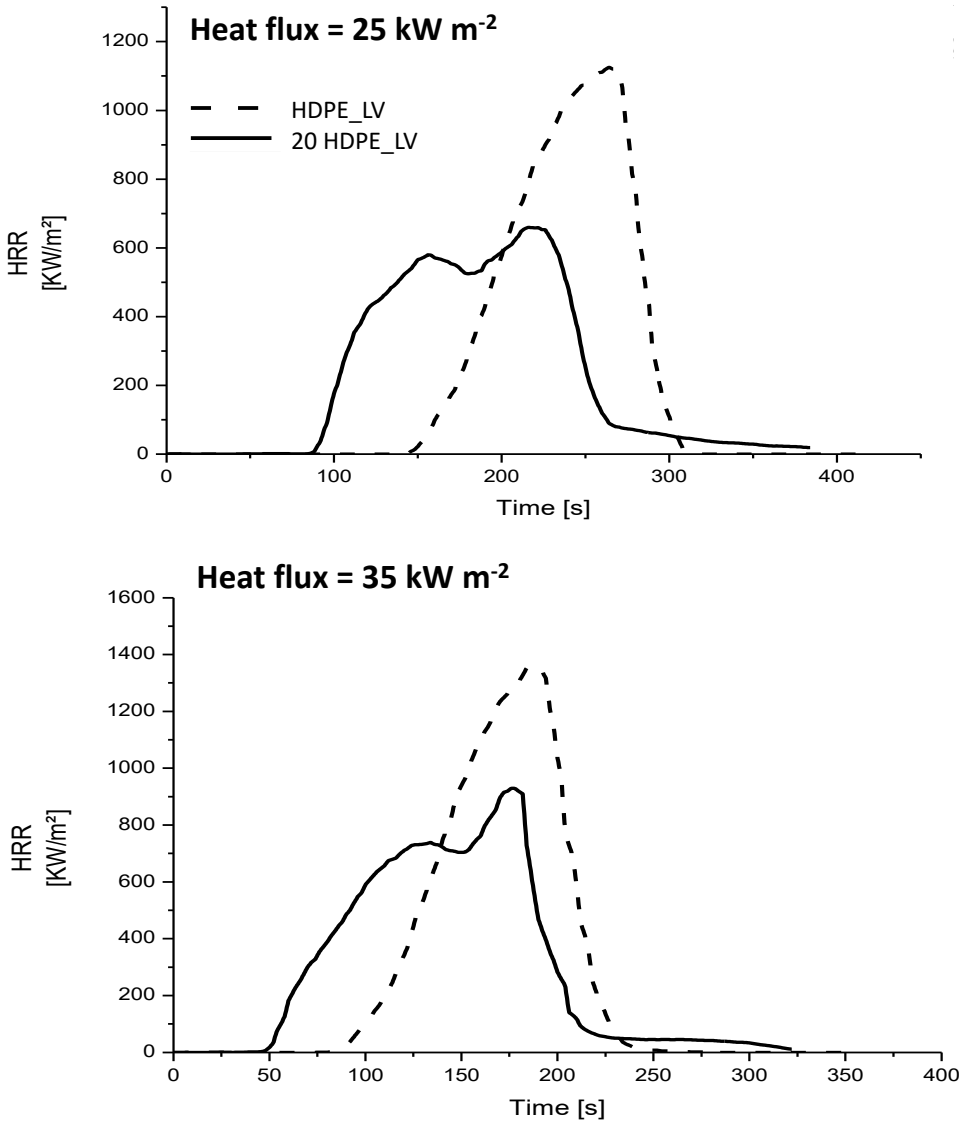
Heat flux = 25 kW m-2
HDPE_LV
20 HDPE_LV
HRR [KW/m²]
Time [s]
Heat flux = 35 kW m-2
HRR [KW/m²]
Time [s]

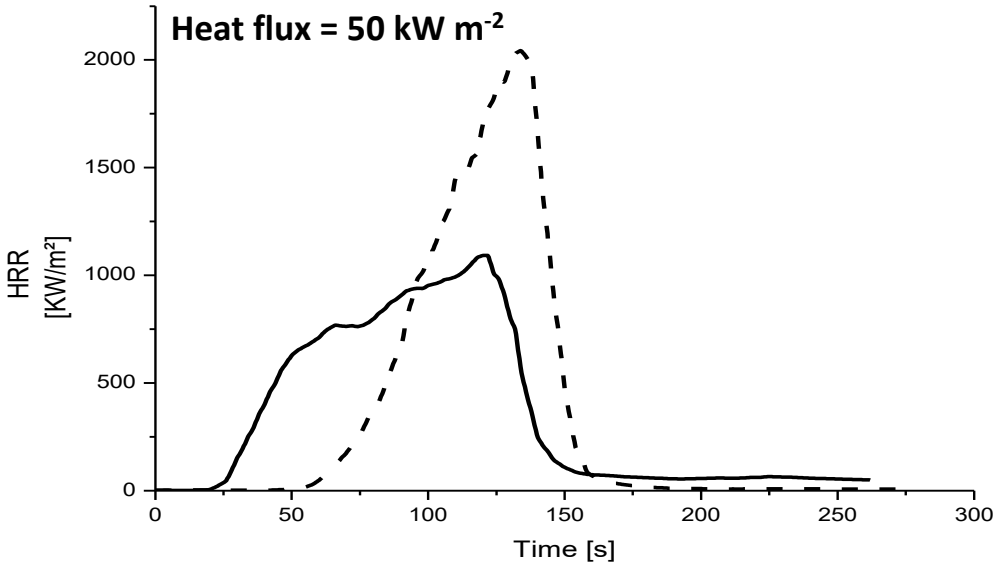

Figure 49. HRR vs time curves for HDPE_LV and its composite containing 20 wt.% of BC at different heat fluxes (i.e. 25, 35, and 50 kW m^{-2}).

7.4.3. Comparison between HDPEs

Figure 50 and Figure 51 display the value of the HRR peaks at different heat fluxes for HDPE_HV and HDPE_LV materials, respectively; the trend lines are marked. The HDPE_HV containing BC shows a peak HRR reduction by 30% at 25 kW m^{-2}, up to 22% at 50 kW m^{-2}, and trend lines with similar slopes. In contrast, HDPE_LV shows a decrease in peak HRR from 41% at 25 kW m^{-2} to 46% at 50 kW m^{-2}, showing an increasing reduction from low to high heat fluxes; in this case, the two trend lines show very different slopes. This opposite behavior means that the flame-retardant effect of BC in HDPE_HV is more effective at low irradiative heat fluxes, while for HDPE_LV it is more efficient at high fluxes. In general, the values of pkHRR of HDPE_LV composites were lower than those of HDPE_HV composites, although the corresponding unfilled polymers showed similar values of peak HRR. This result can be attributed to the different degradation mechanisms involved during combustion [274]: HDPE_HV composites mainly follow degradation by carbon-carbon bonds breaking, with the formation of volatile products; in HDPE_LV composites, on the other hand, the scission between carbon-hydrogen bonds is favorite, which leads to the formation of radicals responsible for char formation.

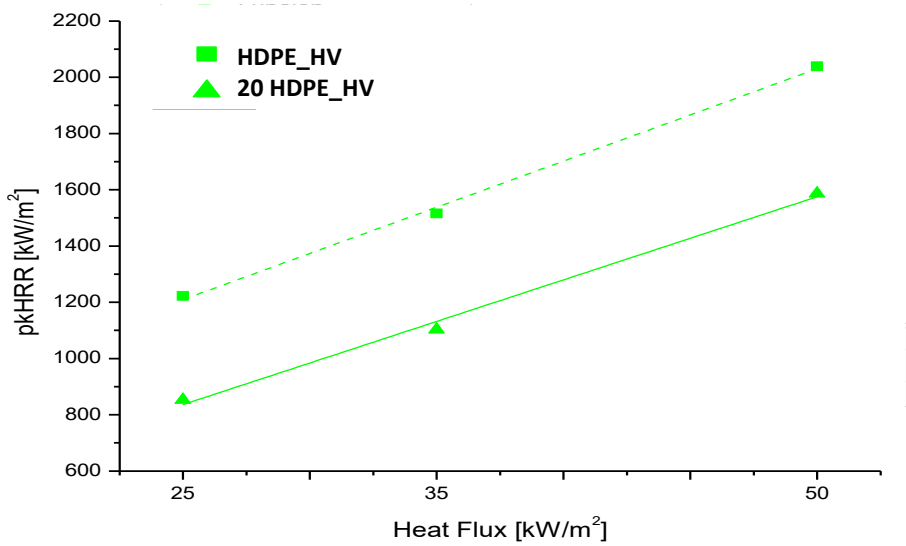

Figure 50. PkHRR vs. heat flux trend lines of HDPE_HV and 20 HDPE_HV.

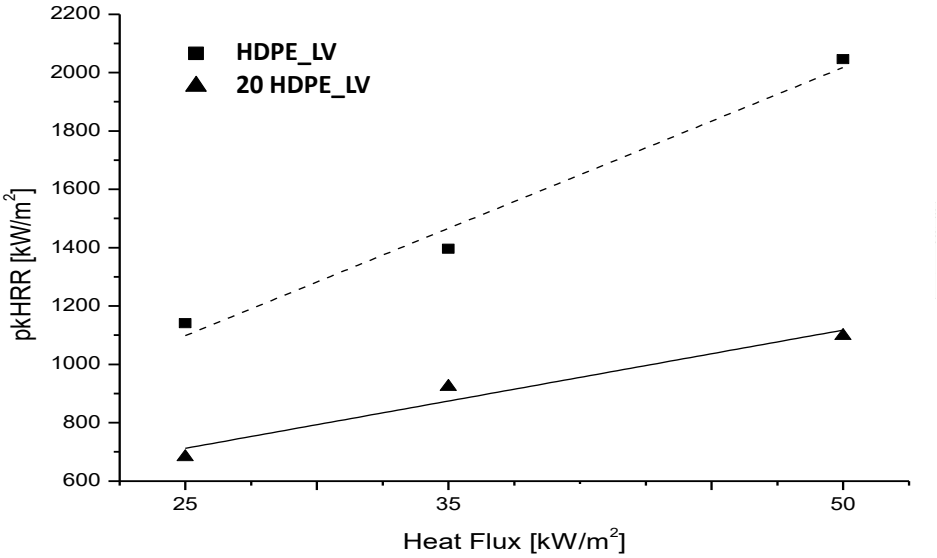

Figure 51. PkHRR vs. heat flux trend lines of HDPE_LV and 20 HDPE_LV.

7.5. Tensile tests

Figure 52 and Figure 53 show the stress-strain curves of HDPEs and respective composites; Table 36 lists their values of tensile modulus and

elongation at break. The presence of BC in HDPE_HV only slightly changes the behavior of its matrix. The composite curve follows the same trend but with a 38 % increase in tensile modulus and a slight decrease in ductility, observed in the decreased elongation at break from 8 to 6 %. On the contrary, the BC particles in the HDPE_LV significantly change the behavior of the polymer. The HDPE_LV presents a very high elongation at break (ε = 164 %), which dramatically drops down to just 6 % when the BC was incorporated, with an increase in elastic modulus of 47%.

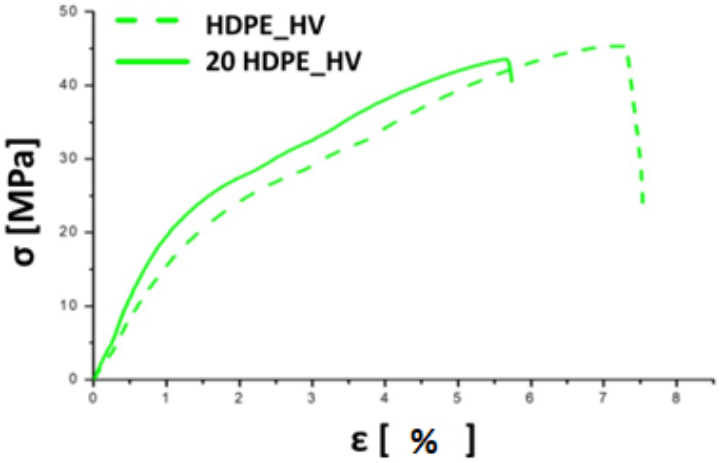

Figure 52. Stress-strain curves for HDPE_HV and its composite containing 20 wt.% of BC.

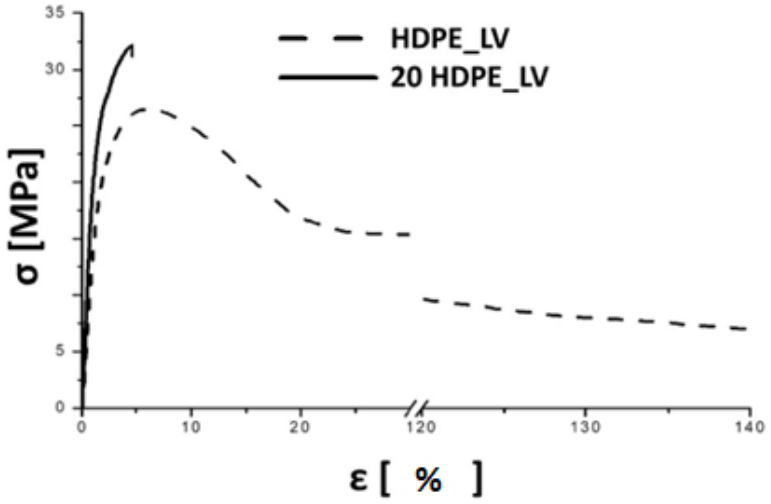

Figure 53. Stress-strain curves for HDPELHV and its composite containing 20 wt.% of BC.

Table 36. Tensile properties of HDPEs and respective composites.

Sample	Tensile modulus (E) [MPa]	Elongation at break (ε) [%]
HDPE_HV	1442 ± 40	8 ± 1
20 HDPE_HV	1986 ± 53	6 ± 1
HDPE_LV	1468 ± 104	164 ± 40
20 HDPE_LV	2162 ± 126	6 ± 1

Chapter 8

General conclusions

This thesis focused on the preparation and study of polymer composites containing flame retardants derived from different waste sources. In detail, the flame retardants were obtained through the char resulting from pyrolysis processes. The pyrolysis was carried on Kraft Lignin, softwood, rapeseed, rice husk, and used Tetra Pak. The solid product of the treatment process, named char, was embedded into different polymer matrices (EVA and HDPE) to obtain by compound technique different flame retardant systems. The prepared flame retardant systems were carefully characterized and the results were shown and discussed in this thesis. The objective was to explore a potential use of chars derived from the pyrolysis of different wastes by embedding it in different thermoplastic polymers and comparing their fire retardancy with typical flame retardants. The main results have been summarized below:

- The first biochars studied in Chapter 3 were derived from kraft lignin pyrolyzed at various temperatures, i.e., 500, 600 and 700 °C, to obtain three different biochars. The EVA composites were prepared with 20 or 40 wt.% of BC, a typical quantity range used to achieve significant fire retardancy results and acceptable mechanical properties. Indeed, the peaks of heat rate release (pkHRR) of these materials significantly lower than that of unfilled EVA (i.e., -23 to -73 %), with a greater effect given by materials with high filler content and using BCs obtained at higher temperatures (i.e., 700 °C). The time to ignition (TTI) was compared and exceeded that of EVA only using BC obtained at 600 and 700 °C at 40 w..%. Similar behavior was observed on EVA composites containing BCs

obtained from various biomasses, as reported in Chapter 4: in these cases, using 40 wt.% of BC from rapeseed accounted for a pkHRR decrease up to 74 % compared to that of EVA. but the TTIs resulted lower, i.e., from 32 to 61 %, compared with that of EVA. In this chapter flame retardant systems with BC-rich surface layer were exploited; these systems showed TTIs similar to that of EVA with just 3 or 6 wt.% of BC, combined with a decrease in pkHRR (from 13 to 30 wt.%).

- Chapter 5 reported the preparation and characterization of EVA composites containing, in addition to BC from rapeseed, another bio-material, humic acid (HA). The combination of these two components have been leading to a decrease in pkHRR of EVA from 70 to 75 %, combined with a TTI higher of 12% respect to that of EVA, for the composites containing 15 wt.% of BC and 25 wt.% of HA.

- The char derived from used Tetra Pak containers was explored in Chapter 6 and 7. EVA composites were prepared using both bulk and surface approaches: the former highlight the decrease in pkHRR, while the latter point out the increase in TTI compared with EVA values. The fire retardancy effect of the char was exploited in HDPE matrices at different heat fluxes (i.e., 25 kW m-2, 35 kW m-2, and 50 kW m-2) showing, from a general point of view, an anticipation of TTI and a decrease in peak HRR, as expected.

In conclusion, this work could be used as a starting point for further work aiming at valorizing pyrolysis process by-products as flame retardants in a circular economy perspective.

Appendix

A.1 Materials

A.1.1 Polymers

EVA (melt flow rate of 12 g/10 min at 190 °C/2.16 kg, density of 0.942 g/cm^3 and vinyl acetate content of 19 wt.%) was supplied by Versalis SPA (San Donato Milanese, Italy) under the trade name Greenflex MQ40 which is a grade for injection molding and compounding.

Different grades of polyethylene have been used. Table 37 reports the commercial names, the codes used, the values of melt flow index (MFI) and density provided by the suppliers. All the materials were used without any further purification.

Table 37: List of polyethylenes used.

Material	Supplier	Code	MFI (g/10min) [190 °C/2.16 kg]	Density (g/cm^3)
Eraclene MP90U	Versalis SPA (San Donato Milanese, Italy)	HDPE_LV	7	0.960
Lupolen 5021DX	LyondellBasell (Rotterdam, Netherlands)	HDPE_HV	0,25	0.950

A.1.2 Biochars

Different types of BCs were obtained by pyrolysis of Kraft Lignin supplied by Domtar (Fort Mill, South Carolina, US). Biomass was dried at 105 °C for 24 hours and pyrolyzed in a mechanical fluidized bed reactor (pilot-scale unit). The feedstock (100 g) was heated in a nitrogen atmosphere at 20 °C min $^{-1}$ to 500, 600 or 700 °C and maintained for 25 min. Pyrolysis gases flux inside a condenser

where they accumulate in the liquid phase, while non-condensable gases are expelled. Samples of these gases can be taken for analysis. After cooling, the char and oils obtained are recovered. The BC was pulverized using a mechanical blender. List and code of obtained BCs are reported in Table 38.

Table 38. BCs obtained from pyrolysis of Kraft lignin.

Code	Pyrolysis temperature
BC500	500
BC600	600
BC700	700

Three types of biochars were purchased from UK Biochar Research Centre and were produced by pyrolysis of mixed softwoods, oil seed rape, and rice husk, using a pilot-scale rotary kiln unit [275]. The highest treatment temperature was set at 550 °C, and each material that resulted from that process was then further annealed at 1000 °C using a vertical furnace and a quartz reactor, heating at a rate of 50 °C min^{-1} while maintaining the final temperature (1000 °C) for 30 min in an argon atmosphere. The annealed biochars were then further mixed for 10 min in a mechanical blender (Savatec BB90E, Turin, Italy), then for 10 min in a ball mill. Their ash content was assessed by incineration at 550 °C for 6 h, using a static furnace. Table 39 reports the names of the samples and their ash content.

Table 39: list of codes used to identify biochar samples and their respective ash content.

Code	Source	Ash Content (%)
BC low	Softwoods	2.3 ± 0.8
BC medium	Rapeseed	23.4 ± 1.1
BC high	Rice husk	47.8 ± 1.3

The BC-T was made using Tetra Pak®, collected from residential and urban waste streams, cleaned, and dried at 105 °C for 72 hours before being converted via pyrolysis. Tetra Pak® was cut into squared pieces measuring about 3 cm2 in size. A tubular furnace (Carbolite TZF 12/65/550) was used to pyrolyze 100 g at a heating rate of 15 °C/min for 30 min at 800 °C in a nitrogen environment. After being allowed to cool at room temperature, BC was collected and mechanically pulverized for 10 minutes while operating at room temperature before being utilized to prepare the composites.

A.1.3 Humic Acid (HA)

Humic acid sodium salt was purchased from Thermo Fisher Scientific (Waltham, MA, USA) in powder form with a purity of 50 to 60% as humic acid. The molecular formula of this substance is $C_9H_8Na_2O_4$ and the chemical structure is reported in Figure 54.

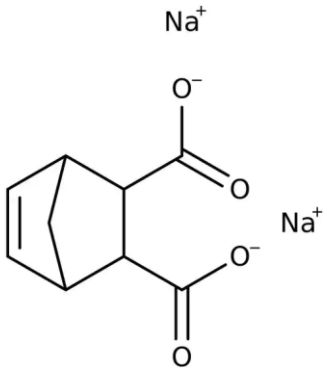

Figure 54. Chemical structure of humic acid sodium salt [data from https://www.fishersci.it/shop/products/humic-acid-sodium-salt-tech-50-60-as-humic-acid-thermo-scientific/15436395].

A.2 Instruments

A.2.1 Compounding

The composites were processed in a co-rotating twin-screw extruder Process 11 from Thermo Fisher Scientific (Waltham, MA, USA) with a screw diameter of 11 mm and L/D ratio of 40. The extruder consisted of 8 blocks and a die with a single hole heated and the adopted temperature profile is reported in Figure 55. On the first block of the extruder and the third block, respectively, two volumetric feeders dosed BC powders and EVA pellets. The die was fitted with a pressure sensor and a thermocouple to measure the melt's temperature (145 °C and 25–30 bar, respectively), and block number seven had a window for degassing. Figure 51 depicts the screw profile, which was selected to maximize the transfer of mechanical energy and enhance BC dispersion. Three kneading blocks were inserted to ensure the appropriate mixing of the BC and molten polymer and to minimize the size of agglomerates or big particles. Every single component of the kneading blocks had a selected orientation of 30°, 60°, and 90° with respect to the subsequent one, as shown in Figure 55. The extruder was running at 500 rpm, the EVA feeder's mass flow was set at 350 g/h, and the powder feeder was calibrated to achieve the necessary filler loading. The finished product was extruded out of the machine into a batch of water where it quickly cooled before being pelletized. The same screw profile was used for the PE-based compounding but with

different conditions: feeding at 250 g/h and temperatures from 185 to 195 °C (specifically, 185 - 185 - 190 - 190 - 190 - 190 - 195 - 195 °C).

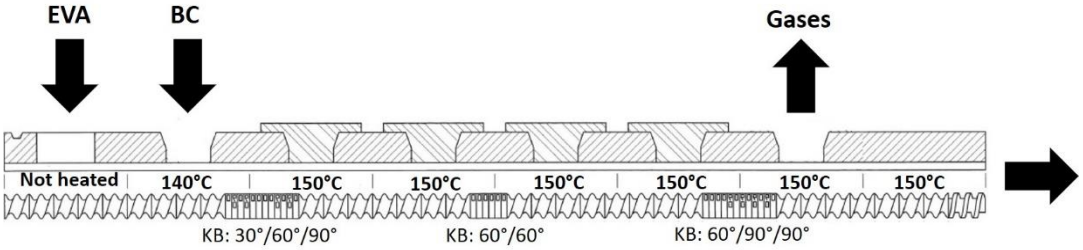

Figure 55. Screw and temperature profile of the instrument used during extrusion process (KB = kneading blocks).

A.2.2 Compression molding

A Collin P200T press (Maitenbeth, Germany) with hot plates for compression molding was used for specimen preparation. For EVA-based materials, square samples (50 × 50 × 3 mm^3) for cone calorimetry were obtained at 150 °C and 100 bar for 3 min. The same conditions were used to mold 500 or 1000 μm thick layers of EVA-BC, which were subsequently joined to the neat EVA square specimens at 80 °C and 100 bar for 1 min. The same method was adopted for molding specimens for flammability tests of size 125 × 16 × 3 mm^3.

The same procedures were used for the compression molding of PEs materials using different conditions: the temperature was set at 190 °C and the time was extended to 6 min.

A.2.3 Injection molding

Specimens with a “dog bone” shape for mechanical tests of size 75 × 4 × 2 mm^3, were molded using a Babyplast 610P Standard injection molding machine, from CRONOPLAST SL (Abrera, Spain). The EVA-based materials were obtained at 150 °C, the first injection time of 8 s at 85 bar for filling the mold, and the second injection time of 25 s at 65 bar of maintenance, with a total time cycle of 45 s. The PE-based materials were processed at 190 °C, first injection time of 8.5 s at 80 bar, second injection time of 12 s at 50 bar.

A.3 Characterization techniques

A.3.1 Raman spectroscopy

BC samples were analyzed through Raman spectroscopy by using a Renishaw InVia apparatus (H43662 model, Gloucestershire, UK) coupled with a green laser line (514 nm) with a 50× objective. Raman spectra were studied in the range between 250 cm^{-1} and 3500 cm^{-1}.

A.3.2 X-Ray photoelectron spectroscopy (XPS)

The BC surface was studied using a PHI 5000 Versaprobe Physical Electronics (Chanhassen, MN, USA) scanning X-ray photoelectron spectrometer (monochromatic Al K-alpha X-ray source with 1486.6 eV energy, 15 kV voltage, and 1 mA anode current) to evaluate the surface chemical composition.

A.3.3 Mechanical tests

An Instron 5966 dynamometer (Norwood, MA, USA) was employed for evaluating the mechanical behavior through tensile tests, according to the ISO 527 standard. A 5 kN load cell was utilized, working at 1 mm/min rate until 0.2% deformation was reached; afterward, the rate was increased up to 50 mm/min till the specimen fracture. At least five specimens were tested for each system and the results in terms of tensile modulus (E), elongation at break (ε), and tensile strength (σ_y) averaged.

A.3.4 Morphological investigations

The morphologies of biochar powders and BC composites were investigated using an EVO 15 scanning electron microscope (SEM) from Zeiss (Oberkochen, Germany), coupled to Ultim Max 40 energy dispersive X-ray (EDX) micro-analyzer by Oxford Instruments (High Wycombe, UK), with AZtecLive

integrated software. Fragments of the composites obtained by a brittle fracture in liquid nitrogen were fixed to conductive adhesive tapes and gold-metallized.

A.3.5 Proximate analysis

The proximate analysis was carried both on BCs and feedstock following the standard ASTM D1762-84 and using a Vulcan muffle furnace model d-550. Moisture content (MC, %), volatile matter (VM, %), and ash (%) were calculated. The fixed carbon (FC, %) content was calculated as the difference from the total. Results were duplicated and averaged.

A.3.6 Ultimate analysis

Ultimate analysis was performed on BCs and feedstocks to investigate the elemental composition of the sample. Carbon, hydrogen, nitrogen and sulfur content was determined using an EA1112 Series CHNS elemental analyzer from Thermo Fisher Scientific. The sample (1-2 mg) was inserted in an aluminum container together with vanadium oxide (8-10 mg). The oxygen content was calculated as a percentage from the difference of the elemental contents plus the ashe percentage obtained from proximate analysis (equation (7)).

$$Oxygen\ \% = 100 - C\ (\%) - H\ (\%) - N\ (\%) - S\ (\%) - ash\ (\%) \qquad (7)$$

A.3.7 Differential scanning calorimetry (DSC)

DSC analyses were carried out using a Q20 TA Instrument apparatus (New Castle, DE, USA), on samples of about 8 mg, placed in sealed aluminum pans. EVA-based samples were first heated up under dry nitrogen from 30 to 150 °C at 10 °C/min, to erase the previous thermal history. Then, samples were cooled from 150 °C to 30 °C at 10 °C min^{-1} and a second heating was applied up to 150 °C at 10 °C min^{-1}. PE-based samples were heated until 200 °C. The crystallization temperature (T_c), crystallization enthalpy (ΔH_c), melting temperature (T_m), and melting enthalpy (ΔH_m) were identified, using the 2nd heating-up trace. The

crystallinity degree (X_c) of the unfilled polymer and of the composites was calculated using the following equation (8):

$$Xc = \frac{\Delta H_m}{\Delta H_{100}\ (1-x)} * 100 \quad (8)$$

where x is the filler weight percentage and ΔH_{100} represents the melting enthalpy of the 100% crystalline polymer matrix equal to 290 J g^{-1} both for EVA and PEs (since it is assumed that EVA crystallization only involves polyethylene segments [276]).

A.3.8 Thermogravimetric analysis (TGA)

The thermal and thermo-oxidative behavior of BC powders and BC composites was assessed through a Q500 system from TA Instrument (New Castle, Delaware, USA). Around 10 mg of each sample was placed into an open alumina crucible and heated up from room temperature to 800 °C (heating rate: 10 °C/min), either in 60 ml/min air or nitrogen gas flow. The following parameters were measured: T_{onset} (temperature, at which the sample starts degrading), T_{max} (temperature of the peak of dTG - derivative - curves) and residues at the related temperatures, as well as at the end of the tests.

A.3.9 Higher Heating Value (HHV)

The determination of HVV was performed using Semi-Automated Calorimeter model C-200 by IKA (Staufen, Germany) and preparing samples of 0.3 - 0.4 grams.

A.3.10 Micro Gas Chromatograph (Micro-GC)

The pyrolysis gases were collected using gas bags at different temperatures (i.e. 300, 400, 500, 600, and 700 °C). In order to identify the compounds, a micro-GC model CP-4900 from Varian Inc. (Palo Alto, California, USA) coupled with a

Thermal Conductivity Detector was employed. Helium and argon gases were employed as carrier gases for the thermal conductivity detector at 80 psi pressure. Each sample was analyzed at least three times and the results were averaged.

A.3.11 Rheological measurements

Rheological measurements were performed using an ARES (TA Instrument, New Castle, DE, USA) strain-controlled rheometer, employing a parallel plate geometry (plate diameter: 25 mm; gap between the plates: 1 mm). The complex viscosity values were measured through frequency scans ranging from 10^{-1} to 10^{2} rad s^{-1} at constant temperature (150 °C). The strain amplitude was chosen for each sample in order to fall in the linear viscoelastic region.

A.3.12 UL-94 test

The UL-94 vertical test was used for studying the flammability of prepared materials. It is a conventional vertical spread flame test that distinguishes materials into V-0, V-1, and V-2 categories. Figure 56 shows the experimental apparatus.

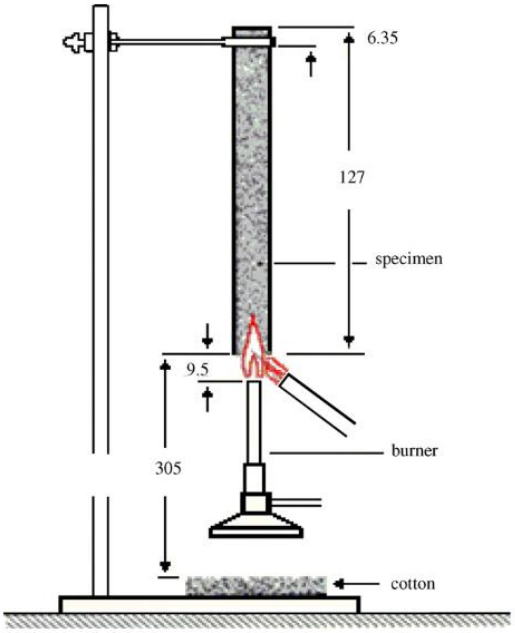

Figure 56. Experimental apparatus for the UL94 V flammability test. Reprinted with the permission from [4]**.**

The burner is configured to generate a blue flame with a center cone height of 20 mm and a power of 50 W. The top of the burner must be 10 mm from the specimen's bottom edge when the flame is applied to the bottom of the specimen. After 10 seconds, the flame is removed. The after-flame time, that is the length of time needed for the flame to be extinguished is given as t_1. After extinguishment, the flame is held for an additional 10 seconds. The after-flame time t2 and the afterglow time t3 (the time required for the fire glow to disappear) are reported. The distance between the burner and the specimen must remain constant during flame application. If drops occur, the burner should be isolated from the test flame or tilted at a 45° angle. During the test, the burning drops that caused a piece of cotton under the specimen to ignite must be recorded. Five samples must be tested, according to the standard. The criteria mentioned in Table 2 are used to classify the specimen as V0, V1, or V2, as reported by the standard [5].

Table 40. Classification of materials for the UL 94 V flammability test.

UL94 V0	t_1 and t_2 less than 10 s for each specimen t_1+t_2 less than 50 s for the five specimens t_2+t_3 less than 30 s for each specimen No after-flame or after-glow up to the holding clamp No burning drops
UL94 V1	t_1 and t_2 less than 30 s for each specimen t_1+t_2 less than 250 s for the five specimens t_2+t_3 less than 60 s for each specimen No after-flame or after-glow up to the holding clamp No burning drops
UL94 V2	t_1 and t_2 less than 30 s for each specimen t_1+t_2 less than 250 s for the five specimens t_2+t_3 less than 60 s for each specimen No after-flame or afterglow up to the holding clamp Burning drops allowed

A3.13 Cone calorimetry

The cone calorimeter was designed in the early 1980s at the National Bureau of Standards (NBS), now the National Institute of Standards and Technology or NIST [277] and nowadays thousands of scientific papers have been published. The equipment and test procedure are internationally standardized as ISO 5660. The cone calorimeter is a bench-scale fire test equipment that creates forced flame

conditions [278] and, as a result, simulates a fire scenario with a very small sample size. The cone calorimeter has found growing application as a characterization tool in the study and development of fire-retarded polymeric materials. In fact, parameters such as peak of HRR (pkHRR), THR and TTI can be compared systematically in relation to the design of new flame-retarded materials.

Cone calorimeter tests work based on measuring the decreasing oxygen concentration in combustion gases of a sample exposed to a specified heat flux (usually in the range 10 and 100 kW/m^2). A cone calorimeter's experimental setup is shown in Figure 57.

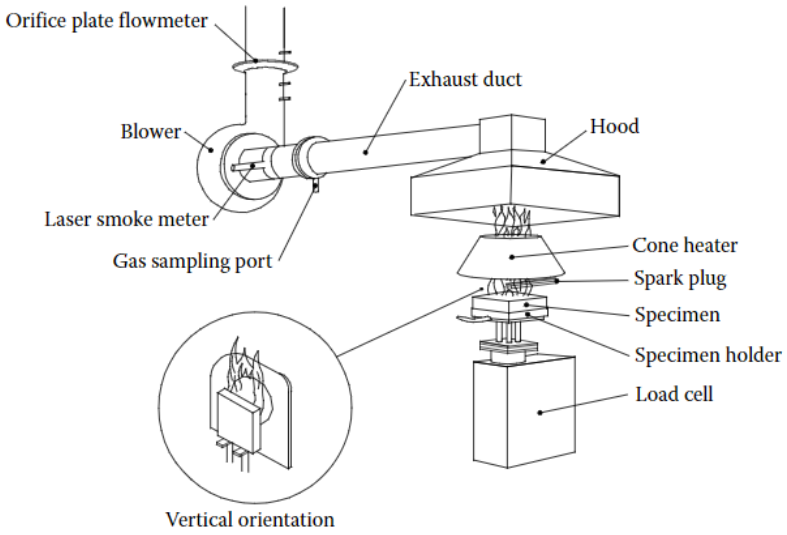

Figure 57. Schematic of cone calorimeter apparatus. Reprinted with the permission from [279]**.**

In order to assess the mass loss during the experiment, the sample is positioned on a load cell. The sample is heated uniformly with a cone-shaped electric radiant heater. An electric spark is used for ignite the sample and start the combustion. The combustion gases generated flow through the heating cone and are collected through an exhaust duct system. Then, gases are sent to analyzers that calculate oxygen content and CO and CO_2 concentrations. The amount of

heat released per unit of time and surface area is calculated using measurements of the gas flow and oxygen content, and represent the HRR (heat release rate), which is expressed in kW m^{-2}. When assessing the fire retardancy of materials, the evolution of the HRR over time, in particular the value of its maximum peak (pkHRR), is a fundamental parameter. The calculation is founded on Huggett's finding that the amount of heat released by the majority of organic materials is proportional to the amount of oxygen used during combustion. The proportionality factor, which is 13.1 kJ/g of consumed oxygen, is constant from one material to the next [280]. The total heat released (THR), expressed in kJ/m^2, is obtained by integrating the HRR vs. time curve. Furthermore, the cone calorimeter test permits evaluation, of the time to ignition (TTI), time of combustion (flame out), mass loss during burning, amounts of CO and CO_2, and total smoke released (TSR), as main parameters.

The different typical combustion behaviors result in distinct HRR versus time curves that provide information about the tested materials. Figure 58 shows the main characteristic HRR vs. time curves.

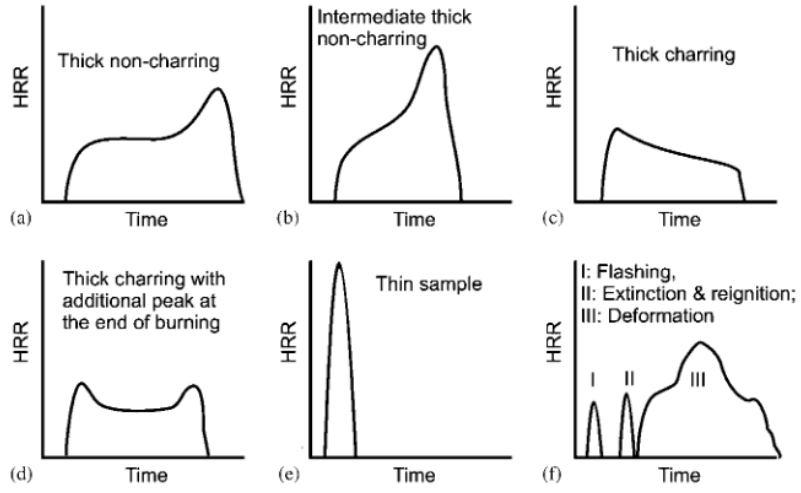

Figure 58. Typical HRR curves for different characteristic burning behaviours. Reprinted with the permission from [10]**.**

a. Thermally thick non-charring specimens present a rapid initial increase of HRR after ignition, reaching a nearly constant HRR value

(averaged or steady HRR). This plateau lasts until the PKHRR takes place close to the end of the test.

b. For intermediate thickness non-charring specimens, the plateau disappears but the steady HRR is highlighted only by a shoulder, followed by the pkHRR.
c. Thermally thick charring (residue forming) specimens form, after an initial increase in HRR, a stable char layer which leads to a progressive decrease in HRR.
d. Some thermally thick charring specimens present two HRR peaks: one at the beginning of the test, before charring, and the other at the conclusion, due to the char cracking.
e. Thermally thin specimens exhibit a pronounced peak in HRR and the pkHRR is dependent on the total fire load.
f. Some materials show HRR curves characterized by unstable combustion trends. The reasons may be intermittency between ignition and self-extinction before a sustained flame or during the entire measurement [10].

The combustion behavior was investigated through cone calorimetry tests according to the ISO 5660 standard, using a Noselab Ats (Nova Milanese, Italy) instrument. Square samples (50 × 50 × 3 mm^3) were exposed to different heat fluxes (i.e., 25, 35, and 50 kW m^{-2}) in horizontal configuration. The specimens were wrapped in aluminum foil except the upper face and placed on a load cell, maintaining 25 mm (increased to 60 mm for intumescent specimens, as recommended by the standard) between specimen surface and cone heater. For each formulation, the test was repeated three times and the results were averaged; the standard deviations are found to be less than 20 % of the averages. Time to ignition (TTI, s), peak of heat release rate (pkHRR, kW m^{-2}), time to peak (s), total heat release (THR, kW m^{-2}), total smoke release (TSR, m^2/m^2), fire performance index (FPI, $(kW/m^2)/s$), fire growth rate index (FIGRA, $(kW/m^2)/s$), Fire Retardancy Index (defined as the ratio of THR∗ (pkHRR/TTI) between the neat polymer and the corresponding thermoplastic composite containing only one flame retardant additive, dimensionless) and final residue were evaluated.

The temperatures involved during combustion were recorded using a K-type thermocouple (diameter of 1 mm) from Tersid (Milan, Italy) and a K-type thermocouple integrated on a heat-resistant plate (size: 100 × 100 mm^2) from Thermo Electra (Pijnacker, Netherlands). The first thermocouple was placed in contact with the sample surface exposed to the cone heater, in the center of the

sample, for collecting the temperature on the top; the second one was used as a support for the specimen, in order to collect the bottom temperature. Specimens of $100 \times 100 \times 3$ mm^3 were used; the tests were repeated at least three times and the results averaged; the standard deviations were found below 20 % of the averages.

References

[1] G. L. Nelson and C. A. Wilkie, “Fire and Polymers: Materials and Solutions for Hazard Prevention,” *J Am Chem Soc*, vol. 124, no. 18, pp. 0–5251, May 2002, doi: 10.1021/ja0153767.

[2] D. A. Purser, “Toxic product yields and hazard assessment for fully enclosed design fires,” *Polym Int*, vol. 49, no. 10, pp. 1232–1255, Oct. 2000, doi: 10.1002/1097-0126(200010)49:10<1232::AID-PI543>3.0.CO;2-T.

[3] D. J. Irvine, J. A. McCluskey, and I. M. Robinson, “Fire hazards and some common polymers,” *Polym Degrad Stab*, vol. 67, no. 3, pp. 383–396, Mar. 2000, doi: 10.1016/S0141-3910(99)00127-5.

[4] F. Laoutid, L. Bonnaud, M. Alexandre, J. M. Lopez-Cuesta, and P. Dubois, “New prospects in flame retardant polymer materials: From fundamentals to nanocomposites,” *Materials Science and Engineering R: Reports*, vol. 63, no. 3. pp. 100–125, Jan. 29, 2009. doi: 10.1016/j.mser.2008.09.002.

[5] S. v. Levchik, “Introduction to Flame Retardancy and Polymer Flammability,” *Flame Retardant Polymer Nanocomposites*. John Wiley & Sons, Inc., pp. 1–29, Jul. 17, 2006. doi: 10.1002/9780470109038.ch1.

[6] B. Camino and G. Camino, “The chemical kinetics of the polymer combustion allows for inherent fire retardant synergism,” *Polym Degrad Stab*, vol. 160, pp. 142–147, Feb. 2019, doi: 10.1016/j.polymdegradstab.2018.12.018.

[7] A. Dasari, Z. Z. Yu, G. P. Cai, and Y. W. Mai, “Recent developments in the fire retardancy of polymeric materials,” *Progress in Polymer Science*, vol. 38, no. 9. pp. 1357–1387, Sep. 2013. doi: 10.1016/j.progpolymsci.2013.06.006.

[8] T. Kashiwagi, “Polymer combustion and flammability-Role of the condensed phase,” *Symposium (International) on Combustion*, vol. 25, no. 1. pp. 1423–1437, 1994. doi: 10.1016/S0082-0784(06)80786-1.

[9] G. Malucelli, F. Carosio, J. Alongi, A. Fina, A. Frache, G. Camino, "Materials engineering for surface-confined flame retardancy," *Materials Science and Engineering: R: Reports*, vol. 84, pp 1-20, Oct. 2014, doi. 10.1016/j.mser.2014.08.001.

[10] B. Schartel and T. R. Hull, "Development of fire-retarded materials - Interpretation of cone calorimeter data," *Fire Mater*, vol. 31, no. 5, pp. 327–354, Aug. 2007, doi: 10.1002/fam.949.

[11] S. Bourbigot and S. Duquesne, "Fire retardant polymers: Recent developments and opportunities," *J Mater Chem*, vol. 17, no. 22, pp. 2283–2300, 2007, doi: 10.1039/b702511d.

[12] S. v Levchik, "INTRODUCTION TO FLAME RETARDANCY AND POLYMER FLAMMABILITY."

[13] A. Richard. Horrocks and D. Price, *Fire retardant materials*. CRC Press, 2001.

[14] "Fire Retardancy of Polymeric Materials Second Edition."

[15] A. B. Morgan, "The Future of Flame Retardant Polymers–Unmet Needs and Likely New Approaches," *Polymer Reviews*, vol. 59, no. 1. Taylor and Francis Inc., pp. 25–54, Jan. 02, 2019. doi: 10.1080/15583724.2018.1454948.

[16] J. de Boer, "Brominated flame retardants in the environment - The price for our convenience?," *Environmental Chemistry*, vol. 1, no. 2, pp. 81–85, 2004, doi: 10.1071/EN04038.

[17] T. R. Hull, A. Witkowski, and L. Hollingbery, "Fire retardant action of mineral fillers," *Polym Degrad Stab*, vol. 96, no. 8, pp. 1462–1469, Aug. 2011, doi: 10.1016/j.polymdegradstab.2011.05.006.

[18] R. N. Rothon and P. R. Hornsby, "Flame retardant effects of magnesium hydroxide."

[19] J. Rychl, K. Vesel, E. Gill, ¢ M Kummer, J. Jancar, and & L. Rychlfi, "Use of Thermal Methods in the Characterization of the High-Temperature Decomposition and Ignition of Polyolefins and EVA Copolymers Filled with Mg(OH)2, A! (OH)3 and CaCO3," 1990.

[20] M. S. Cross, P. A. Cusack, and P. R. Hornsby, “Effects of tin additives on the flammability and smoke emission characteristics of halogen-free ethylene-vinyl acetate copolymer.”

[21] M. A. Cárdenas *et al.*, “Mechanical and fire retardant properties of EVA/clay/ATH nanocomposites – Effect of particle size and surface treatment of ATH filler,” *Polym Degrad Stab*, vol. 93, no. 11, pp. 2032–2037, Nov. 2008, doi: 10.1016/j.polymdegradstab.2008.02.015.

[22] J. Hobson *et al.*, “Synergistic Effect of Cerium Oxide for Improving the Fire-Retardant, Mechanical and Ultraviolet-Blocking Properties of EVA/Magnesium Hydroxide Composites,” *Materials*, vol. 15, no. 17, p. 5867, Aug. 2022, doi: 10.3390/ma15175867.

[23] G. Camino, A. Maffezzoli, M. Braglia, M. de Lazzaro, and M. Zammarano, “Effect of hydroxides and hydroxycarbonate structure on fire retardant effectiveness and mechanical properties in ethylene-vinyl acetate copolymer,” *Polym Degrad Stab*, vol. 74, no. 3, pp. 457–464, Jan. 2001, doi: 10.1016/S0141-3910(01)00167-7.

[24] A. M. Aaronson, “Phosphorus Flame Retardants for a Changing World,” 1992, pp. 218–228. doi: 10.1021/bk-1992-0486.ch017.

[25] G. C. Alfonso *et al.*, “Flame-resistant polycaproamide by anionic polymerization of ε-caprolactam in the presence of suitable flame-retardant agents,” *J Appl Polym Sci*, vol. 31, no. 5, pp. 1373–1382, Apr. 1986, doi: 10.1002/app.1986.070310521.

[26] A. Granzow and J. F. Cannelongo, “The effect of red phosphorus on the flammability of poly(ethylene terephthalate),” *J Appl Polym Sci*, vol. 20, no. 3, pp. 689–701, Mar. 1976, doi: 10.1002/app.1976.070200311.

[27] A. Ballistreri, G. Montaudo, C. Puglisi, E. Scamporrino, D. Vitalini, and S. Calgari, “Mechanism of flame retardant action of red phosphorus in polyacrylonitrile,” *Journal of Polymer Science: Polymer Chemistry Edition*, vol. 21, no. 3, pp. 679–689, Mar. 1983, doi: 10.1002/pol.1983.170210304.

[28] S. Rabe, Y. Chuenban, and B. Schartel, “Exploring the modes of action of phosphorus-based flame retardants in polymeric systems,” *Materials*, vol. 10, no. 5, 2017, doi: 10.3390/ma10050455.

[29] Q. Wu, J. Lü, and B. Qu, “Preparation and characterization of microcapsulated red phosphorus and its flame-retardant mechanism in halogen-free flame retardant polyolefins,” *Polym Int*, vol. 52, no. 8, pp. 1326–1331, Aug. 2003, doi: 10.1002/pi.1115.

[30] Y. F. Shih, Y. T. Wang, R. J. Jeng, and K. M. Wei, “Expandable graphite systems for phosphorus-containing unsaturated polyesters. I. Enhanced thermal properties and flame retardancy,” *Polym Degrad Stab*, vol. 86, no. 2, pp. 339–348, Nov. 2004, doi: 10.1016/j.polymdegradstab.2004.04.020.

[31] S. v. Levchik and E. D. Weil, “Flame retardancy of thermoplastic polyester - A review of the recent literature,” *Polymer International*, vol. 54, no. 1. pp. 11–35, Jan. 2005. doi: 10.1002/pi.1663.

[32] S. V. Levchik, L. Costa, and G. Camino, “Effect of the fire-retardant ammonium polyphosphate on the thermal decomposition of aliphatic polyamides. Part III—Polyamides 6.6 and 6.10,” *Polym Degrad Stab*, vol. 43, no. 1, pp. 43–54, Jan. 1994, doi: 10.1016/0141-3910(94)90224-0.

[33] Y. Chen and Q. Wang, “Preparation, properties and characterizations of halogen-free nitrogen-phosphorous flame-retarded glass fiber reinforced polyamide 6 composite,” *Polym Degrad Stab*, vol. 91, no. 9, pp. 2003–2013, Sep. 2006, doi: 10.1016/j.polymdegradstab.2006.02.006.

[34] S. Duquesne *et al.*, “Mechanism of fire retardancy of polyurethanes using ammonium polyphosphate,” *J Appl Polym Sci*, vol. 82, no. 13, pp. 3262–3274, Dec. 2001, doi: 10.1002/app.2185.

[35] S. v Levchik and E. D. Weil, “Flame retardancy of thermoplastic polyesters?a review of the recent literature,” *Polym Int*, vol. 54, no. 1, pp. 11–35, Jan. 2005, doi: 10.1002/pi.1663.

[36] C. Feng, M. Liang, W. Chen, J. Huang, and H. Liu, “Flame retardancy and thermal degradation of intumescent flame retardant EVA composite with efficient charring agent,” *J Anal Appl Pyrolysis*, vol. 113, pp. 266–273, May 2015, doi: 10.1016/j.jaap.2015.01.021.

[37] J. Bonnet, V. Bounor-Legaré, F. Boisson, F. Melis, G. Camino, and P. Cassagnau, “Phosphorus based organic-inorganic hybrid materials prepared by reactive processing for EVA fire retardancy,” *Polym Degrad Stab*, vol. 97, no. 4, pp. 513–522, Apr. 2012, doi: 10.1016/j.polymdegradstab.2012.01.018.

[38] B. Bann and S. A. Miller, “Melamine And Derivatives Of Melamine,” *Chem Rev*, vol. 58, no. 1, pp. 131–172, Feb. 1958, doi: 10.1021/cr50019a004.

[39] G. Camino, R. Sgobbi, A. Zaopo, S. Colombier, and C. Scelza, “Investigation of flame retardancy in EVA,” *Fire Mater*, vol. 24, no. 2, pp. 85–90, Mar. 2000, doi: 10.1002/1099-1018(200003/04)24:2<85::AID-FAM724>3.0.CO;2-T.

[40] A. S. Luyt *et al.*, “Halogen-free flame-retardant compounds. Thermal decomposition and flammability behavior for alternative polyethylene grades,” *Polymers (Basel)*, vol. 11, no. 9, Sep. 2019, doi: 10.3390/polym11091479.

[41] S. Bourbigot and S. Duquesne, “Char Formation and Characterization,” in *Fire Retardancy of Polymeric Materials*, C. A. Wilkie and A. B. Morgan, Eds. CRC Press, 2009, pp. 239–259.

[42] G. Camino, L. Costa, and M. P. Luda di Cortemiglia, “Overview of fire retardant mechanisms,” *Polym Degrad Stab*, vol. 33, no. 2, pp. 131–154, Jan. 1991, doi: 10.1016/0141-3910(91)90014-I.

[43] G. Camino, L. Costa, and L. Trossarelli, “Study of the mechanism of intumescence in fire retardant polymers: Part II—Mechanism of action in polypropylene-ammonium polyphosphate-pentaerythritol mixtures,” *Polym Degrad Stab*, vol. 7, no. 1, pp. 25–31, Jan. 1984, doi: 10.1016/0141-3910(84)90027-2.

[44] L. Morice, S. Bourbigot, and J.-M. Leroy, “Heat Transfer Study of Polypropylene-Based Intumescent Systems during Combustion,” *J Fire Sci*, vol. 15, no. 5, pp. 358–374, Sep. 1997, doi: 10.1177/073490419701500502.

[45] S. Bourbigot, S. Duquesne, and J.-M. Leroy, “Modeling of Heat Transfer of a Polypropylene-Based Intumescent System during Combustion,” *J Fire Sci*, vol. 17, no. 1, pp. 42–56, Jan. 1999, doi: 10.1177/073490419901700103.

[46] M. le Bras, S. Bourbigot, C. Delporte, C. Siat, and Y. le Tallec, “New Intumescent Formulations of Fire-retardant Polypropylene—Discussion of the Free Radical Mechanism of the Formation of Carbonaceous Protective Material During the Thermo-oxidative Treatment of the Additives,” *Fire Mater*, vol. 20, no. 4, pp. 191–203, Jul. 1996, doi: 10.1002/(SICI)1099-1018(199607)20:4<191::AID-FAM577>3.0.CO;2-S.

[47] J. Alongi, Z. Han, and S. Bourbigot, “Intumescence: Tradition versus novelty. A comprehensive review,” *Progress in Polymer Science*, vol. 51. Elsevier Ltd, pp. 28–73, Oct. 18, 2014. doi: 10.1016/j.progpolymsci.2015.04.010.

[48] M. le Bras, S. Bourbigot, and B. Revel, “Comprehensive study of the degradation of an intumescent EVA-based material during combustion.”

[49] S.-Y. Fu, X.-Q. Feng, B. Lauke, and Y.-W. Mai, “Effects of particle size, particle/matrix interface adhesion and particle loading on mechanical properties of particulate–polymer composites,” *Compos B Eng*, vol. 39, no. 6, pp. 933–961, Sep. 2008, doi: 10.1016/j.compositesb.2008.01.002.

[50] F. Teles, G. Martins, and F. Antunes, “Fire retardancy in nanocomposites by using nanomaterial additives,” *J Anal Appl Pyrolysis*, vol. 163, p. 105466, May 2022, doi: 10.1016/j.jaap.2022.105466.

[51] J. W. Gilman *et al.*, “Flammability Properties of Polymer−Layered-Silicate Nanocomposites. Polypropylene and Polystyrene Nanocomposites,” *Chemistry of Materials*, vol. 12, no. 7, pp. 1866–1873, Jul. 2000, doi: 10.1021/cm0001760.

[52] Y. Komori, Y. Sugahara, and K. Kuroda, “Direct Intercalation of Poly(vinylpyrrolidone) into Kaolinite by a Refined Guest Displacement Method,” *Chemistry of Materials*, vol. 11, no. 1, pp. 3–6, Jan. 1999, doi: 10.1021/cm9804721.

[53] A. B. Morgan and J. W. Gilman, “An overview of flame retardancy of polymeric materials: Application, technology, and future directions,” *Fire and Materials*, vol. 37, no. 4. pp. 259–279, Jun. 2013. doi: 10.1002/fam.2128.

[54] B. N. Jang, M. Costache, and C. A. Wilkie, “The relationship between thermal degradation behavior of polymer and the fire retardancy of polymer/clay nanocomposites,” *Polymer (Guildf)*, vol. 46, no. 24, pp. 10678–10687, Nov. 2005, doi: 10.1016/j.polymer.2005.08.085.

[55] B. N. Jang and C. A. Wilkie, “The thermal degradation of polystyrene nanocomposite,” *Polymer (Guildf)*, vol. 46, no. 9, pp. 2933–2942, Apr. 2005, doi: 10.1016/j.polymer.2005.01.098.

[56] J. W. Gilman, “Flame Retardant Mechanism of Polymer–Clay Nanocomposites,” in *Flame Retardant Polymer Nanocomposites*, Hoboken, NJ, USA: John Wiley & Sons, Inc., pp. 67–87. doi: 10.1002/9780470109038.ch3.

[57] T. Kashiwagi *et al.*, “Flammability properties of polymer nanocomposites with single-walled carbon nanotubes: effects of nanotube dispersion and concentration,” *Polymer (Guildf)*, vol. 46, no. 2, pp. 471–481, Jan. 2005, doi: 10.1016/j.polymer.2004.10.087.

[58] S. Duquesne, C. Jama, M. le Bras, R. Delobel, P. Recourt, and J. M. Gloaguen, “Elaboration of EVA-nanoclay systems - Characterization, thermal behaviour and fire performance,” *Compos Sci Technol*, vol. 63, no. 8, pp. 1141–1148, 2003, doi: 10.1016/S0266-3538(03)00035-6.

[59] L. Costes, F. Laoutid, S. Brohez, and P. Dubois, “Bio-based flame retardants: When nature meets fire protection,” *Materials Science and Engineering R: Reports*, vol. 117. Elsevier Ltd, pp. 1–25, Jul. 01, 2017. doi: 10.1016/j.mser.2017.04.001.

[60] S. v. Vassilev, D. Baxter, L. K. Andersen, and C. G. Vassileva, “An overview of the chemical composition of biomass,” *Fuel*, vol. 89, no. 5, pp. 913–933, May 2010, doi: 10.1016/j.fuel.2009.10.022.

[61] R. Sonnier, A. Taguet, L. Ferry, and J.-M. Lopez-Cuesta, “Biobased Flame Retardants,” in *Towards Bio-based Flame Retardant Polymers*, 1st ed.,

Sonnier Rodolphe, Taguet Aurélie, Ferry Laurent, and Lopez-Cuesta José-Marie, Eds. Springer Cham, 2018, pp. 33–72.

[62] F. Bosco, A. Casale, G. Gribaudo, C. Mollea, and G. Malucelli, "Nucleic acids from agro-industrial wastes: A green recovery method for fire retardant applications," *Ind Crops Prod*, vol. 108, pp. 208–218, Dec. 2017, doi: 10.1016/j.indcrop.2017.06.035.

[63] S. Basak *et al.*, "Flame resistant cellulosic substrate using banana pseudostem sap," *Polish Journal of Chemical Technology*, vol. 17, no. 1, pp. 123–133, Mar. 2015, doi: 10.1515/pjct-2015-0018.

[64] S. Basak and S. W. Ali, "Sustainable fire retardancy of textiles using bio-macromolecules," *Polym Degrad Stab*, vol. 133, pp. 47–64, Nov. 2016, doi: 10.1016/j.polymdegradstab.2016.07.019.

[65] X.-W. Cheng, C.-X. Liang, J.-P. Guan, X.-H. Yang, and R.-C. Tang, "Flame retardant and hydrophobic properties of novel sol-gel derived phytic acid/silica hybrid organic-inorganic coatings for silk fabric," *Appl Surf Sci*, vol. 427, pp. 69–80, Jan. 2018, doi: 10.1016/j.apsusc.2017.08.021.

[66] G. Malucelli *et al.*, "Biomacromolecules as novel green flame retardant systems for textiles: an overview," *RSC Adv.*, vol. 4, no. 86, pp. 46024–46039, Sep. 2014, doi: 10.1039/C4RA06771A.

[67] J. Alongi, A. di Blasio, F. Cuttica, F. Carosio, and G. Malucelli, "Bulk or surface treatments of ethylene vinyl acetate copolymers with DNA: Investigation on the flame retardant properties," *Eur Polym J*, vol. 51, pp. 112–119, Feb. 2014, doi: 10.1016/j.eurpolymj.2013.12.009.

[68] N. Nan, D. B. DeVallance, X. Xie, and J. Wang, "The effect of bio-carbon addition on the electrical, mechanical, and thermal properties of polyvinyl alcohol/biochar composites," *J Compos Mater*, vol. 50, no. 9, pp. 1161–1168, Apr. 2016, doi: 10.1177/0021998315589770.

[69] X. Zhang *et al.*, "Using biochar for remediation of soils contaminated with heavy metals and organic pollutants," *Environmental Science and Pollution Research*, vol. 20, no. 12, pp. 8472–8483, Dec. 2013, doi: 10.1007/s11356-013-1659-0.

[70] M. Ghaedi, A. G. Nasab, S. Khodadoust, M. Rajabi, and S. Azizian, "Application of activated carbon as adsorbents for efficient removal of methylene blue: Kinetics and equilibrium study," *Journal of Industrial and Engineering Chemistry*, vol. 20, no. 4, pp. 2317–2324, Jul. 2014, doi: 10.1016/j.jiec.2013.10.007.

[71] M. Ghaedi, H. Mazaheri, S. Khodadoust, S. Hajati, and M. K. Purkait, "Application of central composite design for simultaneous removal of methylene blue and Pb2+ ions by walnut wood activated carbon," *Spectrochim Acta A Mol Biomol Spectrosc*, vol. 135, pp. 479–490, Jan. 2015, doi: 10.1016/j.saa.2014.06.138.

[72] Z. Liu, B. Fei, Z. Jiang, and X. Liu, "Combustion characteristics of bamboo-biochars," *Bioresour Technol*, vol. 167, pp. 94–99, Sep. 2014, doi: 10.1016/j.biortech.2014.05.023.

[73] M. Barbalini, M. Bartoli, A. Tagliaferro, and G. Malucelli, "Phytic Acid and Biochar: An Effective All Bio-Sourced Flame Retardant Formulation for Cotton Fabrics," *Polymers (Basel)*, vol. 12, no. 4, p. 811, Apr. 2020, doi: 10.3390/polym12040811.

[74] S. Matta, M. Bartoli, and G. Malucelli, "Flame retardant polymer systems containing biochar: current state-of-the-art and perspectives," in *Biochar*, IOP Publishing, 2020. doi: 10.1088/978-0-7503-2660-5ch9.

[75] M. Ahmad *et al.*, "Biochar as a sorbent for contaminant management in soil and water: A review," *Chemosphere*, vol. 99. Elsevier Ltd, pp. 19–33, 2014. doi: 10.1016/j.chemosphere.2013.10.071.

[76] M. Chen, G. Zeng, J. Zhang, P. Xu, A. Chen, and L. Lu, "Global Landscape of Total Organic Carbon, Nitrogen and Phosphorus in Lake Water," *Sci Rep*, vol. 5, no. 1, p. 15043, Dec. 2015, doi: 10.1038/srep15043.

[77] L. Leng *et al.*, "Bio-char derived from sewage sludge by liquefaction: Characterization and application for dye adsorption," *Appl Surf Sci*, vol. 346, pp. 223–231, Aug. 2015, doi: 10.1016/j.apsusc.2015.04.014.

[78] A. S. N. Mahmood, J. G. Brammer, A. Hornung, A. Steele, and S. Poulston, "The intermediate pyrolysis and catalytic steam reforming of

Brewers spent grain," *J Anal Appl Pyrolysis*, vol. 103, pp. 328–342, Sep. 2013, doi: 10.1016/j.jaap.2012.09.009.

[79] X. Tan *et al.*, "Biochar-based nano-composites for the decontamination of wastewater: A review," *Bioresour Technol*, vol. 212, pp. 318–333, Jul. 2016, doi: 10.1016/j.biortech.2016.04.093.

[80] F. R. Oliveira, A. K. Patel, D. P. Jaisi, S. Adhikari, H. Lu, and S. K. Khanal, "Environmental application of biochar: Current status and perspectives," *Bioresour Technol*, vol. 246, pp. 110–122, Dec. 2017, doi: 10.1016/j.biortech.2017.08.122.

[81] T. R. Miles, "Introduction to the biochar world with a focus on new possible applications," in *Biochar*, IOP Publishing, 2020. doi: 10.1088/978-0-7503-2660-5ch1.

[82] M. B. Ahmed, J. L. Zhou, H. H. Ngo, and W. Guo, "Insight into biochar properties and its cost analysis," *Biomass and Bioenergy*, vol. 84. Elsevier Ltd, pp. 76–86, Jan. 01, 2016. doi: 10.1016/j.biombioe.2015.11.002.

[83] J. S. Cha *et al.*, "Production and utilization of biochar: A review," *Journal of Industrial and Engineering Chemistry*, vol. 40. Korean Society of Industrial Engineering Chemistry, pp. 1–15, Aug. 25, 2016. doi: 10.1016/j.jiec.2016.06.002.

[84] B. Chen and Z. Chen, "Sorption of naphthalene and 1-naphthol by biochars of orange peels with different pyrolytic temperatures," *Chemosphere*, vol. 76, no. 1, pp. 127–133, Jun. 2009, doi: 10.1016/j.chemosphere.2009.02.004.

[85] Y.-S. Shen, S.-L. Wang, Y.-M. Tzou, Y.-Y. Yan, and W.-H. Kuan, "Removal of hexavalent Cr by coconut coir and derived chars – The effect of surface functionality," *Bioresour Technol*, vol. 104, pp. 165–172, Jan. 2012, doi: 10.1016/j.biortech.2011.10.096.

[86] Z. Chen, B. Chen, and C. T. Chiou, "Fast and Slow Rates of Naphthalene Sorption to Biochars Produced at Different Temperatures," *Environ Sci Technol*, vol. 46, no. 20, pp. 11104–11111, Oct. 2012, doi: 10.1021/es302345e.

[87] S. Kumar, V. A. Loganathan, R. B. Gupta, and M. O. Barnett, “An Assessment of U(VI) removal from groundwater using biochar produced from hydrothermal carbonization,” *J Environ Manage*, vol. 92, no. 10, pp. 2504–2512, Oct. 2011, doi: 10.1016/j.jenvman.2011.05.013.

[88] D. W. Rutherford, R. L. Wershaw, C. E. Rostad, and C. N. Kelly, “Effect of formation conditions on biochars: Compositional and structural properties of cellulose, lignin, and pine biochars,” *Biomass Bioenergy*, vol. 46, pp. 693–701, Nov. 2012, doi: 10.1016/j.biombioe.2012.06.026.

[89] M. Inguanzo, A. Domínguez, J. A. Menéndez, C. G. Blanco, and J. J. Pis, “On the pyrolysis of sewage sludge: the influence of pyrolysis conditions on solid, liquid and gas fractions,” *J Anal Appl Pyrolysis*, vol. 63, no. 1, pp. 209–222, Mar. 2002, doi: 10.1016/S0165-2370(01)00155-3.

[90] A. Demirbas, “Effects of temperature and particle size on bio-char yield from pyrolysis of agricultural residues,” *J Anal Appl Pyrolysis*, vol. 72, no. 2, pp. 243–248, Nov. 2004, doi: 10.1016/j.jaap.2004.07.003.

[91] G. Chen, J. Andries, Z. Luo, and H. Spliethoff, “Biomass pyrolysis/gasification for product gas production: the overall investigation of parametric effects,” *Energy Convers Manag*, vol. 44, no. 11, pp. 1875–1884, Jul. 2003, doi: 10.1016/S0196-8904(02)00188-7.

[92] M. I. Jahirul, M. G. Rasul, A. A. Chowdhury, and N. Ashwath, “Biofuels production through biomass pyrolysis- A technological review,” *Energies*, vol. 5, no. 12. MDPI AG, pp. 4952–5001, 2012. doi: 10.3390/en5124952.

[93] X. Li *et al.*, “Functional Groups Determine Biochar Properties (pH and EC) as Studied by Two-Dimensional 13C NMR Correlation Spectroscopy,” *PLoS One*, vol. 8, no. 6, p. e65949, Jun. 2013, doi: 10.1371/journal.pone.0065949.

[94] M. Ahmad *et al.*, “Effects of pyrolysis temperature on soybean stover- and peanut shell-derived biochar properties and TCE adsorption in water,” *Bioresour Technol*, vol. 118, pp. 536–544, Aug. 2012, doi: 10.1016/j.biortech.2012.05.042.

[95] O. R. Harvey, B. E. Herbert, R. D. Rhue, and L.-J. Kuo, “Metal Interactions at the Biochar-Water Interface: Energetics and Structure-

Sorption Relationships Elucidated by Flow Adsorption Microcalorimetry," *Environ Sci Technol*, vol. 45, no. 13, pp. 5550–5556, Jul. 2011, doi: 10.1021/es104401h.

[96] W.-K. Kim *et al.*, "Characterization of cadmium removal from aqueous solution by biochar produced from a giant Miscanthus at different pyrolytic temperatures," *Bioresour Technol*, vol. 138, pp. 266–270, Jun. 2013, doi: 10.1016/j.biortech.2013.03.186.

[97] M. E. Boucher, A. Chaala, H. Pakdel, and C. Roy, "Bio-oils obtained by vacuum pyrolysis of softwood bark as a liquid fuel for gas turbines. Part II: Stability and ageing of bio-oil and its blends with methanol and a pyrolytic aqueous phase," *Biomass Bioenergy*, vol. 19, no. 5, pp. 351–361, Nov. 2000, doi: 10.1016/S0961-9534(00)00044-1.

[98] A. K. Sakhiya, A. Anand, and P. Kaushal, "Production, activation, and applications of biochar in recent times," *Biochar*, vol. 2, no. 3. Springer Science and Business Media B.V., pp. 253–285, Sep. 01, 2020. doi: 10.1007/s42773-020-00047-1.

[99] D. Mohan, C. U. Pittman, and P. H. Steele, "Pyrolysis of Wood/Biomass for Bio-oil: A Critical Review," *Energy & Fuels*, vol. 20, no. 3, pp. 848–889, May 2006, doi: 10.1021/ef0502397.

[100] R. Aguado, M. Olazar, B. Gaisán, R. Prieto, and J. Bilbao, "Kinetic Study of Polyolefin Pyrolysis in a Conical Spouted Bed Reactor," *Ind Eng Chem Res*, vol. 41, no. 18, pp. 4559–4566, Sep. 2002, doi: 10.1021/ie0201260.

[101] M. Balat, M. Balat, E. Kirtay, and H. Balat, "Main routes for the thermo-conversion of biomass into fuels and chemicals. Part 1: Pyrolysis systems," *Energy Convers Manag*, vol. 50, no. 12, pp. 3147–3157, Dec. 2009, doi: 10.1016/j.enconman.2009.08.014.

[102] P. M. Lv, Z. H. Xiong, J. Chang, C. Z. Wu, Y. Chen, and J. X. Zhu, "An experimental study on biomass air–steam gasification in a fluidized bed," *Bioresour Technol*, vol. 95, no. 1, pp. 95–101, Oct. 2004, doi: 10.1016/j.biortech.2004.02.003.

[103] A. Heidari, R. Stahl, H. Younesi, A. Rashidi, N. Troeger, and A. A. Ghoreyshi, "Effect of process conditions on product yield and composition

of fast pyrolysis of Eucalyptus grandis in fluidized bed reactor," *Journal of Industrial and Engineering Chemistry*, vol. 20, no. 4, pp. 2594–2602, Jul. 2014, doi: 10.1016/j.jiec.2013.10.046.

[104] S. Papari and K. Hawboldt, "A review on the pyrolysis of woody biomass to bio-oil: Focus on kinetic models," *Renewable and Sustainable Energy Reviews*, vol. 52, pp. 1580–1595, Dec. 2015, doi: 10.1016/j.rser.2015.07.191.

[105] T. Aysu and M. M. Küçük, "Biomass pyrolysis in a fixed-bed reactor: Effects of pyrolysis parameters on product yields and characterization of products," *Energy*, vol. 64, pp. 1002–1025, Jan. 2014, doi: 10.1016/j.energy.2013.11.053.

[106] D. Mohan, A. Sarswat, Y. S. Ok, and C. U. Pittman, "Organic and inorganic contaminants removal from water with biochar, a renewable, low cost and sustainable adsorbent – A critical review," *Bioresour Technol*, vol. 160, pp. 191–202, May 2014, doi: 10.1016/j.biortech.2014.01.120.

[107] C. E. Brewer, K. Schmidt-Rohr, J. A. Satrio, and R. C. Brown, "Characterization of biochar from fast pyrolysis and gasification systems," *Environ Prog Sustain Energy*, vol. 28, no. 3, pp. 386–396, Oct. 2009, doi: 10.1002/ep.10378.

[108] L.-P. Xiao, Z.-J. Shi, F. Xu, and R.-C. Sun, "Hydrothermal carbonization of lignocellulosic biomass," *Bioresour Technol*, vol. 118, pp. 619–623, Aug. 2012, doi: 10.1016/j.biortech.2012.05.060.

[109] S. Román, J. M. V. Nabais, C. Laginhas, B. Ledesma, and J. F. González, "Hydrothermal carbonization as an effective way of densifying the energy content of biomass," *Fuel Processing Technology*, vol. 103, pp. 78–83, Nov. 2012, doi: 10.1016/j.fuproc.2011.11.009.

[110] A. Kruse, "Hydrothermal biomass gasification," *J Supercrit Fluids*, vol. 47, no. 3, pp. 391–399, Jan. 2009, doi: 10.1016/j.supflu.2008.10.009.

[111] S. Gul, J. K. Whalen, B. W. Thomas, V. Sachdeva, and H. Deng, "Physico-chemical properties and microbial responses in biochar-amended soils: Mechanisms and future directions," *Agric Ecosyst Environ*, vol. 206, pp. 46–59, Aug. 2015, doi: 10.1016/j.agee.2015.03.015.

[112] S. Román, J. M. V. Nabais, C. Laginhas, B. Ledesma, and J. F. González, "Hydrothermal carbonization as an effective way of densifying the energy content of biomass," *Fuel Processing Technology*, vol. 103, pp. 78–83, Nov. 2012, doi: 10.1016/j.fuproc.2011.11.009.

[113] E. Sabio, A. Álvarez-Murillo, S. Román, and B. Ledesma, "Conversion of tomato-peel waste into solid fuel by hydrothermal carbonization: Influence of the processing variables," *Waste Management*, vol. 47, pp. 122–132, Jan. 2016, doi: 10.1016/j.wasman.2015.04.016.

[114] W.-H. Chen, J. Peng, and X. T. Bi, "A state-of-the-art review of biomass torrefaction, densification and applications," *Renewable and Sustainable Energy Reviews*, vol. 44, pp. 847–866, Apr. 2015, doi: 10.1016/j.rser.2014.12.039.

[115] M. J. Gronnow *et al.*, "Torrefaction/biochar production by microwave and conventional slow pyrolysis - comparison of energy properties," *GCB Bioenergy*, vol. 5, no. 2, pp. 144–152, Mar. 2013, doi: 10.1111/gcbb.12021.

[116] A. Pimchuai, A. Dutta, and P. Basu, "Torrefaction of Agriculture Residue To Enhance Combustible Properties," *Energy & Fuels*, vol. 24, no. 9, pp. 4638–4645, Sep. 2010, doi: 10.1021/ef901168f.

[117] J. Lehmann and S. Joseph, Eds., *Biochar for Environmental Management*. Routledge, 2015. doi: 10.4324/9780203762264.

[118] B. Zhao *et al.*, "Effect of pyrolysis temperature, heating rate, and residence time on rapeseed stem derived biochar," *J Clean Prod*, vol. 174, pp. 977–987, Feb. 2018, doi: 10.1016/j.jclepro.2017.11.013.

[119] F. Lian, F. Huang, W. Chen, B. Xing, and L. Zhu, "Sorption of apolar and polar organic contaminants by waste tire rubber and its chars in single- and bi-solute systems," *Environmental Pollution*, vol. 159, no. 4, pp. 850–857, Apr. 2011, doi: 10.1016/j.envpol.2011.01.002.

[120] K. Weber and P. Quicker, "Properties of biochar," *Fuel*, vol. 217. Elsevier Ltd, pp. 240–261, Apr. 01, 2018. doi: 10.1016/j.fuel.2017.12.054.

[121] J.-H. Yuan, R.-K. Xu, and H. Zhang, "The forms of alkalis in the biochar produced from crop residues at different temperatures," *Bioresour Technol*,

vol. 102, no. 3, pp. 3488–3497, Feb. 2011, doi: 10.1016/j.biortech.2010.11.018.

[122] J. Lehmann, J. Gaunt, and M. Rondon, “Bio-char Sequestration in Terrestrial Ecosystems – A Review,” *Mitig Adapt Strateg Glob Chang*, vol. 11, no. 2, pp. 403–427, Mar. 2006, doi: 10.1007/s11027-005-9006-5.

[123] K. Y. Chan, L. van Zwieten, I. Meszaros, A. Downie, and S. Joseph, “Agronomic values of greenwaste biochar as a soil amendment,” *Soil Research*, vol. 45, no. 8, p. 629, 2007, doi: 10.1071/SR07109.

[124] X. Cao and W. Harris, “Properties of dairy-manure-derived biochar pertinent to its potential use in remediation,” *Bioresour Technol*, vol. 101, no. 14, pp. 5222–5228, Jul. 2010, doi: 10.1016/j.biortech.2010.02.052.

[125] A. Silber, I. Levkovitch, and E. R. Graber, “pH-Dependent Mineral Release and Surface Properties of Cornstraw Biochar: Agronomic Implications,” *Environ Sci Technol*, vol. 44, no. 24, pp. 9318–9323, Dec. 2010, doi: 10.1021/es101283d.

[126] W. Suliman, J. B. Harsh, N. I. Abu-Lail, A.-M. Fortuna, I. Dallmeyer, and M. Garcia-Perez, “Influence of feedstock source and pyrolysis temperature on biochar bulk and surface properties,” *Biomass Bioenergy*, vol. 84, pp. 37–48, Jan. 2016, doi: 10.1016/j.biombioe.2015.11.010.

[127] J. Li, L. Cao, Y. Yuan, R. Wang, Y. Wen, and J. Man, “Comparative study for microcystin-LR sorption onto biochars produced from various plant- and animal-wastes at different pyrolysis temperatures: Influencing mechanisms of biochar properties,” *Bioresour Technol*, vol. 247, pp. 794–803, Jan. 2018, doi: 10.1016/j.biortech.2017.09.120.

[128] M. I. Al-Wabel, A. Al-Omran, A. H. El-Naggar, M. Nadeem, and A. R. A. Usman, “Pyrolysis temperature induced changes in characteristics and chemical composition of biochar produced from conocarpus wastes,” *Bioresour Technol*, vol. 131, pp. 374–379, Mar. 2013, doi: 10.1016/j.biortech.2012.12.165.

[129] R. C. Bansal, J. B. Donnet, and F. Stoeckli, “Active Carbon,” *J Dispers Sci Technol*, vol. 11, no. 3, p. 323, 1990, doi: 10.1080/01932699008943255.

[130] R. A. Brown, A. K. Kercher, T. H. Nguyen, D. C. Nagle, and W. P. Ball, "Production and characterization of synthetic wood chars for use as surrogates for natural sorbents," *Org Geochem*, vol. 37, no. 3, pp. 321–333, Mar. 2006, doi: 10.1016/j.orggeochem.2005.10.008.

[131] C. E. Brewer *et al.*, "New approaches to measuring biochar density and porosity," *Biomass Bioenergy*, vol. 66, pp. 176–185, 2014, doi: 10.1016/j.biombioe.2014.03.059.

[132] R. Antón-Herrero, C. García-Delgado, M. Alonso-Izquierdo, G. García-Rodríguez, J. Cuevas, and E. Eymar, "Comparative adsorption of tetracyclines on biochars and stevensite: Looking for the most effective adsorbent," *Appl Clay Sci*, vol. 160, pp. 162–172, Aug. 2018, doi: 10.1016/j.clay.2017.12.023.

[133] S. Gul, J. K. Whalen, B. W. Thomas, V. Sachdeva, and H. Deng, "Physico-chemical properties and microbial responses in biochar-amended soils: Mechanisms and future directions," *Agric Ecosyst Environ*, vol. 206, pp. 46–59, Aug. 2015, doi: 10.1016/j.agee.2015.03.015.

[134] H. Wang, B. Gao, S. Wang, J. Fang, Y. Xue, and K. Yang, "Removal of Pb(II), Cu(II), and Cd(II) from aqueous solutions by biochar derived from KMnO4 treated hickory wood," *Bioresour Technol*, vol. 197, pp. 356–362, Dec. 2015, doi: 10.1016/j.biortech.2015.08.132.

[135] O. Das, D. Bhattacharyya, and A. K. Sarmah, "Sustainable eco-composites obtained from waste derived biochar: A consideration in performance properties, production costs, and environmental impact," *J Clean Prod*, vol. 129, pp. 159–168, Aug. 2016, doi: 10.1016/j.jclepro.2016.04.088.

[136] M. Bartoli, R. Arrigo, G. Malucelli, A. Tagliaferro, and D. Duraccio, "Recent Advances in Biochar Polymer Composites," *Polymers*, vol. 14, no. 12. MDPI, Jun. 01, 2022. doi: 10.3390/polym14122506.

[137] O. Das, A. K. Sarmah, and D. Bhattacharyya, "A novel approach in organic waste utilization through biochar addition in wood/polypropylene composites," *Waste Management*, vol. 38, no. 1, pp. 132–140, 2015, doi: 10.1016/j.wasman.2015.01.015.

[138] O. Das, A. K. Sarmah, and D. Bhattacharyya, “Nanoindentation assisted analysis of biochar added biocomposites,” *Compos B Eng*, vol. 91, pp. 219–227, Apr. 2016, doi: 10.1016/j.compositesb.2016.01.057.

[139] S. Gezahegn *et al.*, “Porous graphitic biocarbon and reclaimed carbon fiber derived environmentally benign lightweight composites,” *Science of the Total Environment*, vol. 664, pp. 363–373, May 2019, doi: 10.1016/j.scitotenv.2019.01.408.

[140] S. Ikram, O. Das, and D. Bhattacharyya, “A parametric study of mechanical and flammability properties of biochar reinforced polypropylene composites,” *Compos Part A Appl Sci Manuf*, vol. 91, pp. 177–188, Dec. 2016, doi: 10.1016/j.compositesa.2016.10.010.

[141] D. M. Paleri, A. Rodriguez-Uribe, M. Misra, and A. K. Mohanty, “Pyrolyzed biomass from corn ethanol industry coproduct and their polypropylene-based composites: Effect of heat treatment temperature on performance of the biocomposites,” *Compos B Eng*, vol. 215, Jun. 2021, doi: 10.1016/j.compositesb.2021.108714.

[142] A. A. Alghyamah *et al.*, “Biochar/polypropylene composites: A study on the effect of pyrolysis temperature on crystallization kinetics, crystalline structure, and thermal stability,” *J King Saud Univ Sci*, vol. 33, no. 4, Jun. 2021, doi: 10.1016/j.jksus.2021.101409.

[143] Q. Zhang *et al.*, “Biochar filled high-density polyethylene composites with excellent properties: Towards maximizing the utilization of agricultural wastes,” *Ind Crops Prod*, vol. 146, Apr. 2020, doi: 10.1016/j.indcrop.2020.112185.

[144] Q. Zhang *et al.*, “Production of high-density polyethylene biocomposites from rice husk biochar: Effects of varying pyrolysis temperature,” *Science of the Total Environment*, vol. 738, Oct. 2020, doi: 10.1016/j.scitotenv.2020.139910.

[145] R. Arrigo, P. Jagdale, M. Bartoli, A. Tagliaferro, and G. Malucelli, “Structure-property relationships in polyethylene-based composites filled with biochar derived from waste coffee grounds,” *Polymers (Basel)*, vol. 11, no. 8, Aug. 2019, doi: 10.3390/polym11081336.

[146] S. Li, H. Wang, C. Chen, X. Li, Q. Deng, and D. Li, "Mechanical, electrical, and thermal properties of highly filled bamboo charcoal/ultra-high molecular weight polyethylene composites," *Polym Compos*, vol. 39, pp. E1858–E1866, Jun. 2018, doi: 10.1002/pc.24839.

[147] S. Li, A. Huang, Y. J. Chen, D. Li, and L. S. Turng, "Highly filled biochar/ultra-high molecular weight polyethylene/linear low density polyethylene composites for high-performance electromagnetic interference shielding," *Compos B Eng*, vol. 153, pp. 277–284, Nov. 2018, doi: 10.1016/j.compositesb.2018.07.049.

[148] S. Li, X. Li, Q. Deng, and D. Li, "Three kinds of charcoal powder reinforced ultra-high molecular weight polyethylene composites with excellent mechanical and electrical properties," *Mater Des*, vol. 85, pp. 54–59, Nov. 2015, doi: 10.1016/j.matdes.2015.06.163.

[149] S. Li *et al.*, "Development of electrically conductive nano bamboo charcoal/ultra-high molecular weight polyethylene composites with a segregated network," *Compos Sci Technol*, vol. 132, pp. 31–37, Aug. 2016, doi: 10.1016/j.compscitech.2016.06.010.

[150] E. Watt, M. A. Abdelwahab, A. K. Mohanty, and M. Misra, "Biocomposites from biobased polyamide 4,10 and waste corn cob based biocarbon," *Compos Part A Appl Sci Manuf*, vol. 145, Jun. 2021, doi: 10.1016/j.compositesa.2021.106340.

[151] E. O. Ogunsona, M. Misra, and A. K. Mohanty, "Impact of interfacial adhesion on the microstructure and property variations of biocarbons reinforced nylon 6 biocomposites," *Compos Part A Appl Sci Manuf*, vol. 98, pp. 32–44, Jul. 2017, doi: 10.1016/j.compositesa.2017.03.011.

[152] E. O. Ogunsona, M. Misra, and A. K. Mohanty, "Sustainable biocomposites from biobased polyamide 6,10 and biocarbon from pyrolyzed miscanthus fibers," *J Appl Polym Sci*, vol. 134, no. 4, Jan. 2017, doi: 10.1002/app.44221.

[153] Y. D. Hernandez-Charpak, T. A. Trabold, C. L. Lewis, and C. A. Diaz, "Biochar-filled plastics: Effect of feedstock on thermal and mechanical properties," *Biomass Convers Biorefin*, Oct. 2022, doi: 10.1007/s13399-022-02340-4.

[154] K. Aup-Ngoen and M. Noipitak, “Effect of carbon-rich biochar on mechanical properties of PLA-biochar composites,” *Sustain Chem Pharm*, vol. 15, Mar. 2020, doi: 10.1016/j.scp.2019.100204.

[155] R. Arrigo, M. Bartoli, and G. Malucelli, “Poly(lactic Acid)-biochar biocomposites: Effect of processing and filler content on rheological, thermal, and mechanical properties,” *Polymers (Basel)*, vol. 12, no. 4, Apr. 2020, doi: 10.3390/POLYM12040892.

[156] S. Nizamuddin *et al.*, “Synthesis and characterization of polylactide/rice husk hydrochar composite,” *Sci Rep*, vol. 9, no. 1, Dec. 2019, doi: 10.1038/s41598-019-41960-1.

[157] T. Haeldermans *et al.*, “Poly(Lactic acid) bio-composites containing biochar particles: Effects of fillers and plasticizer on crystallization and thermal properties,” *Express Polym Lett*, vol. 15, no. 4, pp. 343–360, 2021, doi: 10.3144/expresspolymlett.2021.30.

[158] C. May, *Epoxy Resins*. Routledge, 2018. doi: 10.1201/9780203756713.

[159] S. Gantayat, D. Rout, and S. K. Swain, “Carbon Nanomaterial–Reinforced Epoxy Composites: A Review,” *Polym Plast Technol Eng*, vol. 57, no. 1, pp. 1–16, Jan. 2018, doi: 10.1080/03602559.2017.1298802.

[160] A. Montazeri, J. Javadpour, A. Khavandi, A. Tcharkhtchi, and A. Mohajeri, “Mechanical properties of multi-walled carbon nanotube/epoxy composites,” *Mater Des*, vol. 31, no. 9, pp. 4202–4208, Oct. 2010, doi: 10.1016/j.matdes.2010.04.018.

[161] A. Khan *et al.*, “Low-cost carbon fillers to improve mechanical properties and conductivity of epoxy composites,” *Polymers (Basel)*, vol. 9, no. 12, Nov. 2017, doi: 10.3390/polym9120642.

[162] M. Giorcelli, A. Khan, N. M. Pugno, C. Rosso, and A. Tagliaferro, “Biochar as a cheap and environmental friendly filler able to improve polymer mechanical properties,” *Biomass Bioenergy*, vol. 120, pp. 219–223, Jan. 2019, doi: 10.1016/j.biombioe.2018.11.036.

[163] O. P. Minugu, R. Gujjala, O. Shakuntala, P. Manoj, and M. S. Chowdary, “Effect of biomass derived biochar materials on mechanical properties of

biochar epoxy composites," *Proc Inst Mech Eng C J Mech Eng Sci*, vol. 235, no. 21, pp. 5626–5638, Nov. 2021, doi: 10.1177/0954406221990705.

[164] D. Matykiewicz, "Biochar as an effective filler of carbon fiber reinforced bio-epoxy composites," *Processes*, vol. 8, no. 6, pp. 1–13, Jun. 2020, doi: 10.3390/pr8060724.

[165] M. Bartoli *et al.*, "Pressure-Responsive Conductive Poly(vinyl alcohol) Composites Containing Waste Cotton Fibers Biochar," *Micromachines (Basel)*, vol. 13, no. 1, p. 125, Jan. 2022, doi: 10.3390/mi13010125.

[166] N. Nan and D. B. DeVallance, "Development of poly(vinyl alcohol)/wood-derived biochar composites for use in pressure sensor applications," *J Mater Sci*, vol. 52, no. 13, pp. 8247–8257, Jul. 2017, doi: 10.1007/s10853-017-1040-7.

[167] N. Nan, D. B. DeVallance, X. Xie, and J. Wang, "The effect of bio-carbon addition on the electrical, mechanical, and thermal properties of polyvinyl alcohol/biochar composites," *J Compos Mater*, vol. 50, no. 9, pp. 1161–1168, Apr. 2016, doi: 10.1177/0021998315589770.

[168] S. Richard, J. SelwinRajadurai, V. Manikandan, M. Chithambara Thanu, V. Arumugaprabu, and R. Deepak Joel Johnson, "Study of Tribological Properties of Nano-Sized Red Mud Particle-Reinforced Polyester Composites," *Transactions of the Indian Institute of Metals*, vol. 72, no. 9, pp. 2417–2431, Sep. 2019, doi: 10.1007/s12666-019-01694-0.

[169] R. Sundarakannan, V. Arumugaprabu, V. Manikandan, and S. Vigneshwaran, "Mechanical property analysis of biochar derived from cashew nut shell waste reinforced polymer matrix," *Mater Res Express*, vol. 6, no. 12, p. 125349, Jan. 2020, doi: 10.1088/2053-1591/ab6197.

[170] R. O. Akaluzia, F. O. Edoziuno, A. A. Adediran, B. U. Odoni, S. Edibo, and T. M. A. Olayanju, "Evaluation of the effect of reinforcement particle sizes on the impact and hardness properties of hardwood charcoal particulate-polyester resin composites," *Mater Today Proc*, vol. 38, pp. 570–577, 2021, doi: 10.1016/j.matpr.2020.02.980.

[171] J. Andrzejewski, M. Misra, and A. K. Mohanty, "Polycarbonate biocomposites reinforced with a hybrid filler system of recycled carbon

fiber and biocarbon: Preparation and thermomechanical characterization," *J Appl Polym Sci*, vol. 135, no. 28, p. 46449, Jul. 2018, doi: 10.1002/app.46449.

[172] J. Andrzejewski, A. K. Mohanty, and M. Misra, "Development of hybrid composites reinforced with biocarbon/carbon fiber system. The comparative study for PC, ABS and PC/ABS based materials," *Compos B Eng*, vol. 200, p. 108319, Nov. 2020, doi: 10.1016/j.compositesb.2020.108319.

[173] M. R. Ketabchi, M. Khalid, and R. Walvekar, "EFFECT OF OIL PALM EFB-BIOCHAR ON PROPERTIES OF PP/EVA COMPOSITES," 2017. [Online]. Available: https://www.researchgate.net/publication/316629097

[174] S. Lepak-Kuc *et al.*, "Innovative Biochar-Based Composite Fibres from Recycled Material," *Materials*, vol. 14, no. 18, p. 5304, Sep. 2021, doi: 10.3390/ma14185304.

[175] M. G. Faga *et al.*, "Ethylene-Vinyl Acetate (EVA) Containing Waste Hemp-Derived Biochar Fibers: Mechanical, Electrical, Thermal and Tribological Behavior," *Polymers (Basel)*, vol. 14, no. 19, p. 4171, Oct. 2022, doi: 10.3390/polym14194171.

[176] O. Das, D. Bhattacharyya, D. Hui, and K. T. Lau, "Mechanical and flammability characterisations of biochar/polypropylene biocomposites," *Compos B Eng*, vol. 106, pp. 120–128, Dec. 2016, doi: 10.1016/j.compositesb.2016.09.020.

[177] O. Das, N. K. Kim, A. K. Sarmah, and D. Bhattacharyya, "Development of waste based biochar/wool hybrid biocomposites: Flammability characteristics and mechanical properties," *J Clean Prod*, vol. 144, pp. 79–89, Feb. 2017, doi: 10.1016/j.jclepro.2016.12.155.

[178] O. Das, N. K. Kim, A. L. Kalamkarov, A. K. Sarmah, and D. Bhattacharyya, "Biochar to the rescue: Balancing the fire performance and mechanical properties of polypropylene composites," *Polym Degrad Stab*, vol. 144, pp. 485–496, Oct. 2017, doi: 10.1016/j.polymdegradstab.2017.09.006.

[179] Q. Zhang, H. Cai, K. Yang, and W. Yi, “Effect of biochar on mechanical and flame retardant properties of wood – Plastic composites,” *Results Phys*, vol. 7, pp. 2391–2395, 2017, doi: 10.1016/j.rinp.2017.04.025.

[180] N. D. Luong *et al.*, “An eco-friendly and efficient route of lignin extraction from black liquor and a lignin-based copolyester synthesis,” *Polymer Bulletin*, vol. 68, no. 3, pp. 879–890, Feb. 2012, doi: 10.1007/s00289-011-0658-x.

[181] S. Laurichesse and L. Avérous, “Chemical modification of lignins: Towards biobased polymers,” *Progress in Polymer Science*, vol. 39, no. 7. Elsevier Ltd, pp. 1266–1290, 2014. doi: 10.1016/j.progpolymsci.2013.11.004.

[182] C. Chio, M. Sain, and W. Qin, “Lignin utilization: A review of lignin depolymerization from various aspects,” *Renewable and Sustainable Energy Reviews*, vol. 107, pp. 232–249, Jun. 2019, doi: 10.1016/j.rser.2019.03.008.

[183] F. X. Collard and J. Blin, “A review on pyrolysis of biomass constituents: Mechanisms and composition of the products obtained from the conversion of cellulose, hemicelluloses and lignin,” *Renewable and Sustainable Energy Reviews*, vol. 38. Elsevier Ltd, pp. 594–608, 2014. doi: 10.1016/j.rser.2014.06.013.

[184] G. Cazacu, M. C. Pascu, L. Profire, A. I. Kowarski, M. Mihaes, and C. Vasile, “Lignin role in a complex polyolefin blend,” *Ind Crops Prod*, vol. 20, no. 2, pp. 261–273, Sep. 2004, doi: 10.1016/j.indcrop.2004.04.030.

[185] E. Paone, T. Tabanelli, and F. Mauriello, “The rise of lignin biorefinery,” *Curr Opin Green Sustain Chem*, vol. 24, pp. 1–6, Aug. 2020, doi: 10.1016/j.cogsc.2019.11.004.

[186] G. Taylor, “Biofuels and the biorefinery concept,” *Energy Policy*, vol. 36, no. 12, pp. 4406–4409, Dec. 2008, doi: 10.1016/j.enpol.2008.09.069.

[187] J. Hu, Q. Zhang, and D.-J. Lee, “Kraft lignin biorefinery: A perspective,” *Bioresour Technol*, vol. 247, pp. 1181–1183, Jan. 2018, doi: 10.1016/j.biortech.2017.08.169.

[188] N. Mahmood, Z. Yuan, J. Schmidt, and C. Xu, “Production of polyols via direct hydrolysis of kraft lignin: Effect of process parameters,” *Bioresour Technol*, vol. 139, pp. 13–20, 2013, doi: 10.1016/j.biortech.2013.03.199.

[189] S. Farag, B. P. Mudraboyina, P. G. Jessop, and J. Chaouki, “Impact of the heating mechanism on the yield and composition of bio-oil from pyrolysis of kraft lignin,” *Biomass Bioenergy*, vol. 95, pp. 344–353, Dec. 2016, doi: 10.1016/j.biombioe.2016.07.005.

[190] V. Fierro, V. Torné-Fernández, A. Celzard, and D. Montané, “Influence of the demineralisation on the chemical activation of Kraft lignin with orthophosphoric acid,” *J Hazard Mater*, vol. 149, no. 1, pp. 126–133, Oct. 2007, doi: 10.1016/j.jhazmat.2007.03.056.

[191] L. C. P. Araújo, F. M. Yamaji, V. H. Lima, and V. R. Botaro, “Kraft lignin fractionation by organic solvents: Correlation between molar mass and higher heating value,” *Bioresour Technol*, vol. 314, Oct. 2020, doi: 10.1016/j.biortech.2020.123757.

[192] P. Ghetti, L. Ricca, and L. Angelini, “Thermal analysis of biomass and corresponding pyrolysis products,” *Fuel*, vol. 75, no. 5, pp. 565–573, Apr. 1996, doi: 10.1016/0016-2361(95)00296-0.

[193] T. Qu, W. Guo, L. Shen, J. Xiao, and K. Zhao, “Experimental Study of Biomass Pyrolysis Based on Three Major Components: Hemicellulose, Cellulose, and Lignin,” *Ind Eng Chem Res*, vol. 50, no. 18, pp. 10424–10433, Sep. 2011, doi: 10.1021/ie1025453.

[194] A. Demirbas and * Tel, “Relationships between lignin contents and fixed carbon contents of biomass samples,” 2003. [Online]. Available: www.elsevier.com/locate/enconman

[195] J. PARIKH, S. CHANNIWALA, and G. GHOSAL, “A correlation for calculating HHV from proximate analysis of solid fuels,” *Fuel*, vol. 84, no. 5, pp. 487–494, Mar. 2005, doi: 10.1016/j.fuel.2004.10.010.

[196] V. Lago and F. Berruti, “Application of Mechanically Fluidized Reactors to Lignin Pyrolysis,” The University of Western Ontario, 2015. [Online]. Available: https://ir.lib.uwo.ca/etdhttps://ir.lib.uwo.ca/etd/2779

[197] M. M. Hossain, I. M. Scott, F. Berruti, and C. Briens, “Optimizing pyrolysis reactor operating conditions to increase nicotine recovery from tobacco leaves,” *J Anal Appl Pyrolysis*, vol. 112, pp. 80–87, Mar. 2015, doi: 10.1016/j.jaap.2015.02.018.

[198] B. G. Diehl, N. R. Brown, C. W. Frantz, M. R. Lumadue, and F. Cannon, “Effects of pyrolysis temperature on the chemical composition of refined softwood and hardwood lignins,” *Carbon N Y*, vol. 60, pp. 531–537, Aug. 2013, doi: 10.1016/j.carbon.2013.04.087.

[199] F. X. Collard, J. Blin, A. Bensakhria, and J. Valette, “Influence of impregnated metal on the pyrolysis conversion of biomass constituents,” *J Anal Appl Pyrolysis*, vol. 95, pp. 213–226, 2012, doi: 10.1016/j.jaap.2012.02.009.

[200] D. J. Nowakowski, A. V. Bridgwater, D. C. Elliott, D. Meier, and P. de Wild, “Lignin fast pyrolysis: Results from an international collaboration,” *J Anal Appl Pyrolysis*, vol. 88, no. 1, pp. 53–72, May 2010, doi: 10.1016/j.jaap.2010.02.009.

[201] B. Cagnon, X. Py, A. Guillot, F. Stoeckli, and G. Chambat, “Contributions of hemicellulose, cellulose and lignin to the mass and the porous properties of chars and steam activated carbons from various lignocellulosic precursors,” *Bioresour Technol*, vol. 100, no. 1, pp. 292–298, Jan. 2009, doi: 10.1016/j.biortech.2008.06.009.

[202] Z. Ma *et al.*, “In-depth comparison of the physicochemical characteristics of bio-char derived from biomass pseudo components: Hemicellulose, cellulose, and lignin,” *J Anal Appl Pyrolysis*, vol. 140, pp. 195–204, Jun. 2019, doi: 10.1016/j.jaap.2019.03.015.

[203] N. Worasuwannarak, T. Sonobe, and W. Tanthapanichakoon, “Pyrolysis behaviors of rice straw, rice husk, and corncob by TG-MS technique,” *J Anal Appl Pyrolysis*, vol. 78, no. 2, pp. 265–271, 2007, doi: 10.1016/j.jaap.2006.08.002.

[204] K. Crombie, O. Mašek, S. P. Sohi, P. Brownsort, and A. Cross, “The effect of pyrolysis conditions on biochar stability as determined by three methods,” *GCB Bioenergy*, vol. 5, no. 2, pp. 122–131, 2013, doi: 10.1111/gcbb.12030.

[205] B. G. Diehl, N. R. Brown, C. W. Frantz, M. R. Lumadue, and F. Cannon, “Effects of pyrolysis temperature on the chemical composition of refined softwood and hardwood lignins,” *Carbon N Y*, vol. 60, pp. 531–537, Aug. 2013, doi: 10.1016/j.carbon.2013.04.087.

[206] L. Leng *et al.*, “An overview on engineering the surface area and porosity of biochar,” *Science of the Total Environment*, vol. 763. Elsevier B.V., Apr. 01, 2021. doi: 10.1016/j.scitotenv.2020.144204.

[207] J. Zhang, F. Lü, H. Zhang, L. Shao, D. Chen, and P. He, “Multiscale visualization of the structural and characteristic changes of sewage sludge biochar oriented towards potential agronomic and environmental implication,” *Sci Rep*, vol. 5, no. 1, p. 9406, Mar. 2015, doi: 10.1038/srep09406.

[208] A. Tomczyk, Z. Sokołowska, and P. Boguta, “Biochar physicochemical properties: pyrolysis temperature and feedstock kind effects,” *Rev Environ Sci Biotechnol*, vol. 19, no. 1, pp. 191–215, Mar. 2020, doi: 10.1007/s11157-020-09523-3.

[209] H. Yang, R. Yan, H. Chen, D. H. Lee, and C. Zheng, “Characteristics of hemicellulose, cellulose and lignin pyrolysis,” *Fuel*, vol. 86, no. 12–13, pp. 1781–1788, Aug. 2007, doi: 10.1016/j.fuel.2006.12.013.

[210] M. Asmadi, H. Kawamoto, and S. Saka, “Thermal reactivities of catechols/pyrogallols and cresols/xylenols as lignin pyrolysis intermediates,” *J Anal Appl Pyrolysis*, vol. 92, no. 1, pp. 76–87, Sep. 2011, doi: 10.1016/j.jaap.2011.04.012.

[211] Y. Cao *et al.*, “Synthesis Gas Production with an Adjustable H2/CO Ratio through the Coal Gasification Process: Effects of Coal Ranks And Methane Addition,” *Energy & Fuels*, vol. 22, no. 3, pp. 1720–1730, May 2008, doi: 10.1021/ef7005707.

[212] H. Chen and L. Wang, “Sugar Strategies for Biomass Biochemical Conversion,” in *Technologies for Biochemical Conversion of Biomass*, Elsevier, 2017, pp. 137–164. doi: 10.1016/B978-0-12-802417-1.00006-5.

[213] L. Fan *et al.*, “Bio-oil from fast pyrolysis of lignin: Effects of process and upgrading parameters,” *Bioresour Technol*, vol. 241, pp. 1118–1126, Oct. 2017, doi: 10.1016/j.biortech.2017.05.129.

[214] T. Kashiwagi *et al.*, “Thermal and flammability properties of polypropylene/carbon nanotube nanocomposites,” *Polymer (Guildf)*, vol. 45, no. 12, pp. 4227–4239, May 2004, doi: 10.1016/j.polymer.2004.03.088.

[215] Z. Wang, B. Qu, W. Fan, and P. Huang, “Combustion characteristics of halogen-free flame-retarded polyethylene containing magnesium hydroxide and some synergists,” *J Appl Polym Sci*, vol. 81, no. 1, pp. 206–214, Jul. 2001, doi: 10.1002/app.1430.

[216] S. Bourbigot, M. le Bras, F. Dabrowski, J. W. Gilman, and T. Kashiwagi, “PA-6 clay nanocomposite hybrid as char forming agent in intumescent formulations,” *Fire Mater*, vol. 24, no. 4, pp. 201–208, Jul. 2000, doi: 10.1002/1099-1018(200007/08)24:4<201::AID-FAM739>3.0.CO;2-D.

[217] L. Ahmed *et al.*, “Fire reaction properties of polystyrene-based nanocomposites using nanosilica and nanoclay as additives in cone calorimeter test,” *J Therm Anal Calorim*, vol. 132, no. 3, pp. 1853–1865, Jun. 2018, doi: 10.1007/s10973-018-7127-9.

[218] S. Matta, M. Bartoli, A. Frache, and G. Malucelli, “Investigation of different types of biochar on the thermal stability and fire retardance of ethylene-vinyl acetate copolymers,” *Polymers (Basel)*, vol. 13, no. 8, 2021, doi: 10.3390/polym13081256.

[219] A. Merlen, J. Buijnsters, and C. Pardanaud, “A Guide to and Review of the Use of Multiwavelength Raman Spectroscopy for Characterizing Defective Aromatic Carbon Solids: from Graphene to Amorphous Carbons,” *Coatings*, vol. 7, no. 10, p. 153, Sep. 2017, doi: 10.3390/coatings7100153.

[220] A. C. Ferrari and J. Robertson, “Interpretation of Raman spectra of disordered and amorphous carbon.”

[221] M. A. Pimenta, G. Dresselhaus, M. S. Dresselhaus, L. G. Cançado, A. Jorio, and R. Saito, “Studying disorder in graphite-based systems by Raman spectroscopy,” *Phys. Chem. Chem. Phys.*, vol. 9, no. 11, pp. 1276–1290, 2007, doi: 10.1039/B613962K.

[222] J. E. Omoriyekomwan, A. Tahmasebi, J. Zhang, and J. Yu, "Formation of hollow carbon nanofibers on bio-char during microwave pyrolysis of palm kernel shell," *Energy Convers Manag*, vol. 148, pp. 583–592, Sep. 2017, doi: 10.1016/j.enconman.2017.06.022.

[223] A. Tagliaferro, M. Rovere, E. Padovano, M. Bartoli, and M. Giorcelli, "Introducing the novel mixed gaussian-lorentzian lineshape in the analysis of the raman signal of biochar," *Nanomaterials*, vol. 10, no. 9, pp. 1–19, Sep. 2020, doi: 10.3390/nano10091748.

[224] M. Giorcelli *et al.*, "High-Temperature Annealed Biochar as a Conductive Filler for the Production of Piezoresistive Materials for Energy Conversion Application," *ACS Appl Electron Mater*, vol. 3, no. 2, pp. 838–844, Feb. 2021, doi: 10.1021/acsaelm.0c00971.

[225] M. L. Marín, A. Jiménez, J. López, and J. Vilaplana, "Thermal degradation of ethylene (vinyl acetate)," *Journal of Thermal Analysis*, vol. 47, no. 1, pp. 247–258, Jul. 1996, doi: 10.1007/BF01982703.

[226] B. Rimez, H. Rahier, G. van Assche, T. Artoos, M. Biesemans, and B. van Mele, "The thermal degradation of poly(vinyl acetate) and poly(ethylene-co-vinyl acetate), Part I: Experimental study of the degradation mechanism," *Polym Degrad Stab*, vol. 93, no. 4, pp. 800–810, Apr. 2008, doi: 10.1016/j.polymdegradstab.2008.01.010.

[227] A. Fina, H. C. L. Abbenhuis, D. Tabuani, A. Frache, and G. Camino, "Polypropylene metal functionalised POSS nanocomposites: A study by thermogravimetric analysis," *Polym Degrad Stab*, vol. 91, no. 5, pp. 1064–1070, May 2006, doi: 10.1016/j.polymdegradstab.2005.07.013.

[228] J. Schaller *et al.*, "Silicon accumulation in rice plant aboveground biomass affects leaf carbon quality," *Plant Soil*, vol. 444, no. 1–2, pp. 399–407, Nov. 2019, doi: 10.1007/s11104-019-04267-8.

[229] Z. Li, Z. Song, and J.-T. Cornelis, "Impact of rice cultivar and organ on elemental composition of phytoliths and the release of bio-available silicon," *Front Plant Sci*, vol. 5, Oct. 2014, doi: 10.3389/fpls.2014.00529.

[230] L.-J. Wang *et al.*, "Synthesis of Ordered Biosilica Materials," *Chin J Chem*, vol. 20, no. 1, pp. 107–110, Aug. 2010, doi: 10.1002/cjoc.20020200121.

[231] C. L. Thomas, “Chemistry of Cracking Catalysts,” *Ind Eng Chem*, vol. 41, no. 11, pp. 2564–2573, Nov. 1949, doi: 10.1021/ie50479a042.

[232] S. Bourbigot, J. Sarazin, F. Samyn, and M. Jimenez, “Intumescent ethylene-vinyl acetate copolymer: Reaction to fire and mechanistic aspects,” *Polym Degrad Stab*, vol. 161, pp. 235–244, Mar. 2019, doi: 10.1016/j.polymdegradstab.2019.01.029.

[233] X. Wu *et al.*, “Influence of char residues on flammability of EVA/EG, EVA/NG and EVA/GO composites,” *Polym Degrad Stab*, vol. 97, no. 1, pp. 54–63, Jan. 2012, doi: 10.1016/j.polymdegradstab.2011.10.011.

[234] A. Fina and G. Camino, “Ignition mechanisms in polymers and polymer nanocomposites,” *Polym Adv Technol*, vol. 22, no. 7, pp. 1147–1155, Jul. 2011, doi: 10.1002/pat.1971.

[235] S. Bourbigot, M. le Bras, S. Duquesne, and M. Rochery, “Recent Advances for Intumescent Polymers,” *Macromol Mater Eng*, vol. 289, no. 6, pp. 499–511, Jun. 2004, doi: 10.1002/mame.200400007.

[236] F. Yang and M. Antonietti, “The sleeping giant: A polymer View on humic matter in synthesis and applications,” *Prog Polym Sci*, vol. 100, p. 101182, Jan. 2020, doi: 10.1016/j.progpolymsci.2019.101182.

[237] A. Piccolo, “The supramolecular structure of humic substances: A novel understanding of humus chemistry and implications in soil science,” 2002, pp. 57–134. doi: 10.1016/S0065-2113(02)75003-7.

[238] G. Pota *et al.*, “Tuning Functional Behavior of Humic Acids through Interactions with Stöber Silica Nanoparticles,” *Polymers (Basel)*, vol. 12, no. 4, p. 982, Apr. 2020, doi: 10.3390/polym12040982.

[239] G. Liu, H. Shi, C. K. Kundu, Z. Li, X. Li, and Z. Zhang, “Preparation of novel biomass humate flame retardants and their flame retardancy in epoxy resin,” *J Appl Polym Sci*, vol. 137, no. 48, p. 49601, Dec. 2020, doi: 10.1002/app.49601.

[240] S. Matta, M. Bartoli, R. Arrigo, A. Frache, and G. Malucelli, “Flame retardant potential of Tetra Pak®-derived biochar for ethylene-vinyl-acetate

copolymers," *Composites Part C: Open Access*, vol. 8, 2022, doi: 10.1016/j.jcomc.2022.100252.

[241] J. Rybicka, A. Tiwari, and G. A. Leeke, "Technology readiness level assessment of composites recycling technologies," *J Clean Prod*, vol. 112, pp. 1001–1012, Jan. 2016, doi: 10.1016/j.jclepro.2015.08.104.

[242] H. G. Jones, "Tetra pak—a model for successful innovation," *Long Range Plann*, vol. 15, no. 6, pp. 31–37, Dec. 1982, doi: 10.1016/0024-6301(82)90004-8.

[243] E. Chiellini, A. Barghini, P. Cinelli, and V. I. Ilieva, "Overview of environmentally compatible polymeric materials for food packaging," in *Environmentally Compatible Food Packaging*, Elsevier, 2008, pp. 371–395. doi: 10.1533/9781845694784.3.371.

[244] J. Zawadiak, "Tetra Pak Recycling – Current Trends and New Developments," *American Journal of Chemical Engineering*, vol. 5, no. 3, p. 37, 2017, doi: 10.11648/j.ajche.20170503.12.

[245] D. Foti *et al.*, "Microstructure and compressive strength of gypsum-bonded composites with papers, paperboards and Tetra Pak recycled materials," *Journal of Wood Science*, vol. 65, no. 1, p. 42, Dec. 2019, doi: 10.1186/s10086-019-1821-5.

[246] G. Martínez-Barrera *et al.*, "Waste Cellulose from Tetra Pak Packages as Reinforcement of Cement Concrete," *Advances in Materials Science and Engineering*, vol. 2015, pp. 1–6, 2015, doi: 10.1155/2015/682926.

[247] O. Platnieks, A. Barkane, N. Ijudina, G. Gaidukova, V. K. Thakur, and S. Gaidukovs, "Sustainable tetra pak recycled cellulose / Poly(Butylene succinate) based woody-like composites for a circular economy," *J Clean Prod*, vol. 270, p. 122321, Oct. 2020, doi: 10.1016/j.jclepro.2020.122321.

[248] J.-F. Zhang, D. Yan, and Z. Li, "The Recycling of the Tetra-Pak Packages: Research on the Wet Process Separation Conditions of Aluminum and Polythene in the Tetra-Pak Packages," in *2009 3rd International Conference on Bioinformatics and Biomedical Engineering*, Jun. 2009, pp. 1–6. doi: 10.1109/ICBBE.2009.5163649.

[249] J.-F. Zhang, D. Yan, and Z. Li, “The Recycling of the Tetra-Pak Packages: Research on the Wet Process Separation Conditions of Aluminum and Polythene in the Tetra-Pak Packages,” in *2009 3rd International Conference on Bioinformatics and Biomedical Engineering*, Jun. 2009, pp. 1–6. doi: 10.1109/ICBBE.2009.5163649.

[250] L. Xing, J. Gu, W. Zhang, D. Tu, and C. Hu, “Cellulose I and II nanocrystals produced by sulfuric acid hydrolysis of Tetra pak cellulose I,” *Carbohydr Polym*, vol. 192, pp. 184–192, Jul. 2018, doi: 10.1016/j.carbpol.2018.03.042.

[251] C. I. K. Diop and J.-M. Lavoie, “Isolation of Nanocrystalline Cellulose: A Technological Route for Valorizing Recycled Tetra Pak Aseptic Multilayered Food Packaging Wastes,” *Waste Biomass Valorization*, vol. 8, no. 1, pp. 41–56, Jan. 2017, doi: 10.1007/s12649-016-9585-2.

[252] A. Korkmaz, J. Yanik, M. Brebu, and C. Vasile, “Pyrolysis of the tetra pak,” *Waste Management*, vol. 29, no. 11, pp. 2836–2841, Nov. 2009, doi: 10.1016/j.wasman.2009.07.008.

[253] K. Tekin, S. Ucar, and S. Karagöz, “Influence of Co-Pyrolysis of Waste Tetra Pak with Waste Motor Oil on Product Distribution and Properties for Fuel Application,” *Energy & Fuels*, vol. 33, no. 11, pp. 11101–11112, Nov. 2019, doi: 10.1021/acs.energyfuels.9b02634.

[254] A. Undri, L. Rosi, M. Frediani, and P. Frediani, “Fuel from microwave assisted pyrolysis of waste multilayer packaging beverage,” *Fuel*, vol. 133, pp. 7–16, Oct. 2014, doi: 10.1016/j.fuel.2014.04.092.

[255] J. Haydary, D. Susa, and J. Dudáš, “Pyrolysis of aseptic packages (tetrapak) in a laboratory screw type reactor and secondary thermal/catalytic tar decomposition,” *Waste Management*, vol. 33, no. 5, pp. 1136–1141, May 2013, doi: 10.1016/j.wasman.2013.01.031.

[256] W. Jerzak, A. Bieniek, and A. Magdziarz, “Multifaceted analysis of products from the intermediate co-pyrolysis of biomass with Tetra Pak waste,” *Int J Hydrogen Energy*, Jul. 2021, doi: 10.1016/j.ijhydene.2021.06.202.

[257] H. Huo, Y. Ma, and X. Wang, “Recovery of Aluminum and Preparation of Porous Carbon from Tetra Pak Waste,” *ChemistrySelect*, vol. 6, no. 8, pp. 1814–1822, Feb. 2021, doi: 10.1002/slct.202004624.

[258] M. J. Muñoz-Batista, G. Blázquez, J. F. Franco, M. Calero, and M. A. Martín-Lara, “Recovery, separation and production of fuel, plastic and aluminum from the Tetra PAK waste to hydrothermal and pyrolysis processes,” *Waste Management*, vol. 137, pp. 179–189, Jan. 2022, doi: 10.1016/j.wasman.2021.11.007.

[259] Z. Ding, X. Xu, T. Phan, X. Hu, and G. Nie, “High adsorption performance for As(III) and As(V) onto novel aluminum-enriched biochar derived from abandoned Tetra Paks,” *Chemosphere*, vol. 208, pp. 800–807, Oct. 2018, doi: 10.1016/j.chemosphere.2018.06.050.

[260] N. M. Zúñiga-Muro *et al.*, “Recycling of Tetra pak wastes via pyrolysis: Characterization of solid products and application of the resulting char in the adsorption of mercury from water,” *J Clean Prod*, vol. 291, p. 125219, Apr. 2021, doi: 10.1016/j.jclepro.2020.125219.

[261] M. Barbalini, M. Bartoli, A. Tagliaferro, and G. Malucelli, “Phytic Acid and Biochar: An Effective All Bio-Sourced Flame Retardant Formulation for Cotton Fabrics,” *Polymers (Basel)*, vol. 12, no. 4, p. 811, Apr. 2020, doi: 10.3390/polym12040811.

[262] F. Cravero and A. Frache, “Improving Fire Performances of PEAL: More Second-Life Options for Recycled Tetra Pak®,” *Polymers (Basel)*, vol. 12, no. 10, p. 2357, Oct. 2020, doi: 10.3390/polym12102357.

[263] H. Raclavská *et al.*, “Possibilities of the utilization of char from the pyrolysis of tetrapak,” *J Environ Manage*, vol. 219, pp. 231–238, Aug. 2018, doi: 10.1016/j.jenvman.2018.05.002.

[264] Y.-C. Lin, J. Cho, G. A. Tompsett, P. R. Westmoreland, and G. W. Huber, “Kinetics and Mechanism of Cellulose Pyrolysis,” *The Journal of Physical Chemistry C*, vol. 113, no. 46, pp. 20097–20107, Nov. 2009, doi: 10.1021/jp906702p.

[265] S. Wang, Q. Liu, Y. Liao, Z. Luo, and K. Cen, “A study on the mechanism research on cellulose pyrolysis under catalysis of metallic salts,” *Korean*

Journal of Chemical Engineering, vol. 24, no. 2, pp. 336–340, Mar. 2007, doi: 10.1007/s11814-007-5060-x.

[266] N. D. Parkyns, "The surface properties of metal oxides. Part II. An infrared study of the adsorption of carbon dioxide on γ-alumina," *J. Chem. Soc. A*, vol. 0, no. 0, pp. 410–417, 1969, doi: 10.1039/J19690000410.

[267] P. M. A. Sherwood, "Introduction to Studies of Aluminum and its Compounds by XPS," *Surface Science Spectra*, vol. 5, no. 1, pp. 1–3, Jan. 1998, doi: 10.1116/1.1247880.

[268] A. Tagliaferro, M. Rovere, E. Padovano, M. Bartoli, and M. Giorcelli, "Introducing the Novel Mixed Gaussian-Lorentzian Lineshape in the Analysis of the Raman Signal of Biochar," *Nanomaterials*, vol. 10, no. 9, p. 1748, Sep. 2020, doi: 10.3390/nano10091748.

[269] C. Biermann, *Handbook of Pulping and Papermaking*. Elsevier, 1996. doi: 10.1016/B978-0-12-097362-0.X5000-6.

[270] H. Vahabi, B. Kandola, and M. Saeb, "Flame Retardancy Index for Thermoplastic Composites," *Polymers (Basel)*, vol. 11, no. 3, p. 407, Mar. 2019, doi: 10.3390/polym11030407.

[271] V. Babrauskas and W. J. Parker, "Ignitability measurements with the cone calorimeter," *Fire Mater*, vol. 11, no. 1, pp. 31–43, Mar. 1987, doi: 10.1002/fam.810110103.

[272] W. An, L. Jiang, J. Sun, and K. M. Liew, "Correlation analysis of sample thickness, heat flux, and cone calorimetry test data of polystyrene foam," *J Therm Anal Calorim*, vol. 119, no. 1, pp. 229–238, Jan. 2015, doi: 10.1007/s10973-014-4165-9.

[273] S. v. Levchik and E. D. Weil, "Overview of the recent literature on flame retardancy and smoke suppression in PVC," *Polym Adv Technol*, vol. 16, no. 10, pp. 707–716, Oct. 2005, doi: 10.1002/pat.645.

[274] T. Ueno, E. Nakashima, and K. Takeda, "Quantitative analysis of random scission and chain-end scission in the thermal degradation of polyethylene," *Polym Degrad Stab*, vol. 95, no. 9, pp. 1862–1869, Sep. 2010, doi: 10.1016/j.polymdegradstab.2010.04.020.

[275] O. Mašek *et al.*, “Consistency of biochar properties over time and production scales: A characterisation of standard materials,” *J Anal Appl Pyrolysis*, vol. 132, pp. 200–210, Jun. 2018, doi: 10.1016/j.jaap.2018.02.020.

[276] A. Seeger, D. Freitag, F. Freidel, and G. Luft, “Melting point of polymers under high pressure: Part I: Influence of the polymer properties,” *Thermochim Acta*, vol. 424, no. 1–2, pp. 175–181, Dec. 2004, doi: 10.1016/j.tca.2004.05.025.

[277] V. Babrauskas, “Development of the cone calorimeter?A bench-scale heat release rate apparatus based on oxygen consumption,” *Fire Mater*, vol. 8, no. 2, pp. 81–95, Jun. 1984, doi: 10.1002/fam.810080206.

[278] J. J. Shea, “Handbook of building materials for fire protection [Book Review],” *IEEE Electrical Insulation Magazine*, vol. 20, no. 6, pp. 66–66, Nov. 2004, doi: 10.1109/MEI.2004.1367528.

[279] K. T. Paul, “Heat release in fires,” *Fire Saf J*, vol. 21, no. 4, pp. 343–345, Jan. 1993, doi: 10.1016/0379-7112(93)90023-J.

[280] C. Huggett, “Estimation of rate of heat release by means of oxygen consumption measurements,” *Fire Mater*, vol. 4, no. 2, pp. 61–65, Jun. 1980, doi: 10.1002/fam.810040202.